Chapter 3
Numerical Evaluation of Integrals and Derivatives

Abstract The numerical evaluation of integrals referred to as a quadrature is an important aspect of a large number of applied problems in science and engineering. In Chap. 2, we derived several different methods for the numerical evaluation of integrals. These include the trapezoidal and Simpson's rules, the higher order Newton-Cotes algorithms, the Clenshaw-Curtis scheme and the Gauss quadrature methods based on classical and nonclassical polynomials. In this chapter, general principles for the accurate and efficient numerical evaluation of integrals that occur in the modeling of physical systems are provided. This is the basis for an efficient numerical method of solution of integral equations discussed in Chap. 5. The physical systems considered vary considerably from section to section and a brief introduction is provided in each case with numerous references to textbooks and current research publications. We consider radial integrals that occur in density functional theory, integrals for chemical and nuclear fusion rate coefficients and also for the solution of the Boltzmann equation. The numerical evaluation of matrix elements in kinetic theory and quantum mechanics is also presented with important implications for pseudospectral methods. The latter section of the chapter is devoted to the pseudospectral method for numerical differentiation based on the Lagrange and Sinc interpolants. The numerical solution of Sturm-Liouville differential eigenvalue problems for the classical polynomials is also presented.

3.1 Numerical Evaluation of Integrals

The integration of a smooth slowing varying integrand is generally not difficult. With the speed of current personal computers, almost any one-dimensional integral can be evaluated to almost machine accuracy in a finite time. It is well known that a specific numerical method might be efficient for a particular type of integral and not for others. One can always propose a method adapted to work very well for a certain class of integrals but that performs poorly when applied to other integrals.

There have been several discussions of automatic integrators (Davis and Rabinowitz 1975; Lyness 1983) which evaluate one-dimensional integrals for a given integrand, interval and accuracy desired. These automatic integrators have found

some success but are not flawless, as discussed by Lyness (1983). A comprehensive presentation of computational methods for integration with a large number of examples was provided by Kythe and Schaferkotter (2004).

The main objective of this chapter is to present techniques for the evaluation of integrals that arise in physical problems, The precision required will be high but not necessarily of machine accuracy. Specific examples will include radial integrals that arise in density functional theory, electron repulsion integrals in quantum chemistry, integrals in kinetic theory applications and in the evaluation of chemical and nuclear reaction rates, integrals for the efficient evaluation of semi-classical phase shifts in atom-atom scattering and other applications. Often the integrals desired generally have smooth well behaved integrands but in the simulations for which they are required there are a large number of such integral evaluations and thus an efficient scheme is desired. We emphasize the use of Gauss quadratures based on non-classical polynomials.

In kinetic theory, the Boltzmann collision operator is the sum of an integral operator with a well-defined kernel and the collision frequency which is a multiplicative operator. Similarly, the Hamiltonian in the Schrödinger equation is the sum of the kinetic energy second derivative operator and a multiplicative potential function. We consider the calculation of the spectral matrix representations of such multiplicative operators, that is, matrix elements of functions that arise in kinetic theory (Hoare and Kaplinsky 1970; Shizgal and Fitzpatrick 1974; Lindenfeld and Shizgal 1979; Loyalka et al. 2007) and in quantum mechanics (Harris et al. 1965; Dickinson and Certain 1968; Gallas 1980; Bordoni and Manini 2007).

An important example is the matrix representative of the coordinate operator which is the Jacobi matrix, Eq. (2.71). The eigenvalues of this multiplicative operator are the Gaussian quadrature points for the specified weight function and represent the continuous spectrum of the coordinate operator on the specified interval. These continuous eigenvalues do not converge to discrete values with an increase in the number of quadrature points.

The matrix elements of such multiplicative operators can sometimes be calculated exactly in a particular basis set with algebraic methods or approximately by using an appropriate Gaussian quadrature. Harris et al. (1965) and Dickinson and Certain (1968) considered the quadrature evaluation of matrix elements of the potential in the Schrödinger equation. The research lead to the development of a pseudospectral method (Hamilton and Light 1986; Light and Carrington Jr. 2000) for the solution of the Schrödinger equation, primarily for the calculation of the vibrational states of polyatomic molecules.

In quantum chemistry, there is an ongoing interest in the efficient numerical evaluation of three-dimensional integrals over spherical coordinates, (r, θ, ϕ). The theoretical modelling of polyatomic molecules requires the accurate computation of a very large number of similar integrals (Treutler and Ahlrichs 1995; Mura and Knowles 1996; Lindh et al. 2001; Gill and Chien 2003; El-Sherbiny and Poirier 2004; Kakhiani et al. 2009; Mitani 2011). This is an important concern for researchers in quantum chemistry involved with electronic structure calculations. The integration

over solid angle, (θ, ϕ), is generally considered with a cubature separately from the integration over the radial variable, r. In Sect. 3.4.2, the details of the integration of radial integrals is discussed with several examples.

The solution of the Boltzmann equation with a collocation method involves the integral over a kernel which can have a sharp cusp (Gibble and Gallagher 1991; Rogers and Berman 1991; Bovino et al. 2011; Kharchenko et al. 1998; Sospedra-Alfonso and Shizgal 2012). We address the problem of the integration over the cusp for the solution of the Boltzmann equation and similar integral equations discussed in greater detail in Chap. 5. We briefly discuss the challenges presented by oscillatory integrals in physics as well as several integrals that are largely devoid of any physical application (Bornemann et al. 2004).

Pseudospectral methods (Fornberg 1996; Canuto et al. 2006) applied to a multitude of applied problems in diverse fields are defined in terms of global discrete derivative matrix operators generally based on some interpolant. These methods provide first and second order finite derivative matrix operators in physical space and reduce partial differential equations to ordinary differential equations. We will apply these matrix derivative operators to the solution of Sturm-Liouville eigenvalue problems that define the classical polynomials. We also consider the application of pseudospectral methods to the solution of the Fokker-Planck and Schrödinger equations in Chap. 6. There are also finite difference methods (LeVeque 2007; Burden and Faires 2011) that are local representations of the derivative.

3.2 Some General Principles for the Numerical Evaluation of Integrals

We are concerned with the numerical evaluation of a one-dimensional integral of the form

$$I = \int_a^b f(x)dx, \qquad (3.1)$$

with the assumption that the antiderivative, $F(x)$ defined by $dF(x)/dx = f(x)$ is not known analytically. If $F(x)$ is known analytically, then the problem reduces to

$$I = \int_a^b f(x)dx = F(b) - F(a). \qquad (3.2)$$

Since $F(x)$ is generally not known, we consider a numerical approximation to the integral I. In some cases, $F(x)$ is known but expressed in terms of a very complicated function, such as the hypergeometric function, whose evaluation is perhaps more difficult than the numerical calculation of the integral.

For numerical integration, it is important to know in detail the behaviour of the integrand $f(x)$. Of primary interest is the smoothness of $f(x)$ as governed by the continuity of $f(x)$ and its derivatives. If $f(x)$ is continuous, but $df(x)/dx$ is not, special attention is required for the numerical evaluation of I to be accurate as we will show. If $x \in [0, \infty)$ and $f(x)$ decays too slowly as $x \to \infty$, the numerical algorithm chosen must be adapted to take this behaviour into account. Other examples include an integrand that oscillates about zero as $x \to \infty$ or perhaps as $x \to 0$ and the value of I is small. Other special cases include integrands that have singularities in the domain of integration for which a Cauchy principal value is required. For certain functions, a simple variable change $x \to y$, referred to as a mapping, can transform the integrand to a more manageable form suitable for a particular quadrature.

3.3 Scaling Quadrature Points and Weights

For quadratures defined by polynomials on the infinite and semi-infinite intervals such as the Laguerre, Hermite and Maxwell polynomials, an important mapping is the scale change, $z = sx$, to redistribute the quadrature points so as to better capture the integrand. The scaling of quadrature points on the semi-infinite interval for Gauss-Maxwell quadrature with weight function $w(x) = x^2 e^{-x^2}$ often involves this variable change, $z = sx$, and the integral is calculated with the algorithm

$$I = \int_0^\infty G(z)dz = s \int_0^\infty G(sx)dx = s \int_0^\infty x^2 e^{-x^2} \frac{G(sx)}{x^2 e^{-x^2}} dx,$$

$$\approx \sum_{i=1}^N \frac{sw_i}{x_i^2 e^{-x_i^2}} G(sx_i) = \sum_{i=1}^N W_i G(sx_i), \tag{3.3}$$

where the "big" weights are given by $W_i = sw_i/w(x_i)$.

The variable $z = \sqrt{mv^2/2k_BT}$ in the Maxwell weight function is the reduced particle speed with m the particle mass, k_B the Boltzmann constant and T the temperature of the gas. We interpret this mapping in terms of an arbitrary temperature, T_s, different from T so that $x = \sqrt{mv^2/2k_BT_s}$ where the scaling parameter is identified as $s^2 = T_s/T$. This scaling technique has been used in the solution of the Boltzmann equation (Shizgal 1981), the Schrödinger equation (Baye and Heenen 1986; Lo and Shizgal 2008), the Vlasov equation (Schumer and Holloway 1998; Gibelli et al. 2010) and is the basis for the two-temperature model for the solution of the Boltzmann equation for ion mobilities (Mason and McDaniel 1988) in ion-atom binary gases. In the sections that follow, we apply this important technique (Holway 1967; Tang 1993; Holloway 1996; Ordzywolek 2011) to the calculation of radial integrals in density functional theory and to several other applications.

3.4 Integrals in Density Functional Theory

The efficient evaluation of integrals is particularly relevant to the calculation of the electronic energy states of atoms and molecules. Electronic structure modeling in quantum chemistry involves the solution of the Schrödinger equation for the electronic state of a many electron atom or molecule. We provide a very brief overview of this subject to motivate the specific applications in subsequent sections and refer readers to several texts (Karplus and Porter 1970; Szabo and Ostlund 1996; McQuarrie and Simon 1997; Helgaker et al. 2000; Levine 2009; Tsuneda 2014) and research papers (Rys et al. 1983; El-Sherbiny and Poirier 2004; Sandberg and Rinkevicius 2012; Reine et al. 2012; Becke 2014) for a more complete description of this subject and the numerical challenges presented.

The Hamiltonian for the Schrödinger equation is the sum of the electron kinetic energy operators, the electron-nuclei and the electron-electron Coulomb interactions. The only systems for which exact results exist are the hydrogen atom, and one-electron ions such as He^+ (Drake 1999; Drake et al. 2002) and H_2^+ (Cassar and Drake 2004).

The quantum state of the hydrogen atom is represented by the wave function $\psi_{n\ell m}$ (r, Ω) in spherical polar coordinates (r, Ω), $\Omega = (\theta, \phi)$. We showed in Sect. 2.4.6 that the wavefunction for the H-atom separates into the spherical harmonic basis functions $Y_{\ell m}(\Omega) = P_\ell^m(\cos\theta)e^{im\phi}$ and the associated Laguerre polynomials, so that,

$$\psi_{n\ell m}(\rho, \Omega) = N_{n\ell} \exp(-\rho/2)\rho^\ell L_{n-\ell-1}^{(2\ell+1)}(\rho)Y_{\ell m}(\Omega), \tag{3.4}$$

where $\rho = 2r/na_0$, $a_0 = \hbar^2/m_e Z_e^2$ is the Bohr[1] radius and $N_{n\ell}$ is a normalization such that the wave functions are orthonormal,

$$\iint \psi_{nlm}^* \psi_{n'l'm'} r^2 dr d\Omega = \delta_{nn'}\delta_{\ell\ell'}\delta_{mm'}.$$

The spherical harmonic and Laguerre basis functions were discussed in Sects. 2.4.4 and 2.4.5, respectively. In the absence of external fields and spin dependent interactions, the electronic energy states depend only on the principal quantum number n, and the energy is given by $E_n = -e^2/2a_0 n^2$.

The basis functions for the solution of the Schrödinger equation for many electron atoms and molecules are often derived from the eigenfunctions ("orbitals") of the H-atom. The basis functions chosen must be antisymmetric with respect to the exchange of any pair of electrons in order to satisfy the symmetry properties of fermions. The representation of the Hamiltonian in these basis sets is then required and the calculation of the electron-electron pair repulsion integrals presents an ongoing numerical challenge as discussed in Sect. 3.8.1.

An important development in the field was the adoption of an approximate formalism originally developed independently by Thomas (1927) and Fermi (1927)

---

[1] Niels Henrik David Bohr (1885–1962) was a Danish physicist who made fundamental contributions to quantum theory and in particular to the Bohr model of the hydrogen atom. He received the Nobel Prize in Physics in 1922.

for the statistical mechanics of an electron gas and later applied to atomic structure theory (Parr 1983; Parr and Gosh 1986). The electronic ground state is viewed as dependent on the electron density, $\rho(\mathbf{r})$, rather than on the multidimensional electron wavefunction. For many electron systems, the electron density is formally expressed by the integral of the square of the many electron wave function, that is,

$$\rho(\mathbf{r}) = \int |\Psi(\mathbf{r}_1, \mathbf{r}_2, \ldots, \mathbf{r}_n)|^2 d\mathbf{r}_1 \mathbf{r}_2 \ldots \mathbf{r}_{n-1}. \qquad (3.5)$$

The electron-electron and electron-nuclei interactions are then expressed in terms of the density. A variational formalism is applied to the Schrödinger equation written in terms of the electron density appearing as a functional. The theoretical foundations were established by Hohenberg and Kohn (1964) and Kohn and Sham (1965). Excellent reviews of the Thomas-Fermi model and density functional theory are available (Lieb 1981; Jones and Gunnarsson 1989; Morgan 1996) where the original references can be found.

Density functional theory is now routinely employed in electronic structure simulations. The details of this theoretical approach are well beyond the scope of this book. A more complete exposition of this theoretical formalism is available in several textbooks and reviews (Parr 1983; Jones and Gunnarsson 1989; Fiolhais et al. 2003; Burke 2012).

3.4.1 Mapping the Semi-infinite Interval $r \in [0, \infty)$ to $x \in [-1, 1]$

Much of the work on spectral methods (Fornberg 1996; Boyd 2001; Peyret 2002; Canuto et al. 2006; Hesthaven et al. 2007) is based on Fourier series, Chebyshev and Legendre polynomials. Chebyshev polynomials are very closely related to a Fourier series and often referred to as a "Fourier series in disguise" as discussed in Chap. 2. In the next section, we review the evaluation of radial integrals that arise in density functional theory applied to quantum chemistry. The integrals over the semi-infinite domain are often mapped onto the finite interval $[-1, 1]$ as summarized in Table 3.1, and Chebyshev or Legendre quadratures are then used.

Table 3.1 Different mappings of the semi-infinite interval $r \in [0, \infty)$ to $x \in [-1, 1]$

Reference	Mapping
Boyd (1982), Treutler and Ahlrichs (1995)	$x = 1 - 2e^{-r/s}$
Murray et al. (1993)	$x = 2\sqrt[m]{1 - e^{-r/s}} - 1$
Boyd (1987), Becke (1988)	$x = \frac{r-s}{r+s}$
Mura and Knowles (1996)	$x = 2\sqrt{r/(r-s} - 1$
Linear map	$x = \frac{2r}{r_{max}} - 1; \ r \in [0, r_{max}]$

The parameter s is a scaling factor

The accuracy of the different mappings can be tested with the numerical calculation of two integrals on the semi-infinite domain given by

$$\int\limits_0^\infty r^2 e^{-r^2} M_5^2(r) dr = 1,$$

$$\int\limits_0^\infty r^2 e^{-r^2} M_4(r) M_5(r) dr = 0, \tag{3.6}$$

for which the integrands are shown in Fig. 3.1.

Figure 3.1(A) shows the integrand for the normalization of the Maxwell polynomial $M_5(r)$ with respect to the weight function, $w(r) = r^2 e^{-r^2}$, $r \in [0, \infty)$. The integral of this function is the norm which is unity. Figure 3.1(B) shows the integrand for the product of the polynomials $M_4(r)$ and $M_5(r)$ which are orthogonal and the integral for this integrand is zero. We have changed notation from x (originally reduced speed) to r (a radial coordinate) and in the current context we use $x \in [-1, 1]$ as the new variable obtained with variable change or mapping.

These two integrals, one of degree 10 and the other of degree 9, can be done exactly to machine accuracy with the Maxwell ($p = 2$) quadrature points of order 6 shown by the symbols in the graphs. This is a remarkable demonstration of the power of Gaussian quadratures albeit for polynomial integrands. This is no surprise.

This exact quadrature would not be obvious simply from the graphs of the integrands. One could consider the numerical calculation of the integral in Fig. 3.1(A) as the sum of six integrals, each evaluated with a quadrature between the zeros of the function suitably transformed to $[-1, 1]$. The last interval would have to be trun-
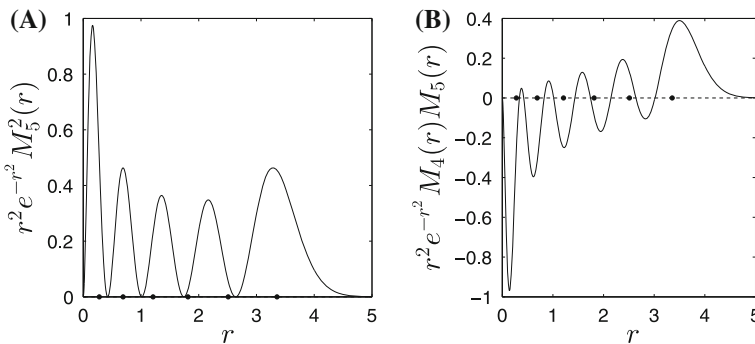
Fig. 3.1 (A) The variation of $r^2 e^{-r^2} M_5^2(r)$ and (B) $r^2 e^{-r^2} M_4(r) M_5(r)$ versus r. The polynomials $M_n(r)$ are orthogonal with the Gauss-Maxwell weight function $w(r) = r^2 e^{-r^2}$, $r \in [0, \infty)$. The integral of the function on the left is 1 and for the function on the right it is zero. The *closed circles* are the quadrature points for the Gauss-Maxwell quadrature for which the integrals in Eq. (3.6) are calculated to machine accuracy with $N = 6$
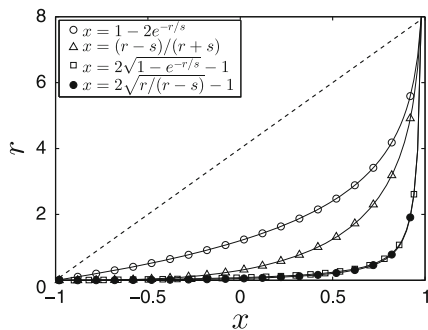
Fig. 3.2 Different variable transformations or mappings from $r \in [0, \infty)$ to $x \in [-1, 1]$ as summarized in Table 3.1. The *dashed line* is the linear map. The scale factor s is chosen such that $r_{max} = 8$ for which the integrands in Fig. 3.1 are considered to be very small

cated at some sufficiently large r_{max}. The integral of the function in Fig. 3.1(B) could also be calculated by evaluating the ten integrals between nodes in the same way. The integrals from node to node can be evaluated with a Chebyshev or Legendre quadrature or a Simpson's rule. This is a commonly used technique for oscillatory integrals.

Five mappings that transform the radial variable $r \in [0, \infty)$ to $x \in [-1, 1]$ are listed in Table 3.1 and shown in Fig. 3.2. A Gauss-Legendre quadrature is then used to evaluate the integrals. These mappings are used in spectral methods (Boyd 1982, 1987) and in particular for the evaluation of integrals in density functional theory. There have been several reviews with numerical comparisons (Lindh et al. 2001; Gill and Chien 2003; El-Sherbiny and Poirier 2004).

The linear map (dashed line) with a truncation at $r = 8$ beyond which there is an insignificant contribution to the integrals does not bias the distribution of quadrature points other than the original clustering near the ends of the interval. An exponential map (open circles) proposed independently by Boyd (1982) and Treutler and Ahlrichs (1995) distributes more quadrature points at small r than at large r. There could be an additional flexibility in the mappings with the use of the scaling parameter which has been chosen as $s = 1$. The main concern is the manner in which the mapping distributes quadrature points and whether the details of the integrand have been captured. A comparison of the distribution of quadrature points for the mappings in Table 3.1 was presented in Fig. 1 of Gill and Chien (2003).

We choose two test integrals of this type to study the different mappings from $[0, \infty)$ to $[-1, 1]$ that have been used as summarized in Table 3.1, namely

$$\langle M_4^2 \rangle = \int_0^\infty r^2 \exp(-r^2) M_4^2 dr = 1,$$

$$\langle M_6^2 \rangle = \int_0^\infty r^2 \exp(-r^2) M_6^2 dr = 1. \tag{3.7}$$
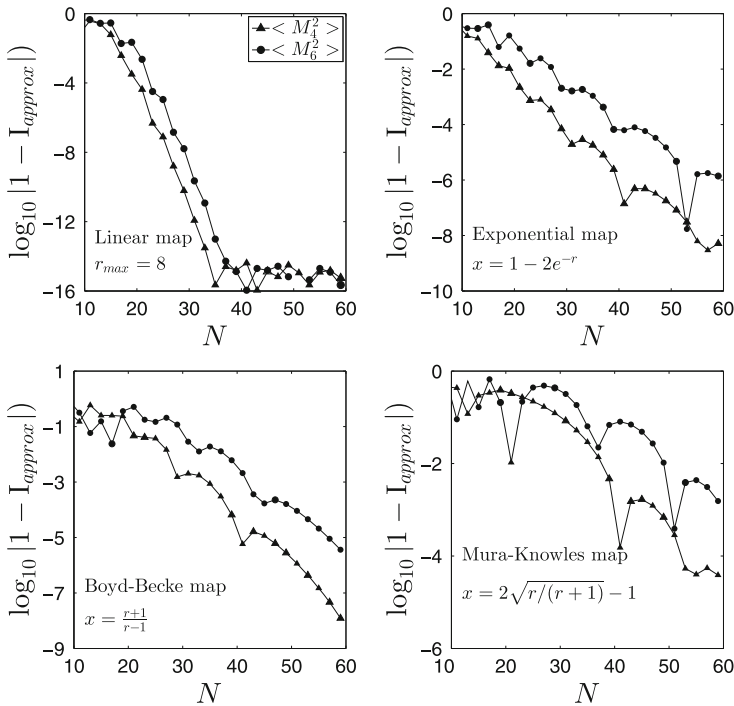
Fig. 3.3 The variation of the relative error for the integrals $\langle M_n^2 \rangle = \int_0^\infty r^2 e^{-r^2} M_n^2(r) = 1$ for $n = 4$ and 6 with four different mappings. The relative error is shown versus the number of Legendre quadrature points, N. The definitions of the mappings are given in Table 3.1

The variation of the relative error for the numerical evaluation of these integrals versus the number of quadrature points, N, is shown for several mappings in Fig. 3.3. The relative error $\log_{10}[1 - I_{approx}]$ for the linear map provides the most rapid convergence. The error with the exponential map is comparable to that with the Boyd-Becke map. The Mura-Knowles map provides the slowest convergence. The different convergence rates depend on the distribution of quadrature points in the transformed interval $[-1, 1]$. These normalization integrals can be evaluated exactly with the Gauss-Maxwell quadrature (p = 2) with $N = 5$ and $N = 7$ quadrature points, respectively.

3.4.2 Radial Integrals in Density Functional Theory

Electron structure calculations in quantum chemistry and density functional theory for polyatomic molecules require the calculation of a large number of three dimensional integrals over a sphere of the form

$$I_{3D} = \int F(\mathbf{r})d\mathbf{r}, \qquad (3.8)$$

where the vector **r** is defined in terms of the three spherical polar coordinates (r, θ, ϕ). The three dimensional integral can be split into an angular integral

$$f(r) = \int_0^{2\pi} \int_0^{\pi} F(r, \theta, \phi) \sin \theta d\theta d\phi, \tag{3.9}$$

over θ and ϕ and the radial integral

$$I_{radial} = \int_0^{\infty} f(r) r^2 dr. \tag{3.10}$$

The angular integral is often evaluated with an algorithm that reduces the two dimensional integral to a single quadrature sum referred to as a cubature (Stroud and Secrest 1966; Lebedev 1977; Cools 2003; Haxton 2007) as discussed in Chap. 2, Sect. 2.8.

There have been several numerical experiments of the calculation of I_{radial} with $f(r)$ approximated by a sum of Gaussians to model the radial variation of the electron density in simple systems such as the inert gas atoms. The mappings from $r \in [0, \infty)$ to $x \in [-1, 1]$ in Table 3.1 have been used (Becke 1988; Murray et al. 1993; Treutler and Ahlrichs 1995; Mura and Knowles 1996; Lindh et al. 2001; Gill and Chien 2003; El-Sherbiny and Poirier 2004; Kakhiani et al. 2009). These studies demonstrate the intense interest in the development of efficient numerical algorithms for the calculation of these three dimensional integrals, Eq. (3.8).

Lindh et al. (2001) considered the integral of a simple (normalized) Gaussian given by,

$$\frac{2\alpha^{(\ell+3)/2}}{\Gamma[(\ell+3)/2]} \int_0^{\infty} r^{\ell} e^{-\alpha r^2} r^2 dr = 1. \tag{3.11}$$

They employed the mappings in Table 3.1 and studied the calculation of this elementary integral for a range of values of α and ℓ versus the number of quadrature points, N. For the integral of the Gaussian in Eq. (3.11), the Gauss-Maxwell quadrature with $p = 2$ provides an exact result for this integral (with $\ell = 0$) and a scale factor $s = 1/\sqrt{\alpha}$.

We evaluate this integral with the Gauss-Maxwell quadrature and the scaling procedure given by Eq. (3.3). The variation of the relative error, defined by

$$\text{Relative Error} = \left| 1 - \frac{I_{approx}}{I_{exact}} \right|, \tag{3.12}$$

versus the scaling parameter s is shown in Fig. 3.4. The integral is evaluated to machine accuracy for $s = 1/\sqrt{\alpha}$ which for $\alpha = 4$ occurs at $s = 0.5$. For $N = 2$ and 4, the range of s values for which the integral is evaluated exactly (to machine accuracy) in the vicinity of $s = 0.5$ is narrower than for the $N = 8$ and 10. It is clear from the graph that there are values of $s > 1/2$, at the inverted cusps, for which the
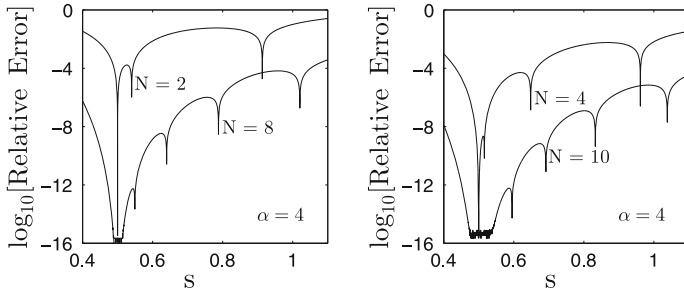
Fig. 3.4 The variation of the relative error for the integral of the Gaussian in Eq. (3.11) versus the scale factor s with the number of Maxwell quadrature points equal to N. The integral is evaluated to machine accuracy for $s = 1/\sqrt{\alpha} = 0.5$ for which the quadrature is exact

integral is also evaluated exactly. This occurs because the error in the integration can overestimate or underestimate the exact value and $(I_{approx} - I_{exact})$ oscillates about zero as s varies. It is difficult to determine a priori where these "roots" of $I_{approx} - I$ versus s occur. We will demonstrate this behaviour versus the scaling parameter in the evaluation of other integrals.

The variation of the relative error for the integral in Eq. (3.11) with the Maxwell quadrature is shown in Fig. 3.5 versus N for $s = 1/2$, $\alpha = 4$ and several values of ℓ. The integral is evaluated to machine accuracy for $\ell = 6, 8, 10$ and 14, with $N = 4, 5, 6$, and 8 quadrature points, respectively. This is not a surprising result as the Gauss-Maxwell integration of a polynomial of degree $2N - 1$ is exact with N quadrature points. The Gaussian in Eq. (3.11) is essentially the Gauss-Maxwell weight function.

The functional forms chosen to simulate realistic radial integrands in Eq. (3.10) include a simple Gaussian

$$f_1(r) = e^{-ar^2}, \tag{3.13}$$
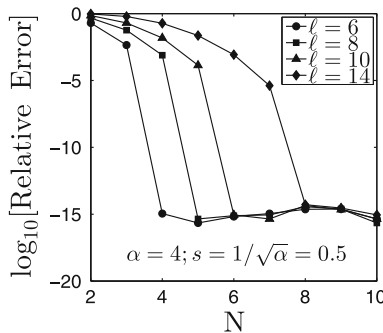
Fig. 3.5 The variation of the relative error for the Gaussian in Eq. (3.11) versus the number of Maxwell quadrature points N for $s = 1$, $\alpha = 4$ and several ℓ values. For $\ell = 6, 8, 10$ and 14, the integrals are evaluated to machine accuracy with $N = 4, 5, 6$, and 8 quadrature points, respectively. This is consistent with the exactness of the Gauss-Maxwell quadrature for polynomials of order $2N - 1$

which is essentially Eq. (3.11). Also studied are the integrands which are the sum of two Gaussians

$$f_2(r) = \left[e^{-r^2} + ae^{-ar^2} \right],$$
(3.14)

and the sum of three Gaussians

$$f_3(r) = \left[e^{-r^2} + ae^{-ar^2} + be^{-br^2} \right].$$
(3.15)

Almost all of the algorithms proposed by different authors to date involve the mapping of the semi-infinite interval, $[0, \infty)$ to the new integration variable $x \in [-1, 1]$ and a quadrature appropriate for the new interval is chosen. These mappings are summarized in Table 3.1. These numerical experiments have been carried out for $a = 10$ and $b = 100$. The quadratures chosen for $x \in [-1, 1]$ are generally Gauss-Legendre, Gauss-Chebyshev and Gauss-Jacobi quadratures.

The variation of the relative error versus the number of Gauss-Maxwell quadrature points, N, for the evaluation of the integrand with a sum of two and three Gaussians, Eqs. (3.14) and (3.15), are shown in Fig. 3.6(A), (B), respectively, for several values of the scaling parameter, s. For the smaller values of s the variation of $\log_{10}$(Relative Error) versus N is almost linear as shown by the dashed lines and also summarized in Table 3.2 for both integrands. The relative error oscillates with N and the linear variation is not accurate for the larger s values.

A Laguerre quadrature which does not involve the mapping to $[-1, 1]$ has also been used as well as a nonclassical quadrature based on the weight function $w(x) = \ln^2 x$ for $x \in [-1, 1]$ (Gill and Chien 2003). The quadrature points and weights for this weight function are easily calculated with a MATLAB code. A comparison and summary of the results of these studies were provided by Gill and Chien (2003) and El-Sherbiny and Poirier (2004). The relative errors obtained vary considerably and are for the most part in the range $-2 \rightarrow -4$ for N in the range $11 \rightarrow 17$. The accuracies
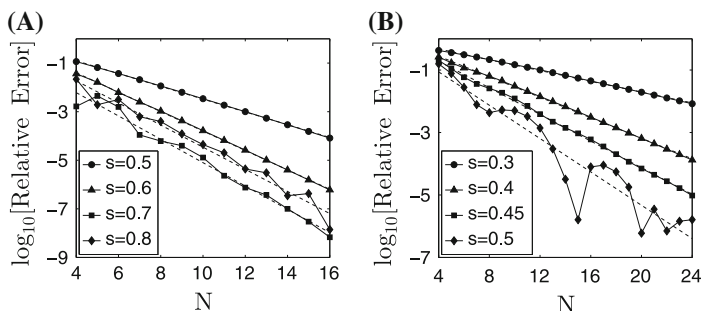
Fig. 3.6 (**A**) The variation of the relative error versus the number of quadrature points N for the integrand in Eq. (3.14) with $a = 10$ and several values of the scaling parameter s. (**B**) The variation of the relative error versus the number of quadrature points N for the integrand in Eq. (3.15) with $a = 10$ and $b = 100$ and several values of the scaling parameter s. The *dashed lines* are the linear fits to the numerical result

Table 3.2 Spectral fits to the convergence of $\log_{10}[|1 - I(N)/I_{exact}|] = A(s)N + B(s)$ and the scaling parameter s

s	A(s)	B(s)
$f_2(r) = [e^{-r^2} + 10e^{-10r^2}]$		
0.5	−0.2630	0.1471
0.6	−0.3996	0.1991
0.7	−0.4804	−0.2947
0.8	−0.4554	0.0915
$f_3(r) = [e^{-r^2} + 10e^{-10r^2} + 100e^{-100r^2}]$		
0.3	−0.08630	0.01899
0.4	−0.01643	0.01015
0.45	−0.02132	0.01369

of the quadratures proposed for the integration of the radial densities for the three atoms mentioned are in the approximate range $-5 \rightarrow -8$ with N up to 25.

In Table 3.3, we compare the results with the Gauss-Maxwell quadrature with the nonclassical Multiexp quadrature of Gill and Chien (2003). Both algorithms converge quickly with a small number of quadrature points with the Gauss-Maxwell quadrature

Table 3.3 Convergence of the integration of $f_2(r)$ and $f_3(r)$, Eqs. (3.14) and (3.15) with the Maxwell quadrature ($p = 2$) and the Multiexp nonclassical quadrature by Gill and Chien (2003) with weight function $w(x) = \ln^2(x)$, $x \in [0, 1]$

N	I(N) (s=0.74)	$\log_{10}$(Relative Error)	I(N)	$\log_{10}$(Relative Error)
	$w(r) = r^2 e^{-r^2}$; $r \in [0, \infty)$		$w(x) = \ln^2(x)$; $x \in [-1, 1]$	
$f_2(r) = [e^{-r^2} + 10e^{-10r^2}]$				
3	0.586161143	−2.30	0.586777664	−2.22
5	0.581900828	−2.64	0.585623383	−2.39
7	0.583287168	−4.08	0.585623383	−2.39
9	0.583232448	−5.00	0.583206200	−4.26
11	0.583238398	−6.58	0.583228705	−4.79
13	0.583238252	−7.81	0.583238660	−6.15
15	0.583238238	−8.09	0.583238152	−6.80
$f_3(r) = [e^{-r^2} + 10e^{-10r^2} + 100e^{-100r^2}]$				
3	0.471897196	−0.606	0.586885435	−1.19
5	0.578862504	−1.11	0.622404076	−2.09
7	0.622639519	−2.11	0.634521349	−1.95
9	0.624246729	−2.28	0.625215372	−2.43
11	0.625501911	−2.49	0.628005273	−3.14
13	0.627361813	−3.52	0.627477032	−3.94
15	0.627548579	−5.79	0.627559616	−4.80

converging slightly faster. The value of s is optimized for the Gauss-Maxwell quadrature. It appears that it is more efficient to develop quadratures on the semi-infinite interval and avoid the mapping to the interval $x \in [-1, 1]$.

3.5 Chemical and Nuclear Reaction Rate Coefficients

In this section, we consider integrals that arise in the calculation of equilibrium reaction rates for chemical and nuclear fusion reactions. The theoretical calculation of reactive cross sections involves a classical or quantal treatment of the collision dynamics between the reactants with a specified interparticle interaction. The macroscopic rate coefficient is then the average of the reactive cross section with Maxwellian distributions for the colliding particles (Ross and Mazur 1961; Truhlar and Wyatt 1976; Chatfield et al. 1991). An important endeavor is the development of efficient algorithms for the calculation of rate coefficients of chemical reactions for numerous applications in shock waves (Brun 2009), in atmospheric science (Seinfeld and Pandis 2006), for nuclear fusion reactions in astrophysics (Clayton 1968) and nuclear fusion machines (Atenzi and Meyer-Ter-Vehn 2004).

3.5.1 Equilibrium Rate Coefficient for Chemical Reactions

The temperature dependence of the binary reactive rate coefficient, $k(T)$, for gas phase chemical reactions as well as nuclear fusion reactions is given in terms of the energy dependence of the total reactive cross section, $\sigma_r(E)$, versus the relative translational energy of the reactants E, and the equilibrium Maxwell-Boltzmann distribution functions of the colliding pair of particles, $F_1(v_1)$ and $F_2(v_2)$, respectively, of the form

$$F(v) = \left[\frac{m}{2\pi k_B T}\right]^{3/2} e^{-mv^2/2k_B T}, \tag{3.16}$$

and normalized according to $4\pi \int_0^\infty F(v)v^2 dv = 1$. In Eq. (3.16), the temperature of the gas is T, k_B is the Boltzmann constant and $m = m_1$ or $m = m_2$ for the particle masses. The temperature dependence of the reactive rate coefficient is given by the average of the reactive flux $g\sigma_r(E)$ over all particle velocities weighted with the distribution functions, that is,

$$k(T) = \iint F_1(v_1)F_2(v_2)g\sigma_r(E)d\mathbf{v}_1 d\mathbf{v}_2, \tag{3.17}$$

where the relative velocity is $\mathbf{g} = \mathbf{v}_2 - \mathbf{v}_1$. We transform to relative velocity, $\mathbf{g}$, and center of mass, $\mathbf{G}$, that is,

$$\mathbf{g} = \mathbf{v}_2 - \mathbf{v}_1,$$
$$\mathbf{G} = \frac{m_1\mathbf{v}_1 + m_2\mathbf{v}_2}{m_1 + m_2}. \tag{3.18}$$

The total kinetic energy can be expressed in terms of G and g given by

$$m_1 v_1^2 + m_2 v_2^2 = m_0 G^2 + \mu g^2, \tag{3.19}$$

where $m_0 = m_1 + m_2$ and the reduced mass is $\mu = m_1 m_2 / m_0$. The Jacobian of the transformation is unity so that $d\mathbf{v_1} d\mathbf{v_2} = d\mathbf{G} d\mathbf{g}$. The integral over G that results from this transformation is

$$4\pi \int_0^\infty e^{-m_0 G^2 / k_B T} G^2 dG = 2\pi \left[\frac{2k_B T}{m_0} \right]^{3/2} \Gamma(\tfrac{3}{2}), \tag{3.20}$$

where $\Gamma(\alpha) = \int_0^\infty e^{-x} x^{\alpha-1} dx$ is the Gamma function. Two useful identities for the Gamma function are $\Gamma(n+1) = n\Gamma(n) = n!$ and $\Gamma(\tfrac{1}{2}) = \sqrt{\pi}$.

With Eq. (3.20), Eq. (3.17) can be reduced to a single integral over g, that is

$$k(T) = 4\pi \left(\frac{\mu}{2\pi k_B T} \right)^{3/2} \int_0^\infty e^{-\mu g^2 / 2k_B T} \sigma_r(E) g^3 dg, \tag{3.21}$$

or in terms of relative energy $E = \mu g^2 / 2$,

$$k(T) = \sqrt{\frac{8}{\pi \mu}} \frac{1}{(k_B T)^{3/2}} \int_0^\infty e^{-E/k_B T} E \sigma_r(E) dE. \tag{3.22}$$

These are standard results that can be found in many texts on chemical kinetics and kinetic theory (McQuarrie and Simon 1997; Gombosi 1994; Kremer 2010; Liboff 2003). The thermal average in Eq. (3.22) is the last step in a detailed theoretical calculation that involves the interaction potential between the reactants followed by the classical or quantal scattering calculation of the reactive cross section (Chatfield et al. 1991).

The temperature dependence of $k(T)$ is determined by the energy dependence of the reactive cross section $\sigma_r(E)$. In fact, one can view $k(T)$ as the Laplace transform of $E\sigma_r(E)$. There are many applications that we can consider each with a different reactive cross section $\sigma_r(E)$. We first consider a simple model system for reactions with activation energy referred to as the line-of-centers reactive cross section given by

$$\sigma_r(E) = \begin{cases} 0, & E \le E^*, \\ \sigma_d(1 - \frac{E^*}{E}), & E > E^*. \end{cases} \tag{3.23}$$

The activation energy is denoted by E^* and there are no reactive collisions if $E < E^*$. For this simple model, the integral in Eq. (3.17) can be done analytically and the result is,

$$k(T) = \sigma_d \sqrt{\frac{8k_B T_b}{\pi \mu}} e^{-E^*/k_B T}, \tag{3.24}$$

where σ_d is a hard sphere cross section.

There is an ongoing effort to determine reactive cross sections experimentally as well as theoretically for a large number of different systems for a wide range of applications. We consider here just one such physically realistic process, namely the collision dissociation reaction $O + O_2$ with applications to planetary atmospheres (Johnson and Tully 2002). The analytic fit to the theoretical scattering results is

$$\sigma_r(E) = \sigma_0 \frac{(E - E_t)^a}{E_0 + E^b}, \tag{3.25}$$

where $\sigma_0 = 4.51$, $E_t = 14.5\,\text{eV}$, $E_0 = 0.21$, $a = 1.03$ and $b = 1.31$. The cross section is in $10^{-16}\,\text{cm}^2$ with E in eV. The variation with energy of this cross section is shown in Fig. 3.7 in comparison with the line-of-centers cross section with the threshold energy $E_t = 1.8\,\text{eV}$ in order to fit the cross sections near threshold.

For such reactions with activation energy, we transform the integral over energy in Eq. (3.17) to an integration over reduced energy $y = E/k_B T$ from which the integral is zero for $y < y_t = E_t/k_B T$. With the additional transformation to $z = y - y_t$ we get the rate coefficient in a form suitable for integration with Gauss-Laguerre quadratures, that is,

$$
k(T) = \sqrt{\frac{8k_B T}{\pi \mu}} \left[y_t e^{-y_t} \int_0^\infty e^{-z} \sigma[(z + y_t)k_B T]dz \right.
$$

$$
\left. + e^{-y_t} \int_0^\infty z e^{-z} \sigma[(z + y_t)k_B T]dz \right]. \tag{3.26}
$$

The first integral suggests the use of Laguerre quadratures based on $L_n^{(\alpha)}(z)$ with $\alpha = 0$ and the second with $\alpha = 1$. The weights and points for each can also be scaled.

In Table 3.4, we show the convergence of the rate coefficient versus the number of Gauss-Laguerre quadrature points for several different scale factors, s. Also shown
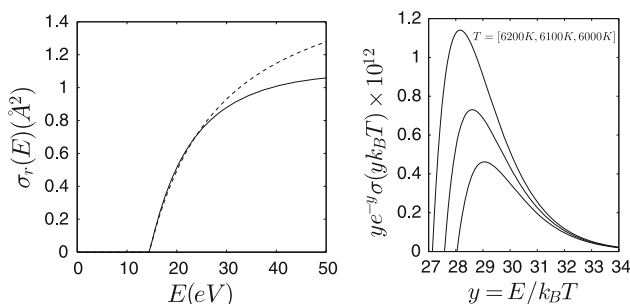
Fig. 3.7 (*Left panel*) Reactive cross section for collisional dissociation for $O + O_2$, Eq. (3.25) (*solid line*) in comparison with the line of centers cross section (*dashed line*; $E^* = E_t$, $\sigma_d = 1.8\,\text{Å}^2$). (*Right panel*) Integrand in Eq. (3.22) versus the reduced energy, $y = E/k_B T$

Table 3.4 Convergence of the integration Eq. (3.26) for the $O + O_2$ reactive cross section, Eq. (3.25), for $T = 6,000\,K$ with a Simpson's rule (SR) integration and the Gauss-Laguerre quadrature for three scalings, s

N	SR	N	$s = 1$	$s = 0.8$	$s = 0.5$
20	1.243617	6	1.257290	1.257398	1.257416
40	1.257156	12	1.257497	1.257522	1.257546
60	1.257661	18	1.257533	1.257544	1.257555
80	1.257671	24	1.257546	1.257551	1.257557
120	1.257625	30	1.257551	1.257555	1.257559
200	1.257586	40	1.257556	1.257558	1.257560
300	1.257572	50	1.257558	1.257559	1.257560

The rate coefficient is in units of $10^{-12}\sqrt{8k_B T/\pi\mu}$

is the convergence with a Simpson's rule. One difficulty with the Simpson's rule integration is the truncation of the grid at some sufficiently large z_{max}. There are therefore two convergence parameters, the number of grid points, N and z_{max}.

The rate of convergence of the integrals is much slower with the Simpson's rule in comparison with the Gauss-Laguerre quadrature. The change with scale factor improves the quadrature result for the smaller N values.

3.5.2 Rate Coefficients for Fusion Reactions; Non-resonant Cross Sections

The accurate calculation of nuclear reaction rate coefficients is a very important for solar and big bang nucleosynthesis (Clayton 1968; Angula 1999; Descouvemont et al. 2004; Bertulani et al. 2013) as well as for nuclear fusion machines (Haubold and John 1981; Heidbrink and Sadler 1994; Atenzi and Meyer-Ter-Vehn 2004). There is considerable research work on the accurate computation of nuclear reaction rates versus the ambient temperature. For time dependent evolutionary simulations, the rate coefficients need be evaluated numerous times as the temperature evolves with time.

In this section, we consider nuclear fusion reactions for which the non-resonant reactive cross sections are of the form

$$\sigma_r(E) = \frac{S(E)}{E} e^{-B/\sqrt{E}}, \tag{3.27}$$

where B is a constant and $S(E)$, often referred to as the astrophysical S-factor, is a slowly varying function of E. There is another important resonant contribution to fusion reactions which we do not consider. The equilibrium rate coefficient from the average of the reactive cross section with the Maxwellian distribution of

relative energies is given by Eq. (3.22). With the reduced energy $y = E/k_BT$, the rate coefficient is given by

$$k(T) = S_0 \sqrt{\frac{8}{\pi \mu k_B T}} I, \tag{3.28}$$

where $S(E)$ is set to a constant, S_0, and the energy average of the cross section can be written in terms of the dimensionless integral

$$I = \int_0^\infty e^{-y-b/\sqrt{y}} dy, \tag{3.29}$$

with $b = B/\sqrt{k_B T}$.

We are interested in the numerical evaluation of the integral in Eq. (3.29). The S_0 and B values of some representative nuclear fusion reactions in stellar interiors are shown in Table 3.5. The details of the integration in Eq. (3.29) are shown in Fig. 3.8(A) as the product of the decreasing Maxwellian and the increasing cross section. The integrand is shown as the Gaussian curve.

The integral in Eq. (3.29) is often approximated with the method of stationary phase also referred to as the saddle-point method (Clayton 1968; Atenzi and Meyer-Ter-Vehn 2004). This is the Gaussian approximation to the bell-shaped curves in Fig. 3.8 which involves the Taylor expansion of the argument of the exponential in

Table 3.5 Representative nuclear fusion reactions (barn $= 10^{-24}$ cm^2)

Reaction	$S(0)$ (keV barn)	B ($\sqrt{\text{keV}}$)
$D + T \rightarrow \alpha + n$	1.2×10^4	34.38
$T + T \rightarrow \alpha + 2n$	138	38.45
$p + p \rightarrow D + e^+ + \nu$	4.0×10^{-22}	22.20
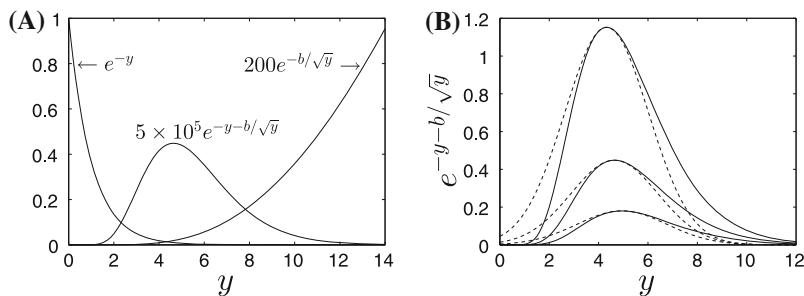
Fig. 3.8 (**A**) The product of decaying Maxwellian distribution and the rising nuclear cross section for $b = 20$. The thermally averaged rate coefficient is the area under the Gaussian shaped curve. (**B**) Integrands for Eq. (3.29) for $b = 18$, 20 and 22, from *top curve* to *bottom curve*. The *dashed curves* are the Gaussian approximations to the actual integrands used in the approximate evaluation of the integral with the saddle-point or stationary phase method as discussed in the text. The exact integrands, Eq. (3.29), are shown by the *solid curves*

Eq. (3.29) up to the quadratic term. The maximum of the function $f(y) = y + b/\sqrt{y}$ occurs at $y_m = \sqrt[3]{b^2/4}$ and the second derivative is $f''(y_m) = \frac{3}{4}b/y_m^{5/2}$. With the extension of the lower limit of the integral to $-\infty$, the analytic evaluation of the integral of the resulting Gaussian, gives the approximate result

$$I_{approx} = \sqrt{\frac{4\pi}{3y_m}} e^{-y_m - b\sqrt{y_m}}. \tag{3.30}$$

The Gaussian approximations to the integrand for $b = 18$, 20 and 22 are shown by the dashed curves in Fig. 3.8(B). The exact value of the integral can be determined with MAPLE and a comparison of the exact value with the approximation, Eq. (3.30), is shown in Table 3.6 versus b. The Gaussian approximation is accurate to several percent.

We use a Simpson's rule integration to estimate the integral in Eq. (3.29). The variation of the accuracy versus the number of integration points, N, is shown in Fig. 3.9 for three different values of y_{max} that defines the integration interval $[0, y_{max}]$. Figure 3.9(A) shows an oscillatory variation of the relative error versus N and there are sharp minima at specific N values for each y_{max}.

Table 3.6 The error of the Gaussian approximation to the integral $I = \int_0^\infty \exp(-y - b/\sqrt{y})dy$, Eq. (3.30), and the exact value computed with MAPLE

b	I_{exact}	I_{approx}	$\log_{10}|(I_{exact} - I_{approx})/I_{exact}|$
5	0.118541084561830544929940 (-1)	1.106 (-2)	-1.18
10	0.567437038339189105890373 (-3)	5.425 (-4)	-1.36
18	0.101229347024099882905469 (-4)	0.9815 (-5)	-1.52
20	0.406891577852032546746999 (-5)	3.953 (-6)	-1.55
22	0.168190705863960574567002 (-5)	1.637 (-6)	-1.56
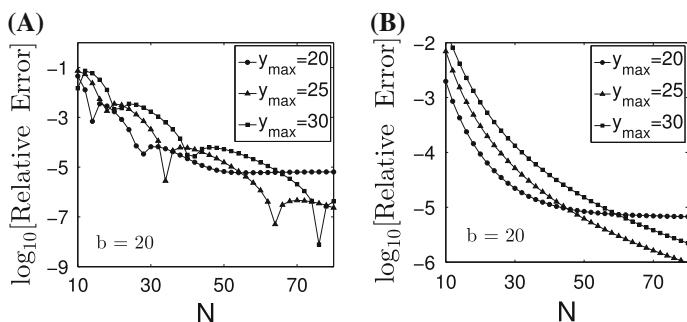
Fig. 3.9 Variation of $\log_{10}$[relative error] versus the number of integration points, N, for the Simpson's rule evaluation of the integral, Eq. (3.29) for $b = 20$. (A) Integration interval is $[0, y_{max}]$, (B) Integration intervals $[0, \sqrt[3]{b^2/4}]$ and $[\sqrt[3]{b^2/4}, y_{max}]$ where the peak in the Gaussian approximation occurs at $y_0 = \sqrt[3]{b^2/4}$ and N integration points in each interval

Figure 3.9(B) shows the results with a Simpson's rule integration using two inter-vals, namely $[0, \sqrt[3]{b^2/4}]$ and $[\sqrt[3]{b^2/4}, y_{max}]$ where the peak in the Gaussian approx-imation occurs at $y_0 = \sqrt[3]{b^2/4}$. The relative error is comparable to that with the full integral and half the number of points but the variation versus N appears monotonic. For the smaller values of N, the accuracy decreases with increasing y_{max} owing to the larger step size. For $y_{max} = 20$, the accuracy attains an asymptotic value because the "tail" of the integrand has not been sampled. This improves with the larger y_{max} val-ues. This exercise illustrates the difficulties of the Simpson's rule on the semi-infinite axis requiring y_{max} to be specified.

We also carry out a comparison of the numerical evaluation of the integral in Eq. (3.29) with a Laguerre quadrature defined by $w(y) = e^{-y}$, and with a quadrature based on the Maxwell weight with $p = 1$ that is, $w(x) = xe^{-x^2}$ with the change of variable $y = x^2$. An important aspect is the distribution of points within the integrand shown in Fig. 3.8. Thus the quadrature points must be scaled so as to be predominantly within the bell shaped curve of the integrand. The results with the Gauss-Laguerre and Gauss-Maxwell quadratures shown in Fig. 3.10 converge much faster versus N than the Simpson's rule integration. The sharp minima in Fig. 3.10
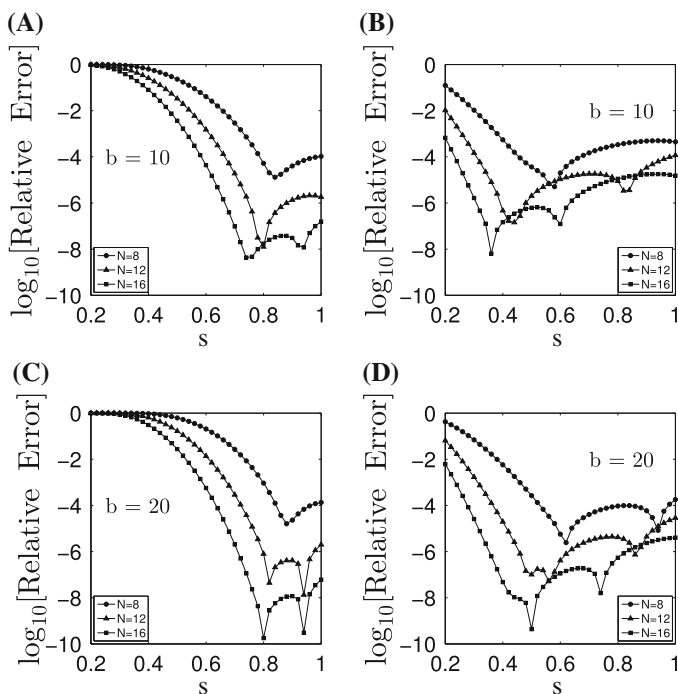
Fig. 3.10 The variation of the $\log_{10}$[relative error] versus the scale factor s for the integral $I = \int_0^\infty \exp(-y - b/\sqrt{y})dy$: (**A**) and (**C**) Gauss-Maxwell quadrature; $w(x) = x\exp(-x^2)$. (**B**) and (**D**) Laguerre quadrature based on $w(y) = \exp(-y)$. The exact value of the integral is calculated with MAPLE listed in Table 3.6

versus the scaling parameter s arise from the change in sign of $I_{approx} - I_{exact}$. Thus, there are several values of the scaling factor for which the numerical result is exact.

There have been several approximate analytical results for the energy integral with the cross section Eq. (3.27) and an energy dependent $S(E)$ which is often expanded in a power series about $E = 0$, that is,

$$S(E) = S(0) + \sum_{n=1}^{N} \frac{1}{n!} \frac{dS(E)}{dE}\bigg|_{E=0} E^n. \tag{3.31}$$

With Eq. (3.31), the reaction rate involves integrals of the form

$$I_n = \int_0^{\infty} y^n e^{-y - \hat{b}/\sqrt{y}} dy. \tag{3.32}$$

This type of parametrization of the cross section and the subsequent analytical approximation of the integrals was carried out by several groups (Haubold and John 1981; Hussein and Pato 1997; Ueda et al. 2000; Mathai and Haubold 2002). This approach yields the integrals in terms of the Meijer G-function related to the hypergeometric function.

We do not pursue this approach here and consider an efficient quadrature evaluation of the integral in Eq. (3.22) with an alternate fit to $S(E)$ in the form of a Padé approximant (Bosch and Hale 1992) of the form

$$S(E) = \frac{a_1 + E(a_2 + E(a_3 + E(a_4 + Ea_5))))}{1 + E(b_1 + E(b_2 + E(b_3 + Eb_4)))}. \tag{3.33}$$

The cross section parameters for some of the more important fusion reactions are provided in Table IV of the review paper by Bosch and Hale (1992). With the change of variable $x^2 = E/k_B T$, the integral in Eq. (3.22) is appropriate for the Gauss-Maxwell quadrature with $p = 1$.

In Table 3.7 we show the rapid convergence of the rate coefficients, $k(T)$, for three nuclear fusion reactions with the Gauss-Maxwell ($p = 1$) quadrature. A small number of quadrature points of the order of 10 yields more accurate results than the corresponding empirical fits of the rate coefficients versus temperature by Bosch and Hale (1992).

3.6 Integrals in Collision Theory and Kinetic Theory

The theoretical description of collisional processes represents an important research effort in chemical physics. This includes the theoretical calculations of reactive cross sections for chemical and nuclear reactions, photoionization, collisional energy transfer and many other applications. In kinetic theory, the collision operator in the Boltzmann equation for translational energy is defined by the differential collision cross section for binary collisions for atom-atom, electron-atom and ion-atom pairs.

Table 3.7 Convergence of the nuclear reaction rate coefficient, $k(T)$ in cm^{3}s^{-1} with the thermal average of the cross section in Eq. (3.33) and the parameters in Table VII of Bosch and Hale (1992)

$k_B T (keV)$	N	^{3}He(d, p)^{4}He	D(d, p)T	D(d, n)^{3}He
1	4	0.2353 (−26)	0.98921 (−22)	9.6908 (−23)
	6	2.8176 (−26)	0.99971 (−22)	9.8165 (−23)
	8	2.9488 (−26)	1.0015 (−22)	9.8340 (−23)
	10	2.9571 (−26)	1.0013 (−22)	9.8328 (−23)
	12	2.9575 (−26)		9.8326 (−23)
	14	2.9576 (−26)		
Bosch and Hale (1992)		3.057 (−26)	1.017 (−22)	9.933 (−23)
10	4	1.6792 (−19)	5.8566 (−19)	6.0804 (−19)
	6	1.6301 (−19)	5.8523 (−19)	6.0798 (−19)
	8	1.6286 (−19)	5.8486 (−19)	6.0766 (−19)
	10	1.6288 (−19)	5.8492 (−19)	
	12		5.8491 (−19)	
Bosch and Hale (1992)		2.126 (−19)	5.781 (−19)	6.023 (−19)
50	4	3.4347 (−17)	9.9370 (−18)	1.1349 (−17))
	6	3.4255 (−17)	9.9725 (−18)	1.1378 (−17)
	8	3.4241 (−17)	9.9668 (−18)	1.1373 (−17)
	10	3.4244 (−17)	9.9678 (−18)	1.1374 (−17)
Bosch and Hale (1992)		5.554 (−17)	9.838 (−18)	1.133 (−17)

The Maxwell weight function $w(x) = x \exp(-x^2)$ is used in the energy integration. The rate coefficients quoted by Bosch and Hale (1992) are taken from their Table VIII

Inelastic collisions between molecules with internal energy transfer are also important processes (McCourt et al. 1991; Brun 2009) as well as inelastic electron or ion atom/molecule collisions (Burke and Joachain 1995; Burke 2011) but these topics are beyond the scope of this book.

In the next five subsections, we consider the quadratures involved in the evaluation of (1) the reactive and elastic collision frequencies, (2) the integration over the cusp in the kernel of the Boltzmann equation, (3) the shear viscosity for a simple gas, (4) the eigenvalues of the collision operator in the Boltzmann equation for the special model referred to as Maxwell molecules and (5) the Jeffries-Wentzel-Brillouin-Kramers (JWKB) approximation to the quantal phase shifts used in the calculation of atom-atom collision cross sections. Some but not all of the physical results discussed are derived in detail and the references provided should be consulted for a better understanding of each topic.

3.6.1 The Reactive and Elastic Collision Frequencies

In the previous sections we showed the relationship between the energy dependence of the reactive cross section and the temperature dependence of the reactive rate

coefficient for reactions of chemical interest as well as for fusion reactions. In this section, we express the reactive rate coefficient in terms of the speed dependence of the reactive collision frequency by assuming that one reactant is distributed in speed with a Maxwellian distribution whereas the distribution function of the second component is not specified. We thus integrate over the velocity of the species m_2 taken to be at equilibrium but we do not transform to centre of mass and relative velocity coordinates as done in the previous section.

We write the reactive rate coefficient as

$$k(T) = \int f_1(v_1)R(v_1)d\mathbf{v}_1, \tag{3.34}$$

where the reactive collision frequency is defined by

$$R(v_1) = \int F(v_2)\sigma_r(E)g d\mathbf{v}_2. \tag{3.35}$$

The analogous elastic collision frequency, $Z(v_1)$, is

$$Z(v_1) = \int F(v_2)\sigma_{el}(E)g d\mathbf{v}_2, \tag{3.36}$$

with the total elastic cross section denoted by $\sigma_{el}(E)$. This elastic collision frequency occurs in the collision operator of the Boltzmann equation. The spectral properties of the linear and linearized operators are considered in detail in Chap. 5, and the elastic collision frequency plays an important role as demonstrated later.

The distribution function of reactant labeled 1, $f_1(v_1)$, is unspecified whereas $F(v_2)$ is a Maxwell-Boltzmann distribution function. We define reduced velocity variables

$$\mathbf{z} = \mathbf{g}\sqrt{\frac{\mu}{2k_BT}}, \qquad \mathbf{x}_i = \mathbf{v}_i\sqrt{\frac{m_i}{2k_BT}}, \qquad i = 1, 2 \tag{3.37}$$

so that

$$R(x_1) = \frac{1}{\pi}\sqrt{\frac{2k_BT}{\pi\mu}}\int e^{-x_2^2}\sigma_r(E)z d\mathbf{x}_2. \tag{3.38}$$

With the change of variable in Eq. (3.38) from x to z where the reduced relative velocity is $\mathbf{z} = \sqrt{M_1}\mathbf{x}_2 - \sqrt{M_2}\mathbf{x}_1$ and the mass fractions are $M_1 = m_1/(m_1 + m_2)$ and $M_2 = m_2(m_1 + m_2)$, we have that

$$R(x_1) = 2\sqrt{\frac{2k_BT}{\pi\mu}}M_1^{-\frac{3}{2}}\int_0^\infty e^{-(z^2+M_2x_1^2)/M_1}\left[\int_{-1}^1 e^{-2\sqrt{M_2}zx_1\hat{\mu}/M_1}d\hat{\mu}\right]\sigma_r(E)z^3 dz. \tag{3.39}$$

The 2π factor results from the integration over the azimuthal angle of $\mathbf{z}$ relative to $\mathbf{x}_1$ as the polar axis and $\hat{\mu} = \cos\theta$ where θ is the angle between $\mathbf{z}$ and $\mathbf{x}_1$. The integration over $\hat{\mu}$ is elementary and we find that,

$$R(x_1) = \sqrt{\frac{2k_BT}{\pi\mu}} \frac{1}{\sqrt{M_1M_2x_1}} [G(-x_1) - G(x_1)], \tag{3.40}$$

where

$$G(x_1) = \int_0^\infty e^{-(z+\sqrt{M_2}x_1)^2/M_1} \sigma_r(E)z^2 dz. \tag{3.41}$$

To evaluate $R(x_1)$, the energy dependence of the reactive cross section must be specified and in the first instance we choose the line-of-centers model, Eq. (3.23), for which we have

$$G(x_1) = \sigma_d\sqrt{M_1}\left[M_1I_2 - 2\sqrt{M_1M_2}I_1 + (M_2x_1 - \epsilon)I_0\right], \tag{3.42}$$

where the I_n integrals are defined by

$$I_n = \int_{t_0}^\infty e^{-t^2}t^n dt, \tag{3.43}$$

where $t_0 = (\sqrt{\epsilon} + \sqrt{M_2}x_1)/M_1$. These integrals are determined by iteration with

$$I_0 = \frac{\sqrt{\pi}}{2}\mathrm{erfc}(t_0),$$

and

$$I_{n+1} = \frac{1}{2}\left[e^{-t_0^2}t_0^n + nI_{n-1}\right].$$

The variation of the reactive collision frequency for this line-of centers cross section versus reduced energy, x_1^2, for several mass ratios is shown in Fig. 3.11. The mass ratio decreases from $m_1/m_2 = 100$ to $m_1/m_2 = 10^{-4}$ as shown in the graph and Table 3.8. The reactive collision frequency changes form with mass ratio and the numerical evaluation of the integral

$$k(T) = \int_0^\infty x^2 e^{-x^2} R(x) dx, \tag{3.44}$$

for the rate coefficient must take this mass ratio variation into account. A straightforward application of the quadrature based on the Maxwellian weight, $w(x) = x^2 e^{-x^2}$,
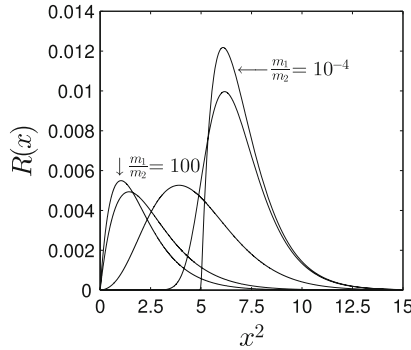
Fig. 3.11 The reactive collision frequency $R(x)$ in units of $\sqrt{2k_BT/\pi\mu}$ versus reduced energy, $x^2 \equiv x_1^2 = mv_1^2/2k_BT$ for reduced threshold energy $\epsilon^* = 5$ for the line-of-centers cross section, Eq. (3.23), and for several mass ratios m_1/m_2 (see Table 3.8). For $m_1/m_2 \to 0$, $R(x) \to 2e^{-x^2}\sigma_r(x^2k_BT)$ and increases rapidly near the threshold energy for small mass ratios m_1/m_2

Table 3.8 The relative error of the Gauss-Maxwell quadrature approximation $(w(x) = x^2e^{-x^2})$ to the integral $I = \int_0^\infty x^2 \exp(-x^2)R(x)dx$ for the line-of-centers cross section, Eq. (3.23)

m_1/m_2	0.0001	0.05	1	10	100
N	Accuracy $= \log[|1 - I(N)/I_{exact}|]$				
4	−0.300	−0.521	−4.34	−6.65	−10.5
6	−0.379	−0.731	−4.56	−10.3	−14.3
8	−0.552	−1.08	−6.17	−14.3	
10	−0.806	−1.66	−7.88		
12	−1.73	−1.98	−9.64		
14	−0.878	−1.87	−11.5		
16	−0.945	−2.69	−14.0		
18	−1.01	−2.45	−14.9		
20	−1.16	−3.14			

The exact value is $I_{exact} = e^{-\epsilon^*}$, $\epsilon^* = 5$; The integrals are in units of $\sqrt{2k_BT/\pi\mu}$

yields excellent results for the larger mass ratios but does not capture the integrand for the small mass ratios as shown in Table 3.8. The results for the two smallest mass ratios in the table are very poor and understandably so. Much better results can be obtained with the appropriate translation of the quadrature points so that the first point is just below the threshold energy.

For $\epsilon^* = 0$, the reactive collision frequency reduces to the well-known elastic collision frequency,

$$Z(x) = \pi d^2 \sqrt{\frac{k_BT_b}{2M}} \left[(2\sqrt{\gamma x} + \frac{1}{\sqrt{\gamma x}}) \frac{\sqrt{\pi}}{2} \text{erf}(\sqrt{\gamma x}) + e^{-\gamma x} \right]. \tag{3.45}$$

This collision frequency appears in the Boltzmann collision operator, Eq. (3.46), and is in part the origin of the continuous portion of the eigenvalue spectrum of the collision operator (Hoare and Kaplinsky 1970). In Sect. 3.9.2, we consider the calculation of matrix elements of the multiplicative operator, $Z(x)$. We compare the matrix representation in Laguerre polynomials with the representation in Maxwell polynomials. We compare the calculation of the matrix elements of the elastic collision frequency with the calculation of the matrix elements of the potential in the Schrödinger equation. The matrix elements of the coordinate operator (Harris et al. 1965; Dickinson and Certain 1968) featured prominently in the development of pseudospectral methods in chemical physics (Light and Carrington Jr. 2000).

3.6.2 Integration Over a Cusp; the Boltzmann Equation

In Chap. 5, we consider the solution of integral equations, in particular the Boltzmann equation, with a kernel $K(x, y)$ defined later. The kernel in this integral equation exhibits a cusp for $x = y$ with a derivative discontinuity at this point. We use a pseudospectral or collocation method (Jerri 1999; Kythe and Puri 2002) to solve the integral equation which requires the integration over the cusp with a chosen quadrature. Other examples of this type of integral equation include Love's integral equation for a circular parallel plate capacitor (Love 1949; Bartlett and Corle 1985; Kumar 2010; Pastore 2011) and a weakly singular Volterra integral equation with sharp gradients reported by Isaacson and Kirby (2011) as well as for quantum mechanical modelling of crystalline solids (Pask et al. 2012). In this section, we consider numerical experiments that involve the integration over the cusp in the kernel for the Boltzmann equation.

We consider a two component system with one component of mass m dilutely dispersed in a second component of mass M which is at equilibrium and at a constant temperature, T_b. The nonequilibrium distribution function, $f(\mathbf{v}, t)$, in the absence of external fields and spatial gradients is given by the linear Boltzmann equation

$$\frac{\partial f(\mathbf{v}, t)}{\partial t} = \int K(\mathbf{u}, \mathbf{v}) f(\mathbf{u}, t) d\mathbf{u} - Z(|\mathbf{v}|) f(\mathbf{v}, t), \qquad (3.46)$$

where $K(\mathbf{u}, \mathbf{v})$ is a kernel that describes the change in the distribution function owing to collisions between the two species (Chapman and Cowling 1970; Kapral and Ross 1970; Ferziger and Kaper 1972; Kharchenko et al. 1997) and is known for arbitrary differential cross section as given explicitly by Eq. (7) in Sospedra-Alfonso and Shizgal (2012). The kernel depends on the mass ratio of the two components defined by $\gamma = M/m$.

The distribution function can be anisotropic and it is often represented as an expansion in Legendre polynomials, that is

$$f(\mathbf{v}, t) = \sum_{\ell=0}^{\infty} f_\ell(v, t) P_\ell(\mu), \qquad (3.47)$$

where $\mu = \cos\theta$ and θ is the angle between $\mathbf{v}$ and the polar axis in velocity space. We consider the relaxation of isotropic and anisotropic distributions in Chap. 5, Sects. 5.6.3 and 5.7.1, respectively. In Chap. 6, Sect. 6.3, we consider the relaxation of electrons in inert gas atoms with the Fokker-Planck equation which is the limiting form of the Boltzmann equation for $\gamma \to \infty$. This mass ratio limit is referred to as the Lorentz limit as discussed in detail later. The other mass ratio limit is the Rayleigh limit, namely $\gamma \to 0$.

If the distribution function of species m is assumed isotropic, only the spherically symmetric component $f_0(v, t)$ in Eq. (3.47) is of concern. In terms of the reduced energies $x = mu^2/2k_B T_b$ and $y = mv^2/2k_B T_b$, respectively, the isotropic distribution satisfies the Boltzmann equation,

$$\frac{\partial f_0(y, t)}{\partial t} = \int_0^\infty k_0(x, y)f_0(x, t)dx - Z(y)f_0(y, t). \tag{3.48}$$

The kernel $k_0(x, y)$ is the spherical component of $K(\mathbf{u}, \mathbf{v})$.

The kernel for the hard sphere differential cross section, $\sigma = d^2/4$, is known as the Wigner[2]-Wilkins[3] kernel and was originally used to describe neutron slowing down (Wigner and Wilkins 1944). The Wigner-Wilkins kernel (Andersen and Shuler 1964; Hoare and Kaplinsky 1970; Hoare 1971) is given by

$$k_{ww}(x, y) = \frac{1}{2}AQ^2\sqrt{\frac{\pi}{x}}\left[\mathrm{erf}(Q\sqrt{y} - R\sqrt{x}) + e^{x-y}\mathrm{erf}(R\sqrt{y} + Q\sqrt{x})\right.$$

$$\left.\pm\left(\mathrm{erf}(Q\sqrt{y} - R\sqrt{x} + e^{x-y}\mathrm{erf}(R\sqrt{y} - Q\sqrt{x}))\right)\right], \tag{3.49}$$

where $A = \pi d^2 n_b \sqrt{k_B T_b/2M}$, $Q = \frac{1}{2}(\gamma^{-1/2} + \gamma^{1/2})$, $R = \frac{1}{2}(\gamma^{-1/2} - \gamma^{1/2})$ and n_b is the density of the background gas of particles of mass M. It is useful to note for later reference that the corresponding kernel for realistic differential cross sections is known and involves two integrations over the scattering angle and relative energy (Kapral and Ross 1970; Sospedra-Alfonso and Shizgal 2012, 2013).

The steady state solution is the equilibrium Maxwellian distribution in dimensionless energy units, (see Eq. (3.16)), that is

$$\hat{F}(y) = \frac{2}{\sqrt{\pi}}\sqrt{y}e^{-y}.$$

There are two important physical principles that yield the dependence of the collision frequency, $Z(y)$, versus the reduced energy, y, originally defined by Eq. (3.36).

---

[2] Eugene Paul Wigner (1902–1995), was an Hungarian American theoretical physicist and mathematician who was awarded the Nobel Prize in Physics in 1963 for his fundamental work on the quantum mechanics of elementary particles and symmetries.

[3] Jesse Ernest Wilkins, Jr. (1923–2011) was an African American nuclear physicist and mathematician who contributed to the Manhattan project and nuclear fission reactions.

The first is conservation of number density so that the integral of Eq. (3.48) gives zero that is, $\partial/\partial t[\int_0^\infty f_0(y, t)\sqrt{y}dy] = 0$, as $f_0(y, t)$ is normalized to unity, and we have that,

$$Z(y) = \int_0^\infty k_0(y, x)dx. \qquad (3.50)$$

The second principle is the detailed balance condition at equilibrium (Hoare and Kaplinsky 1970) so that $\partial f_0/\partial t = 0$ for $f_0 = \hat{F}$, that is,

$$Z(y) = \frac{1}{\hat{F}(y)} \int_0^\infty k_0(x, y)\hat{F}(x)dx. \qquad (3.51)$$

The Maxwellian distributions in Eq. (3.51) symmetrize the kernel, that is

$$G_0(x, y) = \frac{\hat{F}(x)}{\hat{F}(y)} k_0(x, y) = G_0(y, x). \qquad (3.52)$$

The Wigner-Wilkins kernel for the special case of equal masses, $\gamma = 1$, is

$$k_{ww}(x, y) = \frac{1}{2}AQ^2\sqrt{\frac{\pi}{x}}\mathrm{erf}(\sqrt{y}), \quad y < x,$$

$$= \frac{1}{2}AQ^2\sqrt{\frac{\pi}{x}}e^{x-y}\mathrm{erf}(\sqrt{x}), \quad y > x. \qquad (3.53)$$

The three dimensional plot of the symmetrized Wigner-Wilkins kernel for $\gamma = 1$ is shown in Fig. 3.12 (top left graph). The variation of $G(x, y_0)$ versus x for $y_0 = 1, 2, 3, 4$ and 5 for $\gamma = 0.0001, 1$ and $1,000$ is shown in the other three graphs. For $\gamma = 1$, the kernel versus x for each y_0 is much wider than the very narrow cusps for the two disparate mass ratios on the right hand graphs.

It is clear that the kernel is sharply peaked at the disparate mass limits, which are referred to as the Lorentz and Rayleigh limits as discussed previously. This is a result of the small energy transfers in a collision between particles of very different mass. This property of the kernel concerning velocity changing collisions has been reported frequently in the literature (Shizgal and Lindenfeld 1979; Liao et al. 1980; Berman et al. 1986; Rogers and Berman 1991; Gibble and Gallagher 1991; Shapiro 2000; Belai et al. 2007; McGuyer et al. 2012) and impacts on many applications and on Doppler spectroscopy in particular. Examples of a similar localized nature of the kernel in the Boltzmann equation for realistic cross sections are shown in Fig. 4 of Bovino et al. (2011) and Fig. 5 of Zhang et al. (2007).

Our interest in this section is the calculation of the collision frequency with Eq. (3.51). It is clear that in the disparate mass limits a single quadrature for all values of y_0 would be inefficient if the integration algorithm does not take into account the position and width of the cusp over a small interval $[x_{min}, x_{max}]$.
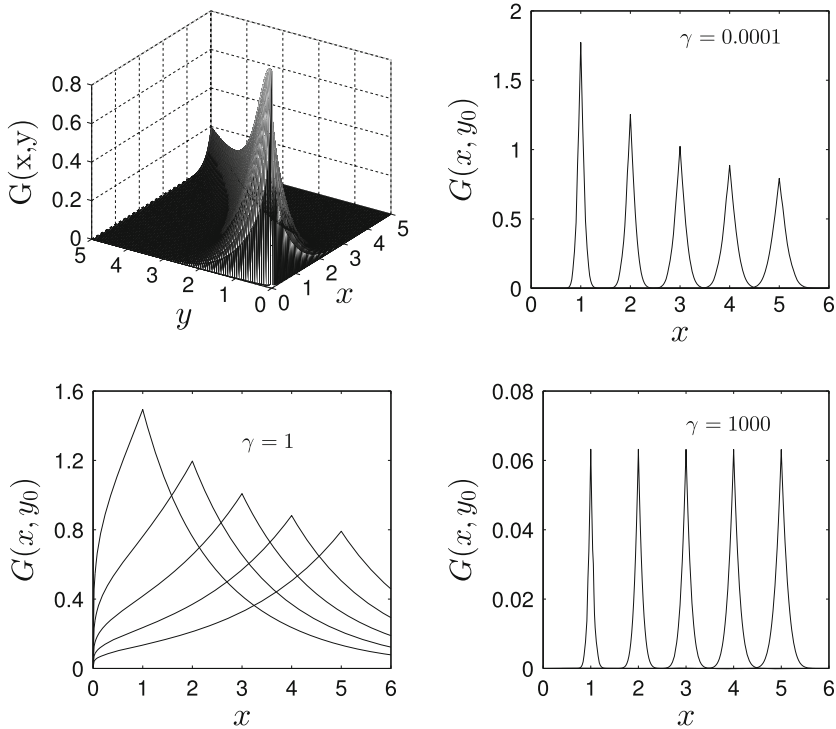
Fig. 3.12 (*Upper left panel*) The three dimensional surface of the Wigner-Wilkins kernel, Eq. (3.53) for equal masses, $\gamma = 1$. Variation of the kernel for fixed argument, $y_0 = 1, 2, 3, 4$ and 5 versus x for $\gamma = 0.0001$, 1 and 1,000

We consider the extreme mass ratio $\gamma = 1,000$, shown in Fig. 3.12 and choose a Simpson rule quadrature to evaluate the integral. In view of the localized nature of the kernel, we consider a narrow interval that brackets the cusp at y_0.

In Fig. 3.13(A), we show for $\gamma = 100$, $y_0 = 1$, the variation of the relative error with a Simpson rule algorithm versus the number of grid points, N, $x_{min} = 0$ and different values of x_{max}. The grid spacing is the same for all x_{max} and as expected the number of integration points required to achieve convergence decreases with x_{max}. The initial decrease in the relative error is rapid for small values of N for all values of x_{max}. In spite of the localized nature of the kernel, the interval has to be sufficiently wide to capture the "tails" on either side of the cusp.

In Fig. 3.13(B), we show for $y_0 = 5$ the variation of the relative error versus the number of grid points, N, for different values of x_{max} with $x_{min} = 0$ (dashed curves) and $x_{min} = 3$ (solid curves). The smaller interval about $y_0 = 5$ gives the more rapid convergence as expected with also a rapid convergence even for small values of N. For all the results shown in Fig. 3.13 there is a grid point at the cusp. The grid spacing, h, is varied as given by $h = 1/m$, and m varies from 10 to 400 in increments of 10. These aspects of the integration over the kernel are important with regard the
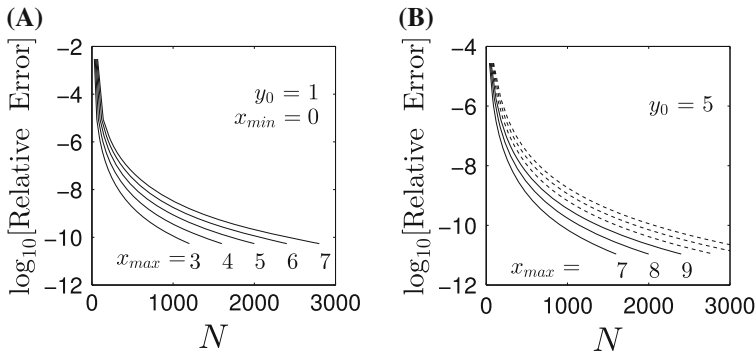
Fig. 3.13 Variation of $\log_{10}$[relative error] for the Simpson rule integration of the symmetrized Wigner-Wilkins kernel $G_0(x, y_0)$, Eq. (3.52) for $\gamma = 1{,}000$. (**A**) $y_0 = 1$; integration is over the interval $x \in [0, x_{max}]$; (**B**) $y_0 = 5$; integration is over the interval $x \in [3, x_{max}]$ (*solid curve*) and $x \in [0, x_{max}]$ (*dashed curve*). In each case, the grid spacing is given by $h = 1/m$ with $m = [10:10:400]$

solution of the time dependent Boltzmann equation, Eq. (3.48), discussed in Chap. 5. However, the choice $\gamma = 1{,}000$ is extreme.

We compare further the results just discussed with integrations that divide the integration interval into two subintervals $x \in [0, y_0]$ and $x \in [y_0, x_{max}]$. We use a Simpson rule integration in both subdomains as well as a Legendre quadrature for each subdomain with the appropriate change of variable. The results for the Simpson rule integration are shown in Fig. 3.14(A) for $y_0 = 1$ (solid curves) and the two intervals [0, 3] and [0, 2] with convergence faster for the smaller interval. The results
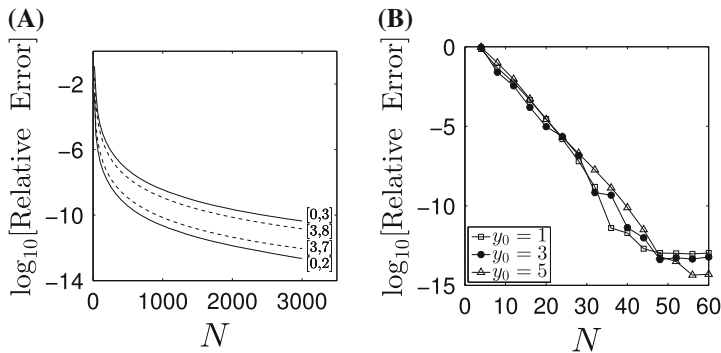
Fig. 3.14 Variation of $\log_{10}$[relative error] for the integration of the symmetrized Wigner-Wilkins kernel $G_0(x, y_0)$, Eq. (3.52) for $\gamma = 1{,}000$. (**A**) Simpson rule integration with $N/2+1$ points in each of the intervals [0, y_0] and [y_0, x_{max}] for $y_0 = 1$ (*solid curves*) and $y_0 = 5$ (*dashed curves*). The intervals used are shown next to the curves. (**B**) Legendre quadrature integration over the intervals [x_{min}, y_0] and [y_0, x_{max}] for $y_0 = 1$, 3 and 5 with $N/2$ points in the intervals [0, 2], [2, 5] and [3, 8], respectively, that bracket y_0

for $y_0 = 5$ (dashed curves) are very similar with the smaller interval providing faster convergence. We notice an initial rapid convergence versus N with a small number of quadrature points as also shown in Fig. 3.13. By contrast with Fig. 3.13, there are $N/2$ points in each interval and many more points between the origin and y_0. Also the grid spacing changes with N as given by $h = 1/m$ with m chosen as before.

In Fig. 3.14(B), the results the Gauss-Legendre quadrature in the two intervals $[x_{min}, y_0]$ and $[y_0, x_{max}]$ with $N/2$ quadrature points in each interval are shown. It is very clear that the Gauss-Legendre quadrature is far superior to the Simpson rule algorithm with results similar for all y_0 provided that the integration domain brackets the cusp. A similar comparison of Simpson and trapezoidal rules for integrations over a cusp were discussed by Secrest and Johnson (1966) in their modelling of atom-diatomic collisional energy transfer.

We consider the Gauss-Maxwell quadrature with $w(x) = x^2 e^{-x^2}$ where $x = \sqrt{mv^2/2k_B T_b}$ is the reduced speed rather than the reduced energy. We calculate $Z(x_i)$ where x_i is the ith quadrature point of the quadrature of order N. This approach does not take into account the cusp in the kernel and we cannot expect the convergence to yield the very small relative errors as in Figs. 3.13 and 3.14. The collision frequency at each x_i calculated with the same set of $N = 80$ quadrature points is shown in Fig. 3.15. The best agreement between the exact and numerical collision frequencies is for mass ratio unity. The departures for the larger and smaller mass ratios arise from the more narrow cusp. The errors are largest for the larger quadrature points as a small number of quadrature points are distributed to the right of the cusp. The calculation of $Z(x_{80} = 14.012)$ does not include the contributions beyond x_{80}. However, this is precisely the approach used, with this or other quadratures, to reduce the integral equation, Eq. (3.46) to a set of coupled ordinary differential equations as discussed further in Chap. 5.
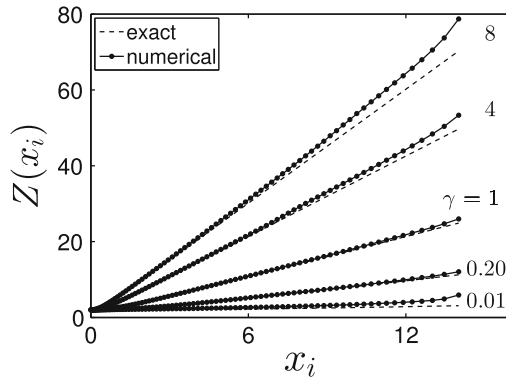
Fig. 3.15 Comparison of the exact hard sphere collision frequency, $Z(x)$ (*dashed curves*) in units of $\pi d^2 \sqrt{k_B T_b/2m}$, Eq. (3.45), with the numerical integration (*solid curves*) of the Wigner-Wilkins kernel with the Gauss-Maxwell quadrature ($p = 2, N = 80$) for several mass ratios. The symbols show each of the 80 quadrature points and $x = \sqrt{mv^2/2k_B T_b}$ is the reduced speed

3.6.3　Viscosity of a Simple Gas

The Chapman-Enskog method of solution of the Boltzmann equation for a one component gas discussed in Chap. 5 is the basis for the calculation of the transport coefficients (Hirschfelder et al. 1954; Huang 1967; Chapman and Cowling 1970; Ferziger and Kaper 1972). For the calculation of the viscosity, the method assumes a small departure of the velocity distribution function from a Maxwellian owing to a small velocity gradient. This perturbation of the distribution function is given by the solution of the linearized Boltzmann equation, Eq. (5.45). The integral collision operator in the Boltzmann equation is defined by the differential scattering cross section for binary collisions of the gaseous particles. We assume that the particle collisions are described by a hard sphere cross section and the integral Boltzmann equation is then given by Eq. (5.88).

The shear viscosity of a simple gas in reduced units is given by

$$\nu = \frac{16\sqrt{2}}{15} \int_{0}^{\infty} e^{-x^2} x^4 B(x) dx, \tag{3.54}$$

as defined in recent publications (Siewert 2002; Sharipov and Bertoldo 2009). We direct our attention to the numerical integration of the integral in Eq. (3.54) given the function $B(x)$ which is determined with the solution of the Boltzmann equation for viscosity (Loyalka et al. 2007).

Loyalka et al. (2007) employed an expansion of the distribution function in the Laguerre (or Sonine) polynomials and used *Mathematica* to algebraically obtain extremely accurate converged solutions to the Boltzmann equation with up to 150 terms and provided the function $B(x)$ in Table 5 of their paper. This is essentially the Galerkin solution of the integral equation. Their work serves as an excellent benchmark and they report the viscosity to 34 significant figures, that is $\nu = 0.44902780628789243460904948953346545$.

We use a spline fit of $B(x)$ from the data provided in Table 5 of Loyalka et al. (2007) which has 44 data points for $x \in [0, 6]$. The values of $B(x)$ are available only up to $x = 6$, but beyond this point the integrand is less than 10^{-15}. With the weight factor $w(x) = x^2 \exp(-x^2)$ in the integrand, it would appear that an optimal quadrature is the one based on the Maxwell polynomials with $p = 2$.

Thus we consider the integral in Eq. (3.54) with the quadratures based on the Maxwell and Laguerre polynomials and we also include a Simpson's rule for comparison. In this case since the data for $B(x)$ is limited up to $x_{max} = 6$ the Simpson's rule is defined on the interval [0, 6]. Also, for the higher order quadratures, the Laguerre quadrature points can be greater than 6^2 so that these have to be scaled as in Eq. (3.3) such that the last point is at $y = 36$ which occurs for $N > 10$. The quadrature point x_N for the Maxwell quadrature and y_N for the Laguerre quadratures for orders $N = 3$ to 10 are compared in Table 3.9. The Laguerre quadrature points are far more diffuse in reduced energy than the Maxwell quadrature in reduced speed for the same N. A similar comparison was shown in Chap. 2.

Table 3.9 The quadrature points, x_N and y_N, for the listed Nth order Gaussian quadratures

N	3	4	5	6	7	8	9	10
Maxwell ($p = 2$)	x_N	2.220	2.640	3.014	3.356	3.671	3.967	4.245	4.509
Laguerre ($\alpha = 3/2$)	y_N	8.471	11.71	15.05	18.46	21.92	25.43	28.98	32.55

The Laguerre quadrature points are far more diffuse than the Maxwell quadrature points with the same N
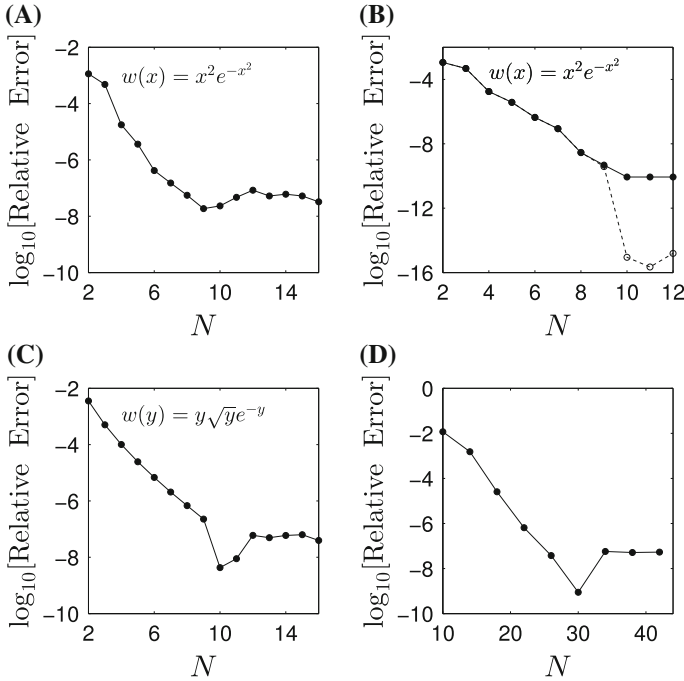
Fig. 3.16 Convergence of the integral for the viscosity of a simple hard sphere gas, Eq. (3.54).
(**A**) Gauss-Maxwell quadrature with spline fit to the data in Table 5 of Loyalka et al. (2007); (**B**)
Gauss-Maxwell quadrature with a 16th order polynomial fit to the data in Table 5 of Loyalka et al.
(2007); *dashed curve* uses the "exact" value with the polynomial fit; (**C**) Gauss-Laguerre quadrature
($\alpha = 3/2$); (**D**) Simpson's rule

A comparison of the convergence of the viscosity, given by Eq. (3.54) versus
the number of quadrature points for these three algorithms is shown in Fig. 3.16.
Figure 3.16(A), (B) are the results for Gauss-Maxwell ($p = 2$) with a spline fit of the
data in Table 5 of Loyalka et al. (2007). For the dashed curve in Fig. 3.16(B), the exact
value from the polynomial fit is used so that machine accuracy obtained is expected.
The results with the Gauss-Laguerre quadrature in Fig. 3.16(C) are comparable to
those with the Gauss-Maxwell quadrature above. The moderately rapid convergence
of the relative errors for this integral for all quadratures are anticipated for this very
smooth integrand. In Chap. 5, Sect. 5.4.5, we consider the solution of the Boltzmann
integral equation for $B(x)$ and the calculation of the shear viscosity in comparison
with the spline method of solution used by Siewert (2002).

3.6.4 Eigenvalues of the Boltzmann Collision Operator
for Maxwell Molecules

In the kinetic theory of gases, the model system based on the atom-atom power law repulsive interaction of the form $V_{MM}(r) = \kappa/r^4$, where r is the atom-atom separation, is referred to as "Maxwell molecules" and κ determines the strength of the interaction. The model was introduced by James Clerk Maxwell[4] long ago as reviewed by Santos (2009). This model is of major significance to the history of the kinetic theory of gases. In spite of the nonphysical nature of this repulsive interaction potential, the model has been used over several decades in many applications (St.-Maurice and Schunk 1976, 1979; Hubert 1983; Shizgal and Hubert 1989; Sabbane et al. 2003; Napier and Shizgal 2008; Santos 2009). The attractive potential, $V(r) = -\kappa/r^4$, is a model for the long range ion atom interaction potential that provides an estimate of ion mobilities in neutral gases with solutions of the Boltzmann equation (McDaniel and Mason 1973; Mason and McDaniel 1988).

The eigenfunctions of the linearized one-component Boltzmann collision operator for the repulsive Maxwell molecule interaction are the direct product of the Sonine-Laguerre polynomials and the spherical harmonics. Thus, the Sonine-Laguerre polynomials have become the basis set of choice for kinetic theory problems. The Maxwell molecule model has also been employed in studies of the approach to equilibrium for the non-linear Boltzmann equation (Krook and Wu 1976; Ernst 1981; Bobylev 1984).

For the interparticle potential, $V_{MM}(r)$, the two body classical scattering problem can be solved exactly (Goldstein et al. 2000; Liboff 2003) and the dependence of the differential cross section on the relative speed, g, and scattering angle, θ, is given by

$$\sigma(g, \theta) = 2\sqrt{\frac{\kappa}{m}}\frac{1}{g}I_4(\theta). \tag{3.55}$$

The dependence on the scattering angle is given by

$$I_4(\theta) = -\frac{1}{\sin(\theta)}\frac{d\cot(2\phi)}{d\theta}, \tag{3.56}$$

with the scattering angle θ defined in terms of ϕ

$$\theta = \pi - 2\sqrt{\cos(\phi)}K(\sin^2 \phi), \tag{3.57}$$

where

$$K(\sin^2 \phi) = \int\limits_0^{\pi/2} \frac{1}{[1 - \sin^2 \phi \sin^2 \alpha]}d\alpha, \tag{3.58}$$

is the Elliptic integral.

---

[4] James Clerk Maxwell (1831–1879) was a Scottish mathematical physicist who made a large number of fundamental contributions to electromagnetic theory, kinetic theory and thermodynamics.

It is very important to notice that for this interaction the product $g\sigma(g, \theta)$ is independent of g (see Eq. (3.55)). An important consequence of this model is that the collision frequency $Z(v)$ that occurs in the collision operator in the Boltzmann equation as given by Eq. (3.35) is independent of the particle speed. The collision operator is greatly simplified and the eigenvalue spectrum of the operator is completely discrete.

It can be shown (Ford 1968; Foch and Ford 1970) that the eigenvalues, $\lambda_{n,\ell}$, of the linearized one-component collision operator for this interaction are given explicitly by the integral

$$\lambda_{n,\ell} = -4\pi\sqrt{\frac{\kappa}{m}} \int_0^\pi I_4(\theta)\left[\cos^{2n+\ell}(\frac{\theta}{2})P_\ell[\cos(\frac{\theta}{2})] + \sin^{2n+\ell}(\frac{\theta}{2})P_\ell[\sin(\frac{\theta}{2}) - 1]\right.$$

$$\left. - \delta_{n0}\delta_{\ell,0}\right]\sin\theta d\theta. \tag{3.59}$$

We find it convenient to transform the integration variable from θ to ϕ so that the integral in Eq. (3.59) becomes

$$\lambda_{n,\ell} = 8\pi\sqrt{\frac{\kappa}{m}} \int_0^{\pi/4} \left[\frac{\cos^{2n+\ell}(\frac{\theta}{2})P_\ell[\cos(\frac{\theta}{2})] + \sin^{2n+\ell}(\frac{\theta}{2})P_\ell[\sin(\frac{\theta}{2}) - 1] - \delta_{n0}\delta_{\ell,0}}{\sin^2 2\phi}\right]d\phi, \tag{3.60}$$

and the angle θ is determined from ϕ as given by Eq. (3.57). In Fig. 3.17(A) we show the integrands of Eq. (3.60) versus ϕ for $\lambda_{n,0}$ with $n = 4, 8, 12$ and 16 and likewise in Fig. 3.17(B) we show the integrands for $\lambda_{0,\ell}$ with $\ell = 6, 10, 14$ and 16. There is a rapid variation near $\phi = \pi/4$ shown in Fig. 3.17(B).

We choose a Gauss-Legendre quadrature to calculate $\lambda_{n,\ell}$. The convergence of several eigenvalues versus the number of quadrature points increases with n and ℓ as shown in Tables 3.10 and 3.11. The results in the tables are in agreement with
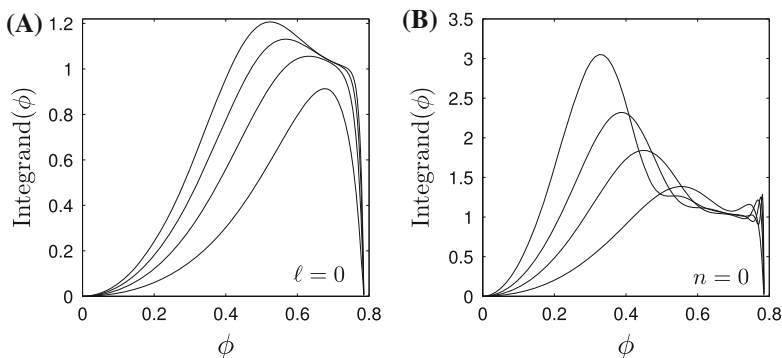
Fig. 3.17 The ϕ variation of the integrand in Eq. (3.60) for the Maxwell molecule eigenvalues, $\lambda_{n,\ell}$. (**A**) $\ell = 0$ and n from top to bottom is 16, 12, 8 and 4. (**B**) $n = 0$ and ℓ from top to bottom is 16, 14, 10 and 6

Table 3.10 Convergence of the Maxwell molecule eigenvalues, $\lambda_{n,0}$ with Gauss-Legendre quadratures

N	$\lambda_{4,0}$	$\lambda_{8,0}$	$\lambda_{12,0}$	$\lambda_{16,0}$
4	7.2473049826	10.6815741779	12.6401640971	13.9560579506
8	7.1404138296	10.3355659392	12.2873384173	13.7368118926
12	7.1402976496	10.3296515433	12.2624669303	13.6902870561
16	7.1402976448	10.3296443968	12.2622077369	13.6886563346
20	7.1402976448	10.3296443951	12.2622072790	13.6886437782
24		10.3296443951	12.2622072788	13.6886437520
32			12.2622072788	13.6886437519
40				13.6886437520

Table 3.11 Convergence of the Maxwell molecule eigenvalues, $\lambda_{0,\ell}$ with Gauss-Legendre quadratures

N	$\lambda_{0,6}$	$\lambda_{0,10}$	$\lambda_{0,14}$	$\lambda_{0,18}$
4	15.0278419641	18.9389440371	21.4348909276	25.4697236812
8	14.2744916100	19.4726281411	23.4800390873	26.5094667009
12	14.2628153767	19.3091338846	23.3459851156	26.8105457092
16	14.2628093775	19.3059204404	23.2863701647	26.7017149499
20	14.2628093771	19.3059159880	23.2852977701	26.6815970246
24		19.3059159869	23.2852954023	26.6812438552
32		19.3059159868	23.2852954009	26.6812426849
40			23.2852954011	26.6812426851
50				26.6812426847

the large number of eigenvalues reported by Alterman et al. (1962) to the significant figures shown and expressed in units of their $A_2 = 9.689818653 \sqrt{\kappa/m}$, that is $\lambda_{02} = 0.6 \times 9.689818653 \sqrt{\kappa/m} = 5.8138911918\sqrt{\kappa/m}$. The authors mention that the integrands in their work were highly oscillatory. They calculated the eigenvalues to 10 significant figures in triple precision with up to 96 Gauss-Legendre quadrature points. The lower order eigenvalues reported recently (Sabbane et al. 2003; Santos 2009) are also in agreement with the results reported here.

3.6.5 The JWKB Phase Shifts and Quantum Elastic Cross Sections

The calculation of the differential and total elastic cross sections for atom-atom collisions with a specified interatomic potential is important for the calculation of transport

coefficients for diffusion, viscosity, heat conduction and ion mobilities (Hirschfelder et al. 1954; Chapman and Cowling 1970; Ferziger and Kaper 1972; Mason and McDaniel 1988; Lemmon and Jacobsen 2004; Danailov et al. 2008; Oh 2013). Other applications include the relaxation to equilibrium of an initial nonequilibrium distribution of energetic atoms by collisional energy transfer (Nan and Houston 1992; Kharchenko and Dalgarno 2004; Zhang et al. 2007; Bovino et al. 2011; Sospedra-Alfonso and Shizgal 2013). Binary collision theory is based on either classical mechanics (Goldstein et al. 2000) or quantum mechanics (Child 1996; Burke 2011).

The quantum mechanical differential elastic cross section for binary collisions between two structureless particles is given in terms of the square of the scattering amplitude, $f(E, \theta)$, which depends on the center-of-mass relative energy, E, and the scattering angle, θ, that is

$$\sigma(E, \theta) = |f(E, \theta)|^2, \tag{3.61}$$

where the scattering amplitude can be expressed in terms of the phase shifts, $\delta_\ell(E)$,

$$f(E, \theta) = \frac{1}{k} \sum_{\ell=0}^{\infty} (2\ell + 1) e^{i\delta_\ell} \sin(\delta_\ell) P_\ell(\cos \theta), \tag{3.62}$$

and $P_\ell(\cos \theta)$ is the Legendre polynomial. In Eq. (3.62), $k = \sqrt{2\mu E / \hbar^2}$ is the wave number and μ is the reduced mass of the colliding pair. The phase shifts can be determined from a solution of the radial Schrödinger equation

$$\frac{1}{r^2} \frac{d}{dr} \left(r^2 \frac{du_{k,\ell}(r)}{dr} \right) + [k^2 - U(r) - \frac{\ell(\ell + 1)}{r^2}] u_{k,\ell}(r) = 0 \tag{3.63}$$

where $U(r) = 2\mu V(r)/\hbar^2$, $k^2 = 2\mu E/\hbar^2$ and the interaction potential is $V(r)$, where r is the distance between the pair of particles considered. The Schrödinger equation is solved for the continuum scattering states with $E > 0$ and the asymptotic boundary condition on the radial wavefunction is

$$u_{k,\ell}(r) \underset{r \to \infty}{\sim} r \frac{\sin(kr - \ell\pi/2 - \delta_\ell)}{kr}, \tag{3.64}$$

which defines the phase shift δ_ℓ. A more detailed discussion of the theoretical approach can be found in several references (Bernstein 1966; Child 1996; Burke 2011; Taylor 2012).

With the scattering amplitude expressed as in Eq. (3.62), the total cross section is given by

$$\sigma_{total}(E) = 2\pi \int_0^\pi \sigma(E, \theta) \sin \theta d\theta = \frac{4\pi}{k^2} \sum_{\ell=0}^{\infty} (2\ell + 1) \sin^2 \delta_\ell(k). \tag{3.65}$$

For heavy particle collisions at high relative energies, many phase shifts contribute to the total cross section, Eq. (3.65), and the time consuming numerical integration

of the radial Shrödinger equation is not necessary in many situations. The Jeffreys-Wentzel-Kramers-Brillouin (JWKB) phase shift (Child 1996; Burke 2011) given by

$$
\delta_\ell = \int_{r_0}^{\infty} \sqrt{\left[k^2 - \frac{(\ell + \frac{1}{2})^2}{r^2} - U(r) \right]} dr - \int_{r_1}^{\infty} \sqrt{k^2 - \frac{(\ell + \frac{1}{2})}{r^2}} dr, \qquad (3.66)
$$

provides a very good approximation. In Eq. (3.66), r_0 is the classical turning point given by the root of the square bracket term in the first integral. Analogously, $r_1 = \sqrt{(\ell + \frac{1}{2})^2/k^2}$ and we have made the familiar Langer modification (Langer 1937) by replacing $\ell(\ell + 1)$ with $(\ell + \frac{1}{2})^2$.

With this very brief overview of semiclassical scattering theory, we now direct attention to our main concern here, namely the numerical evaluation of the phase shift as defined by Eq. (3.66). As with the previous applications discussed in this chapter, the nature of the integrand dictates the choice of numerical quadrature. In this application, it is important to notice that the integral depends on the choice for the potential, $V(r)$, the relative energy as given by k^2, the value of ℓ and the classical turning point, r_0.

We choose the diatom O-H which is important in the estimation of the escape of atomic species from planetary atmospheres (Shizgal 1999; Balakrishnan and Dalgarno 2003; Kharchenko and Dalgarno 2004; Jamieson et al. 2006) and in other applications (Wright and Donaldson 1985; Oneal and Neff 1997). The interaction potentials and collision dynamics were reported in detail in these references. For the purpose of the numerical comparisons presented here it is sufficient to choose the ground $X^2\Pi$ state of OH to be the Morse potential reported by Wright and Donaldson (1985) and given by

$$
V(r) = D_e \left[1 - e^{-\beta(r-r_e)} \right]^2, \qquad (3.67)
$$

where $r_e = 1.821$ au, $D_e = 5.426$ eV and $\beta = 1.189 \, (\text{au})^{-1}$ where $1\text{au} = 0.52917 \, \text{Å}$ and $1 \, \text{Å} = 10^{-8}$ cm. In Chap. 6, we will also consider the bound vibrational states of such diatomic molecules modelled with the Morse potential. There are many other choices for the interatomic potentials including a Lennard-Jones potential (Sospedra-Alfonso and Shizgal 2013) as well the results of quantum mechanical calculations of the electronic structure (Jamieson et al. 2006) for which the potential is often available in tabular rather than in analytic form (Shizgal 1999).

The methods that have been proposed to evaluate the integral in Eq. (3.66) include a modified Clenshaw-Curtis quadrature (Kennedy and Smith 1967), a Gauss-Mehler quadrature (Pack 1974), a Gauss-Legendre quadrature and a non-classical quadrature proposed by Cohen (1978) based on the weight function $w(x) = 1/\sqrt{1-x} \quad x \in [0, 1]$ (see Item 25.4.36 in Abramowitz and Stegun (1964)) with quadrature points and weights related to the Gauss-Legendre quadrature.

A comparison of the Gauss-Legendre and Gauss-Mehler quadratures in the numerical evaluation the integrals for δ_ℓ is presented. It is of interest to note that the use of the

Clenshaw-Curtis quadrature in this application resulted in a study of the convergence properties by O'Hara and Smith (1968) and later by Trefethen (2008).

A detailed comparison of different quadratures is made challenging owing to the variation of the integrand in Eq. (3.66) versus x that depends on the interaction potential, $V(r)$, the energy E and the value of ℓ. Except for the case of short ranged nuclear interactions, a moderately large number of partial waves must be calculated in order to get a converged cross section. Such cross sections for a variety of binary atomic pairs are used in several studies of the approach to equilibrium based on the Boltzmann equation (Bovino et al. 2009, 2011; Sospedra-Alfonso and Shizgal 2013) that we consider in detail in Chap. 5. There are also practical applications concerning gaseous transport properties (Oh 2013; Lemmon and Jacobsen 2004) as well for ion mobilities in gases (Mason and McDaniel 1988; Viehland 1994; Danailov et al. 2008).

The first step in the evaluation of the integral for the phase shift is the determination of the classical turning point which can be done with a simple search to bracket the root and then with a Newton-Raphson iteration to converge to the root. We show in Fig. 3.18 the variation of the "effective" potential, $V_{eff}(r) = V(r) + (\ell + \frac{1}{2})/r^2$ versus r for four values of ℓ at $E = 1.0\,\text{eV}$. For the two lowest ℓ values there is one innermost turning point whereas for $\ell = 60$ there are three turning points and for $\ell = 62$ there is one outermost turning point. We here only consider the one outermost turning point but there is an error introduced (Munn et al. 1964; Viehland and Chang 2010) which is related to the classical orbiting problem when the relative energy is close to the top of the centrifugal barrier depicted by the maximum in $V_{eff}(r)$ in Fig. 3.18.

We make the change of variable $x = r_0/r$ and recognize the classical impact parameter with $b = (\ell + \frac{1}{2})/k$. A very important connection between the semiclassical theory and the classical approach is the relationship between the variation of δ_ℓ versus ℓ and the scattering angle, $\chi(b)$ versus b, given by $\chi(b) = 2\partial\delta_\ell/\partial\ell$ (Child 1996; Viehland and Chang 2010). The phase shift in the new integration variable
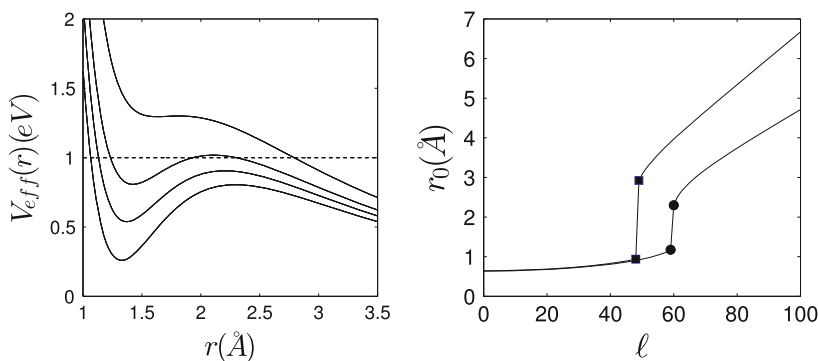
Fig. 3.18   (*Left hand side*) The effective potential $V_{eff}(r) = V(r) + \frac{(\ell+1/2)^2}{r^2}$ where $\ell = 56, 58, 60$ and 62 from bottom to top curves with $E = 1.0\,\text{eV}$ as the *dashed line*. The three turning points are clearly seen for $\ell = 60$. (*Right hand side*) The classical turning points, r_0 versus ℓ, for $E = 0.5\,\text{eV}$ (*square symbols*) and for $E = 1.0\,\text{eV}$. The symbols show the change in the classical turning from the innermost root to the outermost root

appropriate for Gauss-Legendre (GL) quadratures is given by,

$$\delta_\ell^{(GL)} = kr_0 \int\limits_0^1 I_\ell^{(GL)}(x)dx + \frac{\pi[(\ell + \frac{1}{2}) - kr_0]}{2}, \tag{3.68}$$

where

$$I_\ell^{(GL)}(x) = \left[\sqrt{1 - \frac{(\ell + \frac{1}{2})x^2}{kr_0} - \frac{U(r_0/x)}{k^2}} - \sqrt{1 - x^2} \right] \frac{1}{x^2}. \tag{3.69}$$

Pack (1974) suggested the use of a Gauss-Mehler quadrature which is a Chebyshev quadrature $(w(x) = 1/\sqrt{1 - x^2})$ with only the positive quadrature points. The Gauss-Mehler quadrature points and weights are given by

$$x_i = \cos(\frac{i\pi}{2N + 1}), \quad i = 1, \dots N$$

$$w_i = \frac{(1 - x_i^2)\pi}{2N + 1}. \tag{3.70}$$

The algorithm is applied to the integral

$$\delta_\ell^{(GM)} = kr_0 \int\limits_0^1 \frac{1}{\sqrt{1 - x^2}} I_\ell^{(GM)}(x)dx + \frac{\pi[(\ell + \frac{1}{2}) - kr_0]}{2}, \tag{3.71}$$

where

$$I_\ell^{(GM)}(x) = (1 - x^2) \left[\sqrt{1 - \frac{(\ell + \frac{1}{2})x^2}{kr_0} - \frac{U(r_0/x)}{k^2}} - 1 \right] \frac{1}{x^2}. \tag{3.72}$$

It is readily shown that the derivative of the integrand is singular at $x = 1$.

   The phase shifts for a range of energies and ℓ values were determined from the integral in Eq. (3.68) with a Gauss-Legendre quadrature. It is instructive to first show the energy dependence of the total cross section in Fig. 3.19(A). The actual value of the cross section is somewhat larger than previously reported for more realistic potentials for OH (Wright and Donaldson 1985; Shizgal 1999; Bovino et al. 2009, 2011). The differential cross section for $E = 0.5$ eV is shown in Fig. 3.19(B). The number of phase shifts required to get convergence of the cross sections increases with E and for the energy range shown in the figure up to 400 phase shifts were required. Thus a large number of phases shifts are required for the results shown in Fig. 3.19.

   The details of the integrand in Eq. (3.68) vary considerably with E and ℓ and of course the choice of the potential. We choose two energies, $E = 0.5$ and 1.0 eV and four ℓ values as shown in Fig. 3.20.
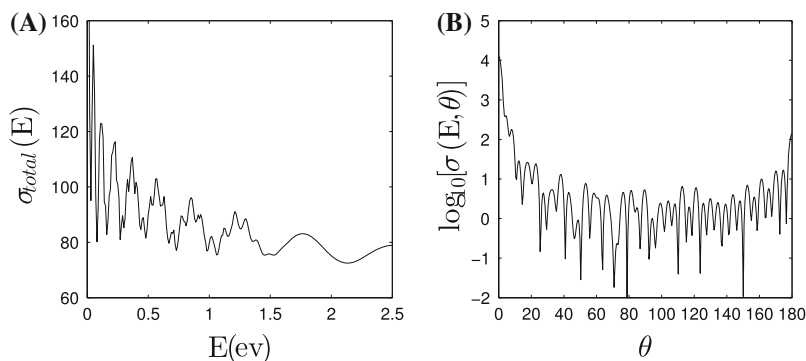
Fig. 3.19 (**A**) The total cross section in Å^2 versus relative energy, E, for O-H; (**B**) The differential cross section in Å^2 versus scattering angle for $E = 0.5\,\text{eV}$
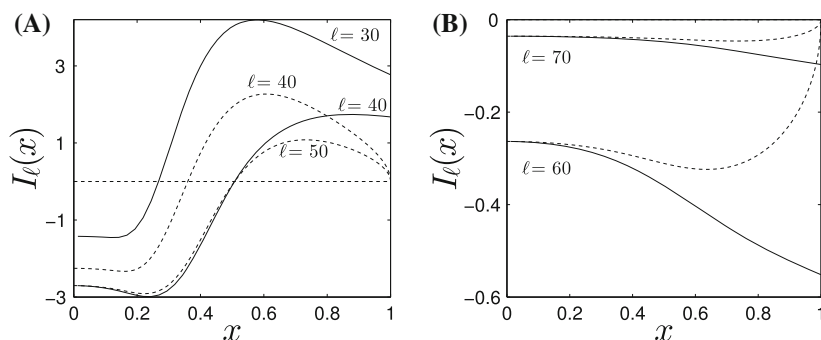
Fig. 3.20 The integrand, $I_\ell(x)$ for $E = 1.0\,\text{eV}$ for Gauss-Legendre quadrature (*dashed line*), Eq. (3.69), and Gauss-Mehler quadrature (*solid line*), Eq. (3.72)

Table 3.12 Convergence of the Gauss-Legendre evaluation of the JWKB phase shifts, Eq. (3.66), versus the number of quadrature points, N, at two energies

N	$E = 0.5\,\text{eV}$			$E = 1.0\,\text{eV}$		
	$\ell = 20$	$\ell = 50$	$\ell = 80$	$\ell = 20$	$\ell = 50$	$\ell = 80$
20	49.72877	1.73645	0.017339	41.81695	32.97958	0.37106
40	49.72806	1.73663	0.017342	41.81610	32.97880	0.36994
60	49.72799	1.73665	0.017342	41.81601	32.97871	0.36982
80	49.72797	1.73666		41.81599	32.97869	0.36979
100				41.81598	32.97868	0.36978

The convergence of the phase shifts with the Gauss-Legendre and Gauss-Mehler quadratures are shown in Tables 3.12 and 3.13, respectively. It is clear that the Gauss-Mehler quadrature outperforms the Gauss-Legendre quadrature. The convergence of the smaller phase shifts for the larger ℓ values is faster than for the larger phase

Table 3.13 Convergence of the Gauss-Mehler evaluation of the JWKB phase shifts, δ_ℓ, Eq. (3.66), versus the number of quadrature points, N, at two energies

N	$E = 0.5\,\mathrm{eV}$			$E = 1.0\,\mathrm{eV}$		
	$\ell = 20$	$\ell = 50$	$\ell = 80$	$\ell = 20$	$\ell = 50$	$\ell = 80$
6	49.72877	1.73645	0.017339	42.21144	32.94304	0.36977
8	49.72806	1.73663	0.017342	42.01845	32.97914	0.36977
12	49.72799	1.73665	0.017342	41.79747	32.97949	
16	49.72797	1.73666		41.81488	32.97895	
20				41.81665	32.97864	
30				41.81595	32.97868	
40				41.81597		

shifts for smaller ℓ values. The reason would appear to be the slower variation of the integrands for the Gauss-Mehler quadrature than for the Gauss-Legendre quadrature as seen in Fig. 3.20. This type of analysis was not considered in the review of the different quadratures by Cohen (1978). A more detailed comparison of the different quadrature procedures and for different potential forms would be useful.

It is important to point out that the numerical calculation of the total cross section with Eq. (3.65) as the integral of the differential cross section shown in Fig. 3.19 would require a very fine grid of points in order to capture the detailed structure. In this case a Simpson's rule would be the method of choice or an adaptive quadrature with subdivision of the domain. This is also the case for the calculation of the elastic collision frequency, Eq. (3.36) with the total cross section also shown in Fig. 3.19 in order to capture the detailed oscillations that occur.

3.7 The Calculation of Matrix Elements of Multiplicative Operators

The collision operator in the Boltzmann equation, Eq. (3.48), is the difference of the integral collision operator and the elastic collision frequency, $Z(y)$, defined by Eq. (3.50). The eigenvalue spectrum of the collision operator has in general a discrete set of eigenvalues as well as a continuum. Similarly, the Hamiltonian for a quantum problem can have bound states of negative energy (discrete eigenvalues) as well as scattering states of positive energy (continuum states). These eigenvalue spectra can be modelled approximately from the matrix representatives of the respective operators in suitable basis sets as discussed in the sections that follow.

In Chap. 1, we outlined the spectral Galerkin solution of differential and/or integral equations based on the method of weighted residuals (Finlayson and Scriven 1966; Finlayson 1972). The Boltzmann or Fokker-Planck equation for a spatially uniform

system in the absence of external forces is the time dependent equation of the form

$$\frac{\partial f(x, t)}{\partial t} = Lf(x, t) \quad x \in [a, b], \tag{3.73}$$

where L is a linear self-adjoint operator and an initial condition, $f(x, 0) = g(x)$, is specified.

An approximate solution is given by the finite expansion in a set of orthonormal basis functions $P_n(x)$ where $P_n(x)$ are classical or nonclassical polynomials and $\int_a^b w(x)P_n(x)P_m(x)dx = \delta_{nm}$. We thus have the Nth order approximation to $f(x, t)$,

$$f^{(N)}(x, t) = \sum_{n=0}^{N-1} c_n(t)P_n(x). \tag{3.74}$$

The initial values, $c_n(0)$, are provided by the expansion of the initial condition, that is,

$$g(x) = \sum_{n=0}^{N-1} c_n(0)P_n(x). \tag{3.75}$$

The departure of the approximate solution from the actual solution is measured by the "residue" defined by

$$R_N(x, t) = \frac{\partial f^{(N)}(x, t)}{\partial t} - Lf^{(N)}(x, t),$$

$$= \sum_{n=0}^{N-1} P_n(x)\frac{dc_n(t)}{dt} - \sum_{n=0}^{N-1} c_n(t)LP_n(x). \tag{3.76}$$

The method of weighted residuals (Finlayson and Scriven 1966; Finlayson 1972; Shen et al. 2011) is a procedure to calculate $c_n(t)$ so as to minimize the residual $R_N(x, t)$ in some average way. We impose the condition that the residue is minimized subject to

$$\int_a^b t(x)R_N(x, t)dx = 0, \tag{3.77}$$

where we choose the "test function" as $t(x) = w(x)P_m(x)$, $m = 0, 1, \ldots$ $(N-1)$. The partial differential equation is approximated by the set of $N-1$ coupled ordinary differential equations with the Galerkin procedure, that is,

$$\frac{dc_m(t)}{dt} = \sum_{n=0}^{N-1} L_{mn}c_n(t) \quad m = 0, 1, \ldots, N-1, \tag{3.78}$$

where

$$L_{mn} = \int_a^b w(x)P_m(x)LP_n(x)dx, \tag{3.79}$$

is the matrix representative of the operator L in spectral space. An important consideration is the condition number of the matrix L_{mn} which determines the stability of the linear set of equations, Eq. (3.78), and their numerical time integration. The preceding discussion follows closely the presentation in Sect. 1.3.

The Nth order transformation from spectral space, c_n, to physical space, $f_i \equiv f(x_i)$, is given by

$$f_i = \sum_{n=0}^{N-1} T_{in}^{(N)} c_n. \tag{3.80}$$

The transformation matrix is defined by

$$T_{ni}^{(N)} = \sqrt{w_i}P_n(x_i) \quad i = 1, 2, \ldots N; \quad n = 0, 1, \ldots (N-1) \tag{3.81}$$

and is symmetric at all orders N, that is

$$\left(\mathbf{T}^{(N)}\right)^t \cdot \mathbf{T}^{(N)} = \mathbf{I}^{(N)}, \tag{3.82}$$

where ^{t} denotes the transpose of the real matrix of order N. Equation (3.82) written in component form is

$$\sum_{n=0}^{N-1} T_{in}^{(N)} T_{nj}^{(N)} = \sqrt{w_i w_j} \sum_{n=0}^{N-1} P_n(x_i)P_n(x_j)$$

$$= \sqrt{w_i w_j} \frac{\delta_{ij}}{\sqrt{w_i w_j}}$$

$$= \delta_{ij}. \tag{3.83}$$

which is exact to any order N. This is a direct consequence of the cardinality condition for the underlying interpolation at any order N.

In the following sections, we direct our attention to the calculation of the matrix elements of multiplicative operators denoted by $G(x)$. The matrix representative in some basis set is

$$G_{mn} = \int_a^b w(x)P_m(x)G(x)P_n(x)dx. \tag{3.84}$$

If this is approximated with the quadrature associated with the basis functions $P_n(x)$, then the Nth order approximation is

$$G_{mn}^{(N)} = \sum_{k=1}^N w_k P_m(x_k)G(x_k)P_n(x_k). \tag{3.85}$$

What is remarkable is that if we transform this (approximate) spectral space representation, $G_{nm}^{(N)}$, to the discrete space, G_{ij}, we have that

$$
\begin{aligned}
G_{ij} &= \sum_{n=0}^{N-1} \sum_{m=0}^{N-1} T_{in} G_{nm}^{(N)} T_{mj}, \\
&= \sum_{n=0}^{N-1} \sum_{m=0}^{N-1} \sqrt{w_i} P_n(x_i) \left[\sum_{k=1}^{N} w_k P_m(x_k) G(x_k) P_n(x_k) \right] \sqrt{w_j} P_m(x_j), \\
&= \sqrt{w_i w_j} \sum_{k=1}^{N} w_k G(x_k) [\sum_{n=0}^{N-1} P_n(x_j) P_n(x_k)] [\sum_{m=0}^{N-1} P_m(x_i) P_m(x_k)], \\
&= \sqrt{w_i w_j} \sum_{k=1}^{N} w_k G(x_k) \frac{\delta_{jk}}{\sqrt{w_j w_k}} \frac{\delta_{ik}}{\sqrt{w_i w_k}}, \\
&= G(x_i) \delta_{ij},
\end{aligned}
\tag{3.86}
$$

where the definition of T_{in} was used in the 2nd line and the "finite completeness" of the basis set in the 3rd line. The transform of the exact G_{nm} matrix elements would not give a diagonal physical space representation of the multiplicative operator as we demonstrate later.

For the Schrödinger equation, the multiplicative operator of interest is the potential, $V(x)$, in a one-dimensional Hamiltonian. The approximate calculation of the matrix elements of the potential function with a quadrature has served as the basis in chemical physics (Harris et al. 1965; Dickinson and Certain 1968) for the development of a pseudospectral or collocation solution of the Schrödinger equation (Light et al. 1985; Light and Carrington Jr. 2000) referred to as the Discrete Variable Representation (DVR).

An analogous procedure was developed by Shizgal (1981) and Shizgal and Blackmore (1984) for the Boltzmann equation and later applied to the Fokker-Planck and the Schrödinger equations (Shizgal and Chen 1996, 1997; Lo and Shizgal 2006, 2008). There is also the analogous Lagrange mesh method developed by Baye (1994, 2006) and coworkers (Baye and Heenen 1986; Baye et al. 2002). These methods of solution of the Schrödinger equation are studied in detail in Chap. 6. The objective in this section is to demonstrate the relationship of the spectral representation of multiplicative operators in an orthonormal basis set evaluated by quadrature and the physical space representation as described in Eq. (3.85).

For the Boltzmann equation the multiplicative operator is the collision frequency,

$$
Z_{nm} = \frac{2}{\sqrt{\pi}} \int_0^\infty w(y) P_n(y) Z(y) P_m(y) dy,
\tag{3.87}
$$

which depends on the mass ratio, $\gamma = M/m$. We will compare these calculations with similar calculations for the matrix elements of the potential in the Schrödinger equation of the form

$$V_{nm} = \int_0^\infty w(x)Q_n(x)V(x)Q_m(x)dx, \tag{3.88}$$

where $Q_n(x)$ are "appropriate" orthonormal basis functions. It should be clear that the choice of basis functions in different applications is crucial so as to get the "best" approximation to the operators. In Sect. 3.7.2, we consider the analogous calculation of the matrix elements of the potential in the Schrödinger equation for the quantum harmonic oscillator. It is the quadrature calculation of the matrix elements of the potential in the Schrödinger equation (Harris et al. 1965; Dickinson and Certain 1968) that inspired the discrete variable representation pseudospectral method in chemical physics (Light and Carrington Jr. 2000).

3.7.1 Matrix Representation of the Collision Frequency in Laguerre and Maxwell Polynomials

The collision operator of the Boltzmann equation, Eq. (3.48), includes the sum of the integral operator and the elastic collision frequency, $Z(y)$, Eq. (3.50) which for the hard sphere cross section is given by Eq. (3.45). The physical system of interest is the binary system of a test particle of mass m dilutely dispersed in a background gas of particles of mass M at equilibrium at temperature T_b. The mass ratio is $\gamma = M/m$.

We are interested in the analytic evaluation of the matrix elements of the collision frequency, $Z(y)$, for a binary gas with the hard sphere cross section. This calculation illustrates some of the techniques used in kinetic theory with the so-called moment method of solution which is a spectral solution of the Boltzmann equation with the distribution expanded in a basis set of functions. The basis set that is commonly used is the Sonine-Laguerre polynomials (Hoare and Kaplinsky 1970). The reason for this choice is that for a particular collisional model, namely for "Maxwell molecules", particles that interact with an inverse power law potential, $(V(r) \approx r^{-4})$, the collision frequency is a constant and the eigenvalue spectrum of the Boltzmann collision operator is discrete. Further details are discussed in Chap. 5.

The Sonine-Laguerre polynomials of order $\alpha = 1/2$ can be defined by their explicit polynomial representation,

$$L_n^{(\frac{1}{2})}(y) = \sum_{k=0}^{n} S_{nk}y^k, \tag{3.89}$$

where $y = mv^2/2k_BT_b$ is reduced energy and the coefficients are given by

$$S_{nk} = \frac{(-1)^k \Gamma(k + \frac{3}{2})}{\Gamma(n + \frac{3}{2})(n - k)!k!} y^k. \tag{3.90}$$

The $L_n^{(\frac{1}{2})}(y)$ basis functions are orthogonal as given by

$$\int_0^\infty \sqrt{y} e^{-y} L_n^{(\frac{1}{2})}(y) L_m^{(\frac{1}{2})}(y) dy = \frac{\Gamma(n + \frac{3}{2})}{n!} \delta_{nm}. \tag{3.91}$$

It is important to note that the coefficients in Eq. (3.90) alternate in sign owing to the factor $(-1)^k$.

With Eqs. (3.89) and (3.90), the matrix elements of the collision frequency, $Z(x)$, Eq. (3.45), are given by

$$Z_{nm} = \frac{A}{\sqrt{\gamma}} \sum_{k=0}^{n} \sum_{\ell=0}^{m} S_{nk} S_{m\ell} \int_0^\infty \sqrt{y} e^{-y} y^{(k+\ell)}$$

$$\times \left(e^{-\gamma y} + \frac{\sqrt{\pi}}{2} \left[\frac{1}{\sqrt{\gamma y}} + 2\sqrt{\gamma y} \right] \mathrm{erf}(\sqrt{\gamma y}) \right) dy, \tag{3.92}$$

with $A = \pi d^2 \sqrt{k_B T_b / 2M}$. The integrals of powers of the collision frequency can be evaluated exactly in terms of two sets of integrals, defined by,

$$I_1(n) = \int_0^\infty y^n e^{-(\gamma+1)y} dy = \frac{1}{(\gamma+1)^{n+1}} \Gamma(n+1), \tag{3.93}$$

and

$$I_2(n) = \int_0^\infty y^n e^{-y} \mathrm{erf}(\sqrt{\gamma y}) dy, \tag{3.94}$$

which satisfies the recurrence relation

$$I_2(n) = nI_2(n-1) + \sqrt{\frac{\gamma}{\pi}} \frac{\Gamma(n+1)}{(\gamma+1)^{(n+1)}}. \tag{3.95}$$

The matrix elements can be written in terms of these integrals as given by

$$Z_{nm} = \frac{A}{\sqrt{\gamma}} \sum_{k=0}^{n} \sum_{\ell=0}^{m} S_{nk} S_{m\ell} \left[I_1(k+\ell+\tfrac{1}{2}) + \frac{1}{2}\sqrt{\frac{\pi}{\gamma}} I_2(k+\ell) + \sqrt{\pi\gamma} I_2(k+\ell+1) \right]. \tag{3.96}$$

As noted earlier, the terms in the sum in Eq. (3.96) alternate in sign and we can expect significant round-off errors for n and m of the order of 15–20. We only consider the lower order matrix elements.

The matrix elements of the collision operator are calculated exactly with Eqs. (3.93)–(3.96) and approximately by quadrature. An important consideration is the mass dependence of the collision frequency that is shown in Table 3.14.

The exact matrix elements for $\gamma = 1$ and order $N = 5$ in Table 3.14 are calculated with Eq. (3.96). The approximate results evaluated with only $N = 5$ quadrature points are shown in Table 3.15. If $Z(y)$ were unity, the matrix is diagonal with the diagonal elements equal to the normalization of the Laguerre polynomials and would require at least $N = (n + 1)/2$ quadrature points for their exact evaluation. Whereas the lower order matrix elements are in agreement (to 4 significant figures), the higher order matrix elements are not exact owing to the departure of $Z(y)$ from a polynomial of some finite order. The convergence of Z_{22} and Z_{44} is shown in Fig. 3.21 for much large numbers of quadrature points.

If we transform the "approximate" matrix representative, Table 3.15, to physical space we recover a diagonal matrix with the diagonal elements equal to $Z_{ij} = Z(y_i)\delta_{ij}$ which for $N = 5$ is represented by the vector

$$\frac{A}{\sqrt{\gamma}}[2.5681 \quad 3.3945 \quad 4.5452 \quad 5.9259 \quad 7.6095].$$

with the components equal to the "exact" $Z(y_i)$ values for the five Laguerre quadrature points 0.43140, 1.75975, 4.10447, 7.74670, 13.45768, in accordance with Eq. (3.86).

Table 3.14 Exact matrix elements, Z_{nm}, in units of $A/\sqrt{\gamma}$ for $\gamma = M/m = 1$, Eq. (3.96), of the hard sphere collision frequency $Z(x)$

n/m	0	1	2	3	4
0	3.1915	−0.6515	−0.0728	−0.0169	−0.0050
1	−0.6515	4.1224	−0.9961	−0.1273	−0.0331
2	−0.0728	−0.9961	4.8688	−1.2693	−0.1755
3	−0.0169	−0.1273	−1.2693	5.5103	−1.5018
4	−0.0050	−0.0331	−0.1755	−1.5018	6.0819

Table 3.15 Approximate matrix elements of the hard sphere collision frequency, $Z(x)$, in units of $A/\sqrt{\gamma}$ for $\gamma = M/m = 1$ evaluated with $N = 5$ Gauss-Laguerre quadrature points

n/m	0	1	2	3	4
0	3.1915	−0.6515	−0.0728	−0.0167	−0.0044
1	−0.6515	4.1225	−0.9958	−0.1261	−0.0292
2	−0.0728	−0.9958	4.8703	−1.2637	−0.1585
3	−0.0167	−0.1261	−1.2637	5.5297	−1.4388
4	−0.0044	−0.0292	−0.1585	−1.4388	6.3291

Fig. 3.21 The convergence of the diagonal matrix elements Z_{22} and Z_{44} versus the number of Laguerre quadrature points, N. The exact values are determined as given by Eqs. (3.93)–(3.96); Accuracy $= \log_{10} |1 - Z_{nn}^{(N)}/Z_{nn}|$
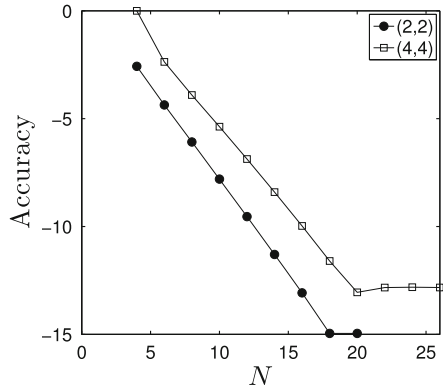
By contrast, the transform of the "exact" spectral space representation of Z_{nm} in Table 3.14 gives the "approximate" non-diagonal physical space representation,

$$\mathbf{T}^{\dagger} \cdot \mathbf{Z} \cdot \mathbf{T} = \frac{A}{\sqrt{\gamma}} \begin{pmatrix} 2.5540 & 0.0243 & -0.0296 & 0.0313 & -0.0308 \\ 0.0243 & 3.3527 & 0.0512 & -0.0544 & 0.0540 \\ -0.0296 & 0.0512 & 4.4822 & 0.0675 & -0.0676 \\ 0.0313 & -0.0544 & 0.0675 & 5.8527 & 0.0742 \\ -0.0308 & 0.0540 & -0.0676 & 0.0742 & 7.5333 \end{pmatrix}. \quad (3.97)$$

This remarkable result between the exact and quadrature evaluated matrix elements and the corresponding physical space representation might be unexpected, but it is consistent with the analysis given by Eq. (3.85). The variation of the matrix representation of the collision frequency with mass ratio is of interest and shown in Tables 3.16 and 3.17 for two different mass ratios.

For $M/m \to 0$, the Rayleigh limit, the matrix representative is becoming diagonal in this basis set, whereas in the larger mass limit, $M/m \to \infty$, the Lorentz limit, the off-diagonal elements are increasing.

It is of interest to examine the reduced energy dependence of the collision frequency in the Rayleigh limit for which $\gamma \to 0$. With the Taylor series expansion of

Table 3.16 Exact matrix elements in units of $A/\sqrt{\gamma}$ for $\gamma = M/m = 0.1$ with Eq. (3.96)

n/m	0	1	2	3	4
0	2.367	−0.088	−0.002	−0.000	−0.000
1	−0.088	2.507	−0.155	−0.004	−0.000
2	−0.002	−0.155	2.640	−0.217	−0.008
3	−0.000	−0.004	−0.217	2.767	−0.275
4	−0.000	−0.000	−0.008	−0.275	2.888

Table 3.17 Exact matrix elements in units of $A/\sqrt{\gamma}$ for $\gamma = M/m = 100$ with Eq. (3.96)

n/m	0	1	2	3	4
0	22.680	−9.167	−2.030	−0.930	−0.543
1	−9.167	33.945	−12.570	−2.693	−1.213
2	−2.030	−12.570	42.397	−15.191	−3.199
3	−0.930	−2.693	−15.191	49.443	−17.411
4	−0.543	−1.213	−3.199	−17.411	55.608

the exponential and error functions, we find that

$$Z(y) \overset{\gamma \to 0}{\approx} \frac{2A}{\sqrt{\gamma}} \left[1 - \frac{1}{3}\gamma y - \frac{1}{30}(\gamma y)^2 + \frac{1}{210}(\gamma y)^3 - \cdots \right]. \qquad (3.98)$$

Therefore in this mass ratio limit, the Laguerre basis set is a good choice for the representation of $Z(y)$ as the collision frequency is approaching a polynomial in the reduced energy, y. In the Lorentz limit for which $\gamma \to \infty$ we use $\mathrm{erf}(\sqrt{\gamma y}) = 1 - \mathrm{erfc}(\sqrt{\gamma y})$ and with the asymptotic expansion of the $\mathrm{erfc}(\sqrt{\gamma y})$, that is

$$\mathrm{erfc}(y) = \frac{e^{-y^2}}{y\sqrt{\pi}} \left(1 - \frac{1}{2y^2} + \frac{3}{4y^4} - \frac{15}{8y^6} + \cdots + (-1)^n \frac{(2n-1)!!}{(2y^2)^n} + \cdots \right) \qquad (3.99)$$

we get

$$Z(y) \overset{\gamma \to \infty}{\approx} A \left[\sqrt{\pi y}(1 + \frac{1}{2\gamma y}) - \frac{e^{-\gamma y}}{2(\gamma y)^2} \left[1 - \frac{3}{2\gamma y} + \frac{15}{4(\gamma y)^2} \cdots \right] \right]. \qquad (3.100)$$

and the limiting dependence is $\sqrt{y}$ with the resulting slow convergence with Laguerre polynomials. On the other hand, if Z(y) is expressed in reduced speed $x = \sqrt{y}$, we recognize that the expansion in Maxwell polynomials would be exact with $N = 2$. This demonstrates the manner in which a particular problem dictates the optimal choice of basis functions, namely Laguerre polynomials for the Rayleigh limit and Maxwell polynomials for the Lorentz limit.

3.7.2 Matrix Representation of the Harmonic Oscillator Potential in Hermite Polynomials

An instructive calculation of the pseudopsectral representation of the Hamiltonian for the quantum harmonic potential is the evaluation of the matrix elements of the harmonic potential, $V(x) = x^2$ for the quantum harmonic oscillator problem, that is,

$$-\frac{d^2\psi_n}{dx^2} + x^2 \psi_n(x) = \lambda_n \psi_n(x), \qquad (3.101)$$

where $\lambda_n = 2n + 1$ in dimensionless units. The Hermite polynomials, Sect. 2.4.7, (Liboff 2002) are the eigenfunctions of the Hamiltonian and are a logical choice for the basis functions. The matrix representative of the potential in the set of basis functions $h_n(x) = e^{-x^2/2}H_n(x)/\sqrt{M_n}$, $M_n = \sqrt{\pi}2^n n!$ is given by

$$V_{nm} = \int_{-\infty}^{\infty} h_n(x)x^2 h_m(x)dx = \begin{cases} \frac{1}{2}(2n+1), & n = m, \\ \frac{1}{2}\sqrt{(n+1)(n+2)}, & n = m \pm 2, \\ 0, & \text{otherwise} \end{cases} \quad (3.102)$$

where we have used the recurrence relation

$$xH_n(x) = \frac{1}{2}[H_{n+1}(x) + 2nH_{n-1}(x)], \quad (3.103)$$

twice. We use M_N to denote the normalization factor of the Hermite polynomials to distinguish it from N.

We are interested in the evaluation of these matrix elements with the Gauss-Hermite quadrature, that is,

$$V_{nm}^{(N)} = \frac{1}{\sqrt{M_n M_m}} \sum_{i=1}^{N} w_i H_n(x_i)x_i^2 H_m(x_i). \quad (3.104)$$

The matrix V_{nm} without the term in x^2 in the integral in Eq. (3.102) represents the orthonormality of the basis functions. We can verify this result to order N with exactly N Gauss-Hermite quadrature points and weights since the largest element would be a polynomial of order $2N$ and the use of N quadrature points would yield an exact result. However, with the additional term in x^2 in Eq. (3.102), the matrix element $V_{N-1,N-1}^{(N)}$ in the bottom rightmost corner of the matrix is not calculated accurately with N quadrature weights and points. The error in this one matrix element can be determined exactly.

The matrix element $V_{N-1,N-1}^{(N)}$ of the potential for the harmonic oscilator is given by Eq. (3.104)

$$V_{N-1,N-1}^{(N)} = \frac{2}{M_{N-1}} \sum_{i=1}^{N/2} w_i x_i^2 H_{N-1}^2(x_i), \quad (3.105)$$

and the quadrature sum is twice the sum over the positive quadrature points. With $M_{N-1} = \sqrt{\pi}2^{N-1}(N-1)!$, the use of the recurrence relation, Eq. (3.103) and $H_N(x_i) = 0$ which defines the quadrature points, we get that,

$$\begin{aligned} V_{N-1,N-1}^{(N)} &= \frac{1}{M_{N-1}} \sum_{i=1}^{N} w_i H_{N-2}^2(x_i), \\ &= (N-1)^2 \frac{M_{N-2}}{M_{N-1}}, \\ &= \frac{N-1}{2}, \end{aligned} \quad (3.106)$$

where the quadrature sum is the normalization of H_{N-2} which is "exact" with N quadrature points. The approximate result, Eq. (3.106), should be compared with the exact result given by Eq. (3.102), that is

$$V_{N-1,N-1} = \frac{2N-1}{2}. \tag{3.107}$$

The transform of the "approximate" quadrature evaluated matrix representative gives the "exact" physical space representation of the potential as the diagonal matrix,

$$V_{ij} = \sum_{m=0}^{N-1} \sum_{n=0}^{N-1} T_{im} V_{nm}^{(N)} T_{mj} = x_i^2 \delta_{ij}. \tag{3.108}$$

This is expected as the transformation of the matrix representation of a multiplicative operator evaluated with an Nth order quadrature, namely $G_{nm}^{(N)}$ in Eq. (3.85) gives on transformation to physical space the diagonal representation, $G(x_i)\delta_{ij}$.

If the exact spectral representation of the harmonic oscillator potential is transformed to physical space it gives an inexact result. This can be seen by considering the transform of the difference of the two spectral space representations,

$$(\Delta V)_{nm} = \frac{N}{2} \delta_{m,N-1} \delta_{n,N-1}, \tag{3.109}$$

which is the null matrix except for the one element $V_{N-1,N-1} = N/2$. We transform the matrix, Eq. (3.109) to physical space and recognize that it is the last row of **T** that plays a role which is the vector with components

$$T_{N-1,j} = (-1)^{N+j} \frac{1}{\sqrt{N}}. \tag{3.110}$$

Thus we have analogous to Eq. (3.108)

$$(\Delta V)_{ij} = \sum_{m=0}^{N-1} \sum_{n=0}^{N-1} T_{im}(\Delta V)_{nm} T_{mj} = \frac{N}{2} \sum_{n=0}^{N-1} \sum_{m=0}^{N-1} T_{in} T_{jm} \delta_{m,N-1} \delta_{n,N-1}$$

$$= \frac{1}{2} (-1)^{i+j}. \tag{3.111}$$

where Eqs. (3.109) and (3.110) have been used. These results were noted by others (Eq. 4.1 in Baye and Heenen (1986) and Eq. (14) in Szalay (1993)) and are important in connection with the convergence properties of pseudospectral methods in kinetic theory and also in quantum mechanics (Szalay et al. 2003). The analysis in this section explains in part the accuracy of pseudospectral methods based on approximate quadrature evaluated matrix elements (Baye et al. 2002; Szalay et al. 2012). Further details are presented in Sect. 6.7.3, in Chap. 6.

3.8 Challenging Integrals

We complete our discussion of the quadrature evaluation of integrals with a brief summary of some challenging integrals, the majority of which are characterized by integrands that oscillate and decay very slowly for $x \to \infty$ on the semi-infinite interval (Lyness 1985). Integrals with oscillatory integrands, especially those defined on the infinite or semi-infinite domains abound in the physical sciences and engineering (Safouhi 2001; Fornberg et al. 2002; Asheim et al. 2014). The use of the Distorted Wave Born Approximation (DWBA) for quantum inelastic cross sections (Rasch and Whelan 1997) leads to oscillatory integrands for the matrix elements between continuum eigenstates. A good example is the calculation of the rate of nuclear spin transitions in ^{3}He-^{3}He collisions (Shizgal 1973; Mullen and Richards 1990; Newbury et al. 1993). We also consider an integral from the SIAM 100-Digit Challenge (Bornemann et al. 2004) that exhibits a similar behaviour.

The numerical evaluation of the six-dimensional electron repulsion integrals that are required for molecular electronic structure calculations is summarized. In these simulations, many integrals are required so as to estimate the electronic states of atoms and molecules. There is a very large effort devoted to the efficient calculation of such integrals. Our discussion in this section is an overview of current work with emphasis on the choice of basis functions and the numerical calculation of the integrals that occur for the different choices. The use of nonclassical Rys quadratures is one of several different methods to calculate the integrals.

3.8.1 Molecular and Atomic Electronic Structure; Electron Pair Repulsion Integrals

The description of the electronic energies of an atom or molecule is based on the Schrödinger equation for the motion of the electrons and nuclei which interact via Coulomb potentials. Owing to the much smaller mass of the electrons relative to the nuclei, one can uncouple the electronic and nuclear motions in accordance with the Born[5]-Oppenheimer[6] approximation (Levine 2009; Szabo and Ostlund 1996). Thus one can write the Schrödinger equation for the electronic motion with the nuclei in fixed positions at $\mathbf{R}_n$ for the nucleus labelled by n. In this way, the Schrödinger equation is the eigenvalue problem

$$(H_{el} + V_{nn})\psi(\mathbf{r}_1, \mathbf{r}_2, \ldots, \mathbf{r}_n) = E_{el}(\mathbf{R_n})\psi(\mathbf{r}_1, \mathbf{r}_2, \ldots, \mathbf{r}_n), \qquad (3.112)$$

---

[5] Max Born (1882–1970) was a German-British physicist and mathematician who made significant contributions to quantum mechanics, solid-state physics and optics, and won the 1954 Nobel Prize in Physics for the statistical interpretation of wavefunctions.

[6] Julius Robert Oppenheimer (1904–1967) was an American theoretical physicist and played a prominent role in the Manhattan Project for which he became known as the "father of the atomic bomb".

where $\mathbf{r_i}$ is the position vector of the ith electron. The electronic Hamiltonian is

$$H_{el} = -\frac{\hbar^2}{2m_e}\sum_i \nabla_i^2 - \sum_n \sum_i \frac{Z_n e^2}{|\mathbf{R}_n - \mathbf{r}_i|} + \sum_i \sum_{i>j} \frac{e^2}{|\mathbf{r}_j - \mathbf{r}_i|}, \qquad (3.113)$$

where Z_n is the charge of the nth nucleus and e is the charge of the electron. The first term in Eq. (3.113) is the kinetic energy of the ith electron. The second term is the Coulomb interaction with the ith electron and the nth nucleus and the last term is the electron-electron repulsion between different electrons. The $\mathbf{R}_n$ positions relative to some space fixed axes are considered known. The rotational and vibrational states are the solution of the Schrödinger equation for the motion of the nuclei in the potential $E_{el}(\mathbf{R}_n)$ considered separately in Chap. 6.

The situation simplifies considerably if we consider atoms with one nucleus and in particular atomic hydrogen with one electron moving about a proton for which an analytic solution is known (Karplus and Porter 1970; Levine 2009; Liboff 2003). The eigenfunctions of the H-atom are

$$\psi_{n\ell m}(r, \theta, \phi) = R_{n\ell}(r)Y_\ell^{(m)}(\theta, \phi), \qquad (3.114)$$

where $R_{n\ell}(r)$ can be written in terms of the associated Laguerre polynomials as discussed in Chap. 2, Sect. 2.4.6. These atomic orbitals are often used as the basis functions for larger molecular systems. Another one-electron system that can be solved analytically is H_2^+ (Wind 1965; Levine 2009; Liu and Zhao 2010). The Helium atom is the simplest two electron problem for which the Hamiltonian is,

$$H = -\frac{\hbar^2}{2m_e}\nabla_1^2 - \frac{\hbar^2}{2m_e}\nabla_2^2 - \frac{2e^2}{r_1} - \frac{2e^2}{r_2} + \frac{e^2}{|\mathbf{r}_1 - \mathbf{r}_2|}, \qquad (3.115)$$

where the last term is the electron repulsion potential. This is a prototypical quantum system that provides some of the main concepts for quantum chemical problems (Karplus and Porter 1970; Levine 2009).

Our main interest is with respect to the quadrature evaluation of electron repulsion integrals which is central to quantum chemistry computer codes (Becke 1988; Lindh et al. 2001; Gill and Chien 2003; El-Sherbiny and Poirier 2004; Kakhiani et al. 2009; Mitani 2011). Any speed-up in the computational time of these integrals represents an enormous advance toward the treatment of larger molecular systems. The subject is very technical and it is not our intention to treat this in any detailed manner here. It has become a very computationally intensive problem that occupies the interests of a large number of computational theoretical chemists and physicists. Additional presentations of the problem are in several textbooks (Karplus and Porter 1970; Szabo and Ostlund 1996; Helgaker et al. 2000; Levine 2009; Tsuneda 2014) and review papers (Gill 1994; Reine et al. 2012). The objective is to introduce the reader to the ongoing efforts of many researchers in the development of efficient methods for the evaluation of integrals over the basis functions of electrons in atoms and molecules.

This subject area often involves very technical aspects of Fortran codes and the nomenclature for the basis sets used can be found in Chap. 3 in the book by Szabo and Ostlund (1996). This brief summary will hopefully provide the reader with the essential aspects as it relates to numerical quadratures and the evaluation of integrals.

The only exact solution of the Schrödinger equation is for the hydrogen atom and other one-electron atoms such as He^+, Li^{++}, etc. with a Hamiltonian which is separable and consequently with eigenfunctions that are expressed as a direct product of the associated Laguerre polynomials and the spherical harmonics, Eq. (3.4). In the absence of external fields, the allowed energy levels depend only on n. The eigenfunctions $\psi_{nlm}(r, \theta, \phi)$ are referred to as orbitals.

The Schrödinger equation for two-electron atoms such as He, is not separable in the same way owing to the Coulomb electron-electron interaction dependent on the distance, $r_{12} = |\mathbf{r_1} - \mathbf{r_2}|$ between the two electrons. There are several variational treatments for He that provide useful analytical approximations to the electronic ground eigenstate (Frankowski and Pekeris 1966; Levine 2009). The choice of basis functions is a key element in current computational methods in atomic electronic structure calculations. As always, the basis functions should be chosen so as to best describe the anticipated behaviour of the eigenfunctions and at the same time provide for an efficient numerical treatment.

For many electron atoms, one useful choice of basis functions or "orbitals" are those that mimic the orbitals for the single electron for the H-atom and are the product of a radial function $R_{n\ell}(r)$ and the spherical harmonic $Y_{\ell m}(\theta, \phi)$. One such basis function is the set of Slater[7]-type orbitals (STO) given by

$$\phi_{n\ell m}^{sto}(\mathbf{r}) = N_{n\ell m} r^{n-1} e^{-\alpha r} Y_{\ell m}(\theta, \phi), \qquad (3.116)$$

where $N_{n\ell m}$ is a normalization and α is a parameter. An added complexity is that electrons are fermions with spin 1/2 states and the eigenfunctions must be made anti-symmetric with respect to an exchange of the two electrons. In order to reduce the Schrödinger equation for He to a set of matrix equations, a large number of matrix elements of the Hamiltonian between basis functions must be evaluated. The situation for He has been considered by numerous researchers and exact numerical results are known (Drake 1999; Drake et al. 2002) including the application of pseudospectral methods (Cassar and Drake 2004; Grabowski and Chernoff 2011). Electronic structure calculations for many electron atoms is an active area of research.

Another level of complexity occurs for diatomic molecules such as H_2 with two nuclei, that is "two centers", as shown in Fig. 3.22. The protons are at a fixed separation R in keeping with the Born-Oppenheimer approximation and the relative electron-electron distance is $r_{12} = |\mathbf{r_1} - \mathbf{r_2}|$. The other solid lines are the four electron-proton interactions. The two electrons can move in space and their positions specified with cartesian coordinates (x_1, y_1, z_1) and (x_2, y_2, z_2) or preferably in terms of spherical polar coordinates which is made difficult owing to the two centers.

---

[7] John Clarke Slater (1900–1976) was an American physicist who pioneered theoretical methods in atomic and molecular electronic structure.
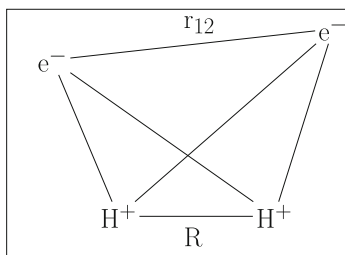
Fig. 3.22 Electron-electron separation is denoted by $r_{12} = |\mathbf{r_1} - \mathbf{r_2}|$ and then fixed separation of the protons by R. The other *solid lines* are the four electron-proton interactions

Thus, one of the main difficulties is the choice of coordinates and the basis functions in which to express the three-dimensional eigenfunctions. The ground state eigenenergy depends on the nuclear separation R and provides the potential $V(R)$ for the subsequent study of the nuclear motion or vibration. For H_2^+, with only one electron and no electron-electron repulsion the problem is simplified (Wind 1965). Further details of the theoretical treatment for this molecular ion can be found elsewhere (Cassar and Drake 2004; Levine 2009).

For molecular systems, the evaluation of matrix elements between Slater type orbitals is difficult and a better choice are the basis sets constructed from Gaussian type orbitals,

$$\phi_{n\ell m}^{gto}(\mathbf{r}) = N_{n\ell m} r^\ell e^{-\alpha r^2} Y_{\ell m}(\theta, \phi), \tag{3.117}$$

where the main difference with Slater type orbitals is the exponential dependence on r^2 rather than r. The main advantage is that the product of two Gaussians is another Gaussian which can be easily understood by completing the square of the argument of the exponential. Another suggestion for basis function are those discussed by Weniger (2009) referred to as B-functions with the radial portion expressed as a Bessel function. In this approach, we once again encounter integrals with oscillating integrands as discussed in Sect. 3.8.2 (Safouhi 2001). The importance of choosing the appropriate basis functions is clear.

In either case, the problem reduces to an expansion of the multi-electron ground state eigenfunction in these basis sets and the reduction of the Schrödinger equation to a set of linear equations for the eigenvalues. This is easier said than done. In the course of this calculation, the matrix elements of the kinetic energy operator and, in particular, of the electron-electron Coulomb repulsion potential must be calculated. These are integrals of the form

$$\langle ij| \frac{1}{r_{12}} |k\ell\rangle = \iint \phi_i(\mathbf{r_1}) \phi_j(\mathbf{r_2}) \frac{1}{r_{12}} \phi_k(\mathbf{r_1}) \phi_\ell(\mathbf{r_1}) d\mathbf{r_2} d\mathbf{r_2}. \tag{3.118}$$

These are 6-dimensional integrals with the position, r_i, of each basis function (or orbital) with reference to the position of a particular nucleus. Even for diatomic molecules, the numerical evaluation of these integrals is difficult and a large number

are required in a simulation of the electronic structure. It might be of interest for the reader to consult some original papers in which some of these integrals were evaluated analytically (Shavitt and Karplus 1965; Kern and Karplus 1965).

3.8.2 Relaxation Times for ^{3}He-^{3}He Spin Exchange Collisions—Oscillatory Integrands

The use of the distorted wave Born approximation to approximate transition probabilities for inelastic collision processes (Child 1996; Canto and Hussein 2013) yields integrals with oscillatory integrands. We choose to apply this theoretical approach to the nuclear spin-exchange that accompanies ^{3}He-^{3}He collisions. The distorted wave Born approximation applies to systems for which the interaction potential is the sum of two distinct potentials, a spherical potential, $V_0(r)$, that defines the elastic scattering of the He atoms and another much weaker spin dependent interaction, $\mathbf{V}_1(\mathbf{r}; \mathbf{I}_1, \mathbf{I}_2)$ that is responsible for the changes in the ^{3}He nuclear spin states, $\mathbf{I}_1$ and $\mathbf{I}_2$. With this assumption, the continuum scattering eigenfunctions are very well approximated with the solution of the Schrödinger equation with only $V_0(r)$.

The integrals required in the distorted wave Born approximation are the diagonal matrix elements between the radial wavefunctions $u_{k,\ell}(r)$, of the form $\int_0^\infty u_{k,\ell}^2/r^8 d\mathbf{r}$ or $\int_0^\infty u_{k,\ell}^2 e^{-\alpha r}/r^2 d\mathbf{r}$ for the spin dependent interactions (Shizgal 1973, 1974a). The radial wavefunction, $u_{k,\ell}(r)$, are the solutions of Eq. (3.63). However, the continuum radial eigenfunctions can also be approximated with the JWKB eigenfunctions. The difficulty with the numerical evaluation of these integrals is that the integrands are highly oscillatory and may decay slowly for $r \rightarrow \infty$. Shizgal (1974b) evaluated such integrals by searching for the roots of the integrands and evaluating the integrals between successive roots with a Gauss-Mehler quadrature. This technique provides acceptable results but the convergence of the partial sums is slow. The results compared favorably with the exact quantum results obtained with a direct numerical integration of the radial Schrödinger equation. Dickinson and Shizgal (1975) later employed a classical analogue to the JWKB approximation and found excellent agreement with the semi-classical and quantal results.

We will not discuss the details of these calculations but instead consider analogous integrals with the replacement of the radial wavefunctions with the plane wave analogues so that $u_{k,\ell}(r) \rightarrow j_\ell(kr)$ where $j_\ell(kr)$ is the spherical Bessel function (Abramowitz and Stegun 1964). A typical example is the integral

$$\int_0^\infty \frac{j_\ell^2(x)}{x} dx = \frac{1}{2\ell(\ell+1)}, \tag{3.119}$$

with the oscillatory integrand shown in Fig. 3.23. The partial sums of the integrals between the successive zeros (with 8 Gauss-Legendre quadrature points and weights) for the integral in Eq. (3.119) with $\ell = 5$ are 0.01556, 0.01600, 0.01618, 0.01630,
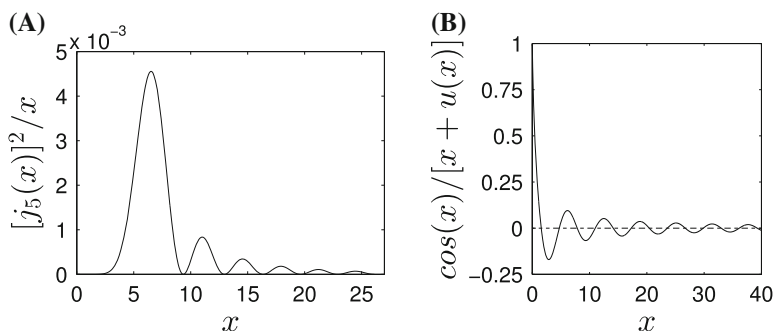
Fig. 3.23 (**A**) Integrand for the integral in Eq. (3.119) for $\ell = 5$; (**B**) The integrand for the integral, Eq. (3.120) in the SIAM 100-Digit Challenge (Gautschi 2008; Slevinsky and Safouhi 2008)

0.01637, 0.01643, etc. The exact value is $1/60 = 0.01666$. More than 93 % of the contribution to the integral is from the first peak and the contributions from the remaining intervals are much smaller and decrease very slowly. For physical applications such as this one, the required accuracy is of several significant figures. Similar integrals involving the squares of Bessel functions occur in the reconstruction of temperature multipole spectrum of cosmic microwave background from measured data (Tomaschitz 2012, 2013) containing the squares of Bessel functions as in Eq. (3.119). An exhaustive discussion of the work on oscillatory integrands is beyond the scope of the book. The original treatment of quadratures for integrals of this type is Filon[8]'s sine and cosine formulae discussed in Sect. 4.11 of the book by Lindfield and Penny (2012). More advanced discussions can be found in recent papers (Iserles and Norsett 2005; Asheim et al. 2014).

3.8.3 The SIAM 100-Digit Challenge; a "Twisted Tail" Integral

It is useful to compare the previous discussion with the integral

$$I = \int\limits_0^\infty \frac{\cos(x)}{x + u(x)} dx \qquad (3.120)$$

arising from a change of variable from an original integral (Slevinsky and Safouhi 2008; Gautschi 2008) discussed by Laurie in Chap. 1 in the SIAM 100-Digit

---

[8] Louis Napoleon George Filon (1875–1937) was an English mathematician and worked in classical mechanics, elasticity and continuous media.

Challenge (Bornemann et al. 2004). In Eq. (3.120), $x = u(x) \ln[u(x)]$. The integrand in Eq. (3.120) is shown in Fig. 3.23(B) and shares some of the features of Fig. 3.23(A). The graph is drawn with the spline fit of a table of $u(x)$ versus x. Gautschi (2008) provides a numerical algorithm for the evaluation of this integral. The infinite domain is divided into subdomains with the end points at the roots of $\cos(x)$ that is $x_k = (2k+1)\pi/2$ so that the integral is represented as a sum over each subdomain. The integral in each sub-domain is evaluated with a Gauss-Legendre quadrature over the interval $[-1, 1]$ with the appropriate change of variable as done for the integral in Eq. (3.119). Gautschi also discusses the need to introduce a special acceleration scheme in the summation over subintervals as this series converges very slowly analogous to the results cited for Eq. (3.119).

Further details can be found in recent publications (Gautschi 2008; Slevinsky and Safouhi 2008). In contrast to the applications to physical problems where the precision required is often less than machine accuracy, the "challenge" for this example and others (Bornemann et al. 2004) is to evaluate the integral to 100 digits.

3.9 Numerical Evaluation of Derivatives

The numerical evaluation of the derivatives of a function is the basis of pseudospectral methods of solution of partial differential equations such as the Schrödinger equation and/or differential-integro equations such as the Boltzmann equation. The earliest collocation appears to be the solution of the radiative transfer equation by Wick (1943) and Chandrasekhar (1960). The technique of differential quadrature was later introduced by Bellman (Bellman et al. 1972; Shu 2000) based on either polynomials or Fourier basis sets. The monograph by Gottlieb and Orszag (1977) established the use of spectral methods with a finite basis set expansion and the relationship with a collocation.

Blackmore and Shizgal (1985) applied pseudospectral discretizations of derivatives together with quadratures for integrals to reduce the Boltzmann equation to linear algebraic form. The method was referred to as a discrete ordinate method analogous to the terminology in radiative and neutron transport (Chandrasekhar 1960; Liou 1973) and in kinetic theory (Robson et al. 1991; Robson and Prytz 1993). These discretization techniques were applied to the Schrödinger equation by Light and coworkers (Hamilton and Light 1986; Bacic and Light 1986; Light and Carrington Jr. 2000) and originated from considerations of the quadrature evaluation of matrix elements (Harris et al. 1965; Dickinson and Certain 1968) discussed in Sect. 3.7. The Lagrange mesh method developed by Baye (1994) and coworkers (Baye and Heenen 1986; Baye and Vincke 1999) is based on Lagrange interpolation. A personal chronology of the development of pseudospectral methods in chemistry and physics was provided in Table 1.1. The applications to the Boltzmann, Fokker-Planck and Schrödinger equations are presented in Chaps. 5 and 6.

3.9.1 Finite Difference Formulas for Derivatives

Finite difference methods for the evaluation of derivatives are often used for the solution of differential equations. We present a brief summary in comparison with pseudospectral methods. The finite difference first derivative of a function is simply an approximation to the definition of the derivative as the slope of the function at some point. The method is considered local as the derivative is approximated by neighbouring function values. Specifically, we evaluate the first derivative between uniformly spaced grid points, x_i and x_{i+1}, with $\Delta x = x_{i+1} - x_i$ as

$$\left.\frac{df}{dx}\right|_{x_i} \approx \frac{f(x_{i+1}) - f(x_i)}{\Delta x}. \tag{3.121}$$

Equation (3.121) is the forward finite difference whereas

$$\left.\frac{df}{dx}\right|_{x_i} \approx \frac{f(x_i) - f(x_{i-1})}{\Delta x}, \tag{3.122}$$

is the backward finite difference approximation to the first derivative. It is clear that this is a local method as only neighbouring grid points are involved. The third approximation is the centered difference formula given by,

$$\left.\frac{df}{dx}\right|_{x_i} \approx \frac{f(x_{i+1}) - f(x_{i-1})}{2\Delta x}. \tag{3.123}$$

The error in the above approximations to the first derivative is second order in Δx. Higher order estimates can also be provided. Further details can be found in Chap. 4 of Burden and Faires (2011) and Chap. 7 of Cheney and Kincaid (2008).

The approximation to the second derivative is derived from the expressions above and we have the second order estimate,

$$\left.\frac{d^2f}{dx^2}\right|_{x_i} \approx \frac{f(x_{i+1}) - 2f(x_i) + f(x_{i-1})}{(\Delta x)^2}. \tag{3.124}$$

The diffusion equation of the form

$$\frac{\partial n(x, t)}{\partial t} = \frac{\partial^2 n(x, t)}{\partial x^2} \tag{3.125}$$

can be discretized with Eq. (3.121) on the right-hand side in x and with Eq. (3.124) on the left hand side in t so that

$$\frac{n_i(t + \Delta t) - n_i(t)}{\Delta t} = \frac{n_{i+1}(t) - 2n_i(t) + n_{i-1}(t)}{(\Delta x)^2}. \tag{3.126}$$

where $n_i(t) \equiv n(x_i, t)$. The solution can be advanced in time with an Euler algorithm, that is

$$n_i(t + \Delta t) = n_i(t) + \left[\frac{n_{i+1}(t) - 2n_i(t) + n_{i-1}(t)}{(\Delta x)^2} \right] \Delta t, \qquad (3.127)$$

which is initiated with the initial condition $n_i(0)$.

The differential operators in many different partial differential equations can be discretized in this way and the equations reduced to ordinary differential equations which are then advanced in time with an Euler scheme above or with higher order methods such as a Runge-Kutta scheme (Cheney and Kincaid 2008). An important aspect of these methods is the choice of the grid spacing in x and t, that is Δx and Δt. Further details on finite difference methods can be found in several textbooks (LeVeque 2007; Cheney and Kincaid 2008; Durran 2010). We use a finite difference method for the solution of the nonlinear Boltzmann equation in Chap. 5, Sect. 5.8 (Kabin and Shizgal 2003). We make use of the Chang and Cooper (1970) finite difference scheme for the solution of the Fokker-Planck equation in Chap. 6, Sect. 6.2.3.

3.9.2 Interpolation and Differentiation

In Chap. 2, Sect. 2.3.1, we discussed the role of interpolation in the development of quadrature procedures. A Lagrange interpolation was defined for the set of N points $\{x_i\}$ and the corresponding function values, $y_i = f(x_i)$. The Nth order Lagrange interpolant is of the form

$$f(x) \approx f^{(N)}(x) = \sum_{i=1}^{N} f(x_i) I_i(x), \qquad (3.128)$$

where the interpolation function, $I_i(x)$, is constructed from orthogonal polynomials that is

$$I_i(x) = w_i \sum_{n=0}^{N-1} P_n(x) P_n(x_i), \qquad (3.129)$$

and satisfy the Cardinality condition

$$I_i(x_j) = \delta_{ij}. \qquad (3.130)$$

Thus the interpolation returns the exact values of the function values, $f(x_i)$, at each point x_i, as discussed in Sect. 2.3.1 and shown in Fig. 2.2.

It is clear that an approximation for the derivative of $f(x)$ is given by

$$\frac{df^{(N)}(x)}{dx} = \sum_{i=1}^{N} f(x_i) \frac{dI_i(x)}{dx}. \qquad (3.131)$$

We thus identify the derivative matrix operator used in pseudospectral methods for the solution of differential equations as the derivative of the Lagrange interpolant, that is,

$$\hat{D}_{ij} = \left. \frac{dI_j(x)}{dx} \right|_{x=x_i}$$

$$= w_j \sum_{n=0}^{N-1} P_n'(x_i) P_n(x_j). \tag{3.132}$$

It is straightforward to construct the discrete derivative matrix operator for classical and nonclassical polynomials from the recurrence coefficients α_n and β_n. The quadrature weights and points are calculated with the diagonalization of the Jacobi matrix, Eq. (2.71). The polynomials, $P_n(x)$, and the derivatives, $P_n'(x)$ are determined by recurrence and the discrete derivative matrix operator is given by Eq. (3.132).

It follows that the second derivative matrix operator in physical space is given by

$$\hat{D}_{ij}^{(2)} = w_j \sum_{n=0}^{N-1} P_n''(x_i) P_n(x_j). \tag{3.133}$$

With Eq. (3.132), the approximation to the second derivative that appears in Eq. (3.133) is

$$P_n''(x_i) = \sum_{\ell=1}^{N} \hat{D}_{i\ell} P_n'(x_\ell). \tag{3.134}$$

We substitute Eq. (3.134) into (3.133) and get

$$\hat{D}_{ij}^{(2)} = w_j \sum_{n=0}^{N} \left[\sum_{\ell=0}^{N} \hat{D}_{i\ell} P_n'(x_\ell) \right] P_n(x_j),$$

$$= \sum_{\ell=0}^{N} \hat{D}_{i\ell} w_j \sum_{n=0}^{N} P_n'(x_\ell) P_n(x_j),$$

$$= \sum_{\ell=0}^{N} \hat{D}_{i\ell} \hat{D}_{\ell j}. \tag{3.135}$$

Thus the second derivative matrix operator is the matrix product of the first order derivative matrix operators.

We use nonclassical basis functions for the majority of the applications in Chaps. 5 and 6 and use the definition Eq. (3.132) to construct the derivative matrix operator. For some nonclassical weight functions it is possible to express the spectral space matrix elements, d_{nm}, in terms of the recurrence coefficients and then transform to

Table 3.18 References to explicit first and second derivative matrix operators

Basis	Quadrature	Reference	$\mathbf{D}^{(1)}$	$\mathbf{D}^{(2)}$
Fourier		Schwartz (1985)	Eq. (2)	Eq. (3)
		Baye and Heenen (1986)		Eq. (3.5)
		Colbert and Miller (1992)		Appendix
		Kokoouline et al. (1999)		Appendix
		Shen et al. (2011)	Eq. (2.34)	Eq. (2.37)
	Odd collocation	Peyret (2002)	Eq. (2.30)	Eq. (2.31)
	Even collocation	Peyret (2002)	Eq. (2.32)	Eq. (2.33)
Chebyshev	Gauss	Funaro (1992)	Eq. (7.2.14)	
	Gauss	Shen et al. (2011)	Eq. (3.231)	
	Lobatto	Peyret (2002)	Eq. (3.46)	Eq. (3.47)
	Lobatto	Canuto et al. (2006)	Eq. (2.4.33)	Eq. (2.4.36)
	Lobatto	Shen et al. (2011)	Eq. (3.228)	
	Radau	Shen et al. (2011)	Eq. (3.229)	
Legendre	Gauss	Funaro (1992)	Eq. (7.2.14)	
Jacobi	Gauss	Shen et al. (2011)	Eq. (3.164)	
	Gauss	Funaro (1992)	Eq. (7.2.12)	
	Lobatto	Shen et al. (2011)	Eq. (3.160)–(3.162)	
	Radau	Shen et al. (2011)	Eq. (3.163)	
Laguerre	Radau	Funaro (1992)	Eq. (7.2.15)	
	Gauss	Baye and Heenen (1986)		Eq. (3.17)
Hermite	Gauss	Baye and Heenen (1986)		Eq. (3.14)

the physical space representation as done for Maxwell polynomials (Shizgal and Blackmore 1984). In general, explicit expressions of the physical space derivative matrix operators, $\hat{D}_{ij}$ and $\hat{D}_{ij}^{(2)}$, for nonclassical polynomials are not available. Explicit expressions do exist for derivative operators for the classical polynomials and Table 3.18 provides a partial list to the references where these results can be found.

The Fourier basis is the basis set of choice especially for the second derivative operator representing the kinetic energy in the Hamiltonian for quantum problems. Other definitions of these derivative matrix operators were reported by Baye (1994), Barkley (1995) and by Szalay (1993). There is considerable overlap of the results reported in these references.

If the matrix elements of the derivative operator in spectral space

$$d_{nm} = \int_a^b w(x) P_n(x) \frac{dP_m(x)}{dx} dx, \qquad (3.136)$$

is transformed to physical space with the transform, T_{ni}, then the derivative matrix operator in physical space is,

$$D_{ij} = \sum_{n=0}^{N-1} \sum_{m=0}^{N-1} T_{in} d_{nm} T_{mj},$$

$$= \sum_{n=0}^{N-1} \sum_{m=0}^{N-1} \left[\sqrt{w_i} P_n(x_i) \right] \sum_{k=1}^{N} w_k P_n(x_k) P'_m(x_k) \left[\sqrt{w_j} P_m(x_j) \right],$$

$$= \sqrt{w_i w_j} \left[\sum_{k=1}^{N} w_k \sum_{n=0}^{N-1} P_n(x_i) P_n(x_k) \right] \sum_{m=0}^{N-1} P'_m(x_k) P_m(x_j),$$

$$= \sqrt{w_i w_j} \left[I_k(x_i) \right] \sum_{m=0}^{N-1} P'_m(x_k) P_m(x_j), \tag{3.137}$$

where in the second line we have used the definitions of d_{nm} and of T_{in} in the square brackets. In the third line, we have collected the separate sums over n and m and we recognize the interpolation function in square brackets as noted in the last line. Since $I_k(x_i) = \delta_{ki}$, we have that

$$\boxed{D_{ij} = \sqrt{w_i w_j} \sum_{m=0}^{N-1} P'_m(x_i) P_m(x_j)}. \tag{3.138}$$

This is consistent with Eq. (3.132) since

$$\hat{D}_{ij} = D_{ij} \sqrt{\frac{w_i}{w_j}}. \tag{3.139}$$

In the absence of explicit analytic expressions, we show the physical space first and second derivative matrix operators for Maxwell polynomials, $(w(x) = x^2 e^{-x^2})$, with $N = 5$ in Tables 3.19 and 3.20. The main objective is to show the potential round-off errors that can occur in the calculation of numerical derivatives with these matrix operators. The matrix elements alternate in sign and increase rapidly with N, especially for $\mathbf{D}^{(2)}$.

In Fig. 3.24, we show the first and second derivatives of $f(x) = e^{-x^4}$ and the numerical values as symbols with $N = 20$ and a scale factor $s = 0.3$ so to as

Table 3.19 First derivative operator, **D**, in physical space for Maxwell Polynomials, $w(x) = x^2 e^{-x^2}$

i/j	1	2	3	4	5
1	−3.8890	6.1977	−3.1580	0.9693	−0.1201
2	−0.6768	−0.8170	1.8841	−0.4389	0.0485
3	0.2644	−1.4443	0.5276	0.7112	−0.0588
4	−0.3160	1.3101	−2.7694	1.5640	0.2112
5	1.1631	−4.3053	6.8023	−6.2745	2.6143

Table 3.20 Second derivative operator, $\mathbf{D}^{(2)}$, in physical space for Maxwell Polynomials, $w(x) = x^2 e^{-x^2}$

i/j	1	2	3	4	5
1	9.6484	−22.8180	18.7915	−6.4661	0.8442
2	3.8783	−7.0327	3.1378	0.0515	−0.0349
3	−0.2042	3.2413	−5.6473	2.7466	−0.1364
4	−0.6386	2.1113	−0.8897	−1.7295	1.1467
5	5.2122	−18.5745	26.9635	−18.3623	4.7611

Fig. 3.24 Numerical values of $f'(x)$ (*circles*) and $f''(x)$ (*squares*) versus x for $f(x) = e^{-x^4}$ with Maxwell quadrature points with scaling factor $s = 0.3$. The *solid lines* are the exact results
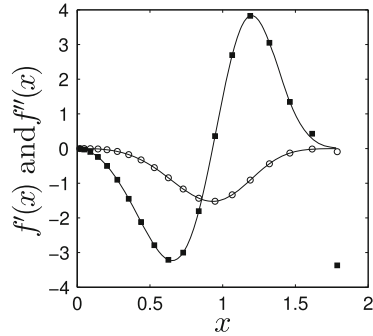
to shorten the effective interval. The effect of the roundoff error in the second derivative is illustrated by the two quadrature points for $n = 18$ and $n = 19$ (solid circles) that deviate significantly from the exact result (solid curve). In fact, the error in the last point, $n = 20$, is too large to show on the graph. Similar round-off errors for physical space derivative matrix operators for Chebyshev polynomials was discussed in Sect. 3.3.4 in Peyret (2002). This was also discussed in greater detail by Baltensperger and Trummer (2003) who provided methods to reduce the errors. Additional detailed discussions of such errors were also reported in the solution of Fisher's equation (Olmos and Shizgal 2006). The errors for the pseudospectral methods based on the Maxwell polynomials in the semi-infinite axis are larger than for Chebyshev pseudospectral methods.

Shizgal and Blackmore (1984) calculated D_{kj} for Legendre polynomials normalized to unity with the transform of

$$d_{nm} = \begin{cases} \sqrt{(2n+1)(2m+1)}, & m > n, \quad \text{m} + \text{n odd}, \\ 0 & \text{otherwise}, \end{cases} \tag{3.140}$$

as given by the first line of Eq. (3.137). In Fig. 3.25, we show the variation of the absolute error in the calculation of the first and second derivatives of the oscillatory function

$$f(x) = \sin\left[3(\sinh(x) + (1-x)^2)\right]. \tag{3.141}$$

The convergence is moderately fast for this non-polynomial function and slow at the interval boundaries relative to the convergence in the middle part of the interval.
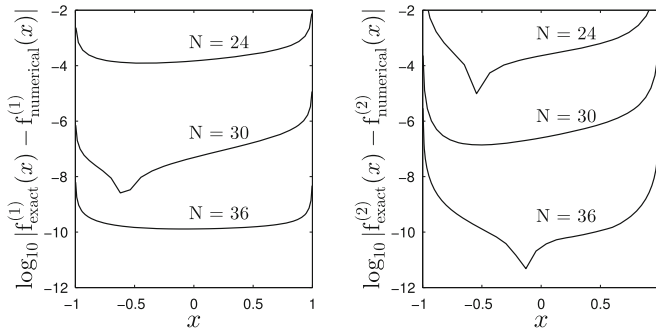
Fig. 3.25 Variation of the absolute error versus x for the numerical first derivative $\mathbf{f}^{(1)} = \mathbf{D} \cdot \mathbf{f}$ and numerical second derivative $\mathbf{f}^{(2)} = \mathbf{D}^{(2)} \cdot \mathbf{f}$ for $f(x) = \sin[3(\sinh(x) + (1+x)^2)]$ with $N = 24, 30,$ and 36 Legendre quadrature points

A comparison with a fourth order finite difference differentiation was shown by Shizgal and Blackmore (1984).

3.9.3 Sturm-Liouville Eigenvalues Problems

The classical polynomials satisfy Sturm-Liouville eigenvalue problems and equivalent Schrödinger equations. We provide a detailed discussion of these problems in Chap. 6. In this section, we introduce the subject so as to show that only the first derivative matrix operator is required for such second order differential equations. To illustrate this result, we note that the Sturm-Liouville equation for Legendre polynomials is given by

$$-\frac{d}{dx}\left[(1-x^2)\frac{dP_\ell(x)}{dx}\right] = \ell(\ell+1)P_\ell(x), \qquad (3.142)$$

which is equivalent to the Schrödinger equation for a rigid rotor, that is

$$-\frac{\hbar^2}{2I}\left[\frac{1}{\sin\theta}\frac{\partial}{\partial\theta}\left(\sin\theta\frac{\partial}{\partial\theta}\right)\right]\psi_\ell(\theta) = E_\ell\psi_\ell(\theta), \qquad (3.143)$$

where I is the moment of the inertia of the diatomic molecule. The change of variable, $x = \cos\theta$ transforms Eq. (3.143) to Eq. (3.142) with $E_\ell = \ell(\ell+1)\frac{\hbar^2}{2I}$.

We wish to construct the physical space representation of the Sturm-Liouville operator on the left hand side of Eq. (3.142). We begin with the spectral space representation given by

$$L_{\ell\ell'} = -\int_{-1}^{1} P_\ell \frac{d}{dx}\left[(1-x^2)\frac{dP_{\ell'}(x)}{dx}\right] dx. \qquad (3.144)$$

An integration by parts gives

$$L_{\ell\ell'} = \int_{-1}^{1} (1-x^2)P'_\ell(x)P'_{\ell'}(x)dx,$$

$$\approx \sum_{k=1}^{N} w_k(1-x_k^2)P'_\ell(x_k)P'_{\ell'}(x_k),$$

$$= \sum_{k=1}^{N} w_k(1-x_k^2) \sum_{\alpha=1}^{N} \hat{D}_{k\alpha}P_\ell(x_\alpha) \sum_{\beta=1}^{N} \hat{D}_{k\beta}P'_\ell(x_\beta), \tag{3.145}$$

where the integral for the matrix elements is evaluated by quadrature in the second line and the derivatives are evaluated with the derivative matrix operator in the third line. The transformation of $L_{\ell\ell'}$ to physical space with the transformation $T_{i\ell} = \sqrt{w_i}P_\ell(x_i)$ gives

$$L_{ij} = \sum_{\ell=0}^{N-1} T_{i\ell}L_{\ell\ell'}T_{\ell'j},$$

$$= \sum_{k=1}^{N} w_k(1-x_k^2) \left[\sum_{\ell=0}^{N-1} \sqrt{w_i}P_\ell(x_i) \sum_{\alpha=1}^{N} \hat{D}_{k\alpha}P_\ell(x_\alpha) \right]$$

$$\times \left[\sum_{\ell'=0}^{N-1} \sqrt{w_j}P_{\ell'}(x_j) \sum_{\beta=1}^{N} \hat{D}_{k\beta}P_{\ell'}(x_\beta) \right]. \tag{3.146}$$

We now use the discrete "completeness" relation

$$\sum_{\ell=0}^{N-1} P_\ell(x_i)P_\ell(x_\alpha) = \frac{\delta_{i\alpha}}{w_i}, \tag{3.147}$$

in each square bracket and the final result is

$$L_{ij} = \sum_{k=1}^{N} (1-x_k^2)D_{ki}D_{kj}, \tag{3.148}$$

where the definition Eq. (3.139) has been used. The eigenfunctions of $\mathbf{L}$ given by Eq. (3.148) for $N = 6$ calculated with a MATLAB code are shown by the solid symbols in Fig. 3.26. These coincide exactly with the solid line which is $P_5(x)$. The eigenvalues calculated in this way are "exactly" the rigid rotor eigenvalues, that is $\lambda_\ell = \ell(\ell+1)$.
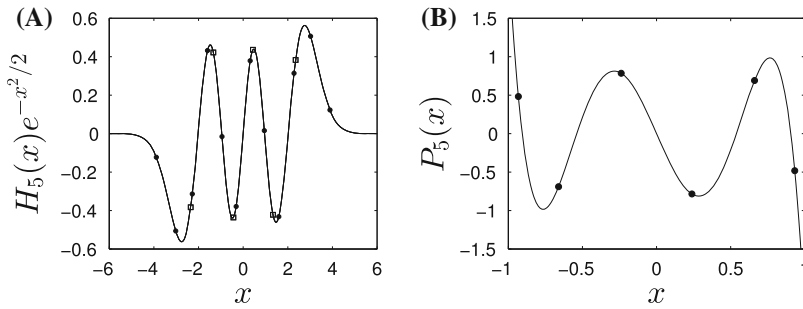
Fig. 3.26 (**A**) *Solid line* is the exact result for the orthonormal Hermite polynomial $H_5(x)e^{-x^2/2}$. The eigenfunctions of H_{ij} of Eq. (3.149) agree with the exact polynomial as shown by the *solid circles* for $N = 12$ and by the *squares* for $N = 6$. (**B**) *Solid line* is the exact result for the orthonormal Legendre polynomial $P_5(x)$. The eigenfunctions of L_{ij} of Eq. (3.148) agree with the exact polynomial as shown by *solid circles* for $N = 6$

Similarly, the eigenfunctions and eigenvalues for the harmonic oscillator are calculated with the diagonalization of the pseudospectral representation of the Schrödinger equation, that is

$$H_{ij} = \sum_{k=1}^{N} D_{ki} D_{kj} \qquad (3.149)$$

with Gauss-Hermite quadratures.

This calculation provides N exact eigenvalues, $\lambda_n = 2n$, relative to the ground state and eigenfunctions that coincide with the Hermite functions $h_n(x)$. In Fig. 3.26, the symbols are the results obtained with the diagonalization of Eq. (3.149) and are in exact agreement with the polynomial $h_5(x) = H_5(x)e^{-x^2/2}$ shown by the solid lines for $N = 6$ and $N = 12$. This calculation for the quantum harmonic oscillator, based on Eq. (3.149), does not involve the calculation of the matrix elements of the harmonic potential (Colbert and Miller 1992; Baye and Heenen 1986).

The evaluation of the potential energy matrix elements by quadrature (Szalay 1993; Baye et al. 2002; Szalay et al. 2012) are of no concern with this pseudospectral approach. Moreover, there is no occurrence of nonphysical "ghost levels" (Wei 1997; Willner et al. 2004; Kallush and Kosloff 2006) as discussed further in Chap. 6, Sect. 6.7.3.

3.9.4 Discrete Singular Convolution; Whittaker's Sinc Interpolation

Fourier basis functions are traditionally associated with pseudospectral methods for the solution of partial differential equations, and the grids associated with Fourier methods are uniform grids. In Sect. 2.6.1, we introduced the sinc function (Whittaker 1929a, b; Stenger 1993)

$$S_k(x) = \frac{\sin[\frac{\pi}{h}(x - x_k)]}{\frac{\pi}{h}(x - x_k)}, \tag{3.150}$$

which satisfies the cardinality condition $S_k(x_j) = \delta_{jk}$. Thus we have the interpolation on a uniform grid of N points $x_k = x_{min} + h(k - 1)$, defined for the finite interval $[x_{min}, x_{xmax}]$ where the grid spacing is $h = (x_{max} - x_{min})/(N - 1)$, that is

$$f_N(x) \approx \sum_{k=0}^{N} S_k(x)f(x_k). \tag{3.151}$$

From the explicit differentiation of Eq. (3.151), the representation of the second derivative operator is,

$$D_{jk}^{(2)} = S_k''(x_j) = \begin{cases} -\frac{2(-1)^{j-k}}{(j-k)^2 h^2}, & j \neq k, \\ -\frac{\pi^2}{3h^2}, & j = k. \end{cases} \tag{3.152}$$

This representation of the second derivative operator has been used frequently for the solution of the Schrödinger equation (Schwartz 1985; Colbert and Miller 1992; Dulieu et al. 1997; Meijering et al. 1999; Boyd 2001; Wei 2000a, b; Amore 2006).

References

Abramowitz, M., Stegun, I.A.: Handbook of Mathematical Functions with Formulas, Graphs, and Mathematical Tables. US Government Printing Office (1964)

Alterman, Z., Frankowski, K., Pekeris, C.L.: Eigenvalues and eigenfunctions of the linearized Boltzmann collision operator for a Maxwell gas and for a gas of rigid spheres. Astrophys. J. Suppl. **7**, 291–331 (1962)

Amore, P.: A variational Sinc collocation method for strong-coupling problems. J. Phys. A: Math. Gen. **39**, L349–L355 (2006)

Andersen, K., Shuler, K.E.: On the relaxation of a hard sphere Rayleigh and Lorentz gas. J. Chem. Phys. **40**, 633–650 (1964)

Angula, C., et al.: A compilation of charged-particle induced thermonuclear reaction rates. Nucl. Phys. A **656**, 3–183 (1999)

Asheim, A., Deano, A., Huybrechs, D., Wang, H.: A Gaussian quadrature rule for oscillatory integrals on a bounded interval. Discret. Contin. Dyn. Syst. **34**, 883–901 (2014)

Atenzi, S., Meyer-Ter-Vehn, J.: The Physics of Inertial Fusion. Clarendon Press, Oxford (2004)

Bacic, Z., Light, J.C.: Highly excited vibrational levels of floppy triatomic-molecules: a discrete variable representation—distributed Gaussian-basis approach. J. Chem. Phys. **85**, 4594–4604 (1986)

Balakrishnan, N., Dalgarno, A.: Nitric oxide production in collisions of hot $O(^3P)$ atoms with N_2. J. Geophys. Res. **108**, 1065 (2003)

Baltensperger, R., Trummer, M.A.: Spectral differencing with a twist. SIAM J. Sci. Comput. **24**, 1465–1487 (2003)

Barkley, D.: Spiral meandering. In: Kapral, R., Showalter, K. (eds.) Chemical Waves and Patterns, pp. 163–189. Kluwer Academic, Norwell (1995)

Bartlett, D.F., Corle, T.R.: The circular parallel plate capacitor: a numerical solution for the potential. J. Phys. A: Math. Gen. **18**, 1337–1342 (1985)

Baye, D.: Lagrange bases for the Fourier, generalized Fourier and Riccati-Bessel grids. J. Phys. B: Atom. Mol. Opt. Phys. **27**, L187–L191 (1994)

Baye, D.: Lagrange-mesh method for quantum-mechanical problems. Phys. Stat. Sol. B **243**, 1095–1109 (2006)

Baye, D., Heenen, P.H.: Generalized meshes for quantum-mechanical problems. J. Phys. A: Math. Gen. **19**, 2041–2059 (1986)

Baye, D., Vincke, V.: Lagrange meshes from nonclassical orthogonal polynomials. Phys. Rev. E **59**, 7195–7199 (1999)

Baye, D., Hesse, M., Vincke, M.: The unexplained accuracy of the Lagrange-mesh method. Phys. Rev. E **65**, 026701 (2002)

Becke, A.D.: A multicenter numerical integration scheme for polyatomic molecules. J. Chem. Phys. **88**, 2547–2553 (1988)

Becke, A.D.: Perspective: fifty years of density-functional theory in chemical physics. J. Chem. Phys. **140**, 18A301 (2014)

Belai, O.Y., Schwartz, O.V., Shapiro, D.A.: Accuracy of one-dimensional collision integral in the rigid-sphere approximation. Phys. Rev. A **76**, 012513 (2007)

Bellman, R.E., Kashef, B.G., Casti, J.: Differential quadrature: a technique for the rapid solution of nonlinear partial differential equations. J. Comput. Phys. **10**, 40–52 (1972)

Berman, P.R., Haverkort, J.E.M., Woerdman, J.P.: Collision kernels and transport coefficients. Phys. Rev. A **34**, 4647–4656 (1986)

Bernstein, R.B.: Quantum effects in elastic molecular scattering. Adv. Chem. Phys. **10**, 75–134 (1966)

Bertulani, C.A., Fuqua, J., Hussein, M.S.: Big bang nucleosynthesis and non-Maxwellian distribution. Astrophys. J. **767**(63), 1–11 (2013)

Blackmore, R., Shizgal, B.: Discrete ordinate method of solution of Fokker-Planck equations with nonlinear coefficients. Phys. Rev. A **31**, 1855–1868 (1985)

Bobylev, A.V.: Exact solutions of the nonlinear Boltzmann equation and the theory of relaxation of a Maxwellian gas. Theor. Math. Phys. **60**, 820–841 (1984)

Bordoni, A., Manini, N.: An optimized algebraic basis for molecular potentials. J. Phys. Chem. A **111**, 12564–12569 (2007)

Bornemann, F., Laurie, D., Wagon, S., Waldvogel, J.: The SIAM 100-Digit Challenge: A Study in High-Accuracy Numerical Computing. SIAM, Philadelphia (2004)

Bosch, H.S., Hale, G.M.: Improved formulas for fusion cross sections and thermal reactivities. Nucl. Fusion **32**, 611–631 (1992)

Bovino, S., Zhang, P., Kharchenko, V., Dalgarno, A.: Trapping hydrogen atoms from a Neon-gas matrix: a theoretical simulation. J. Chem. Phys. **131**, 054302 (2009)

Bovino, S., Zhang, P., Kharchenko, V., Dalgarno, A.: Relaxation of energetic S(^{1}D) atoms in Xe gas: comparison of ab initio calculations with experimental data. J. Chem. Phys. **135**, 024304 (2011)

Boyd, J.P.: The optimization of convergence for Chebyshev polynomial methods in an unbounded domain. J. Comput. Phys. **45**, 43–79 (1982)

Boyd, J.P.: Exponentially convergent Fourier-Chebyshev quadrature schemes on bounded and infinite domains. J. Sci. Comput. **2**, 99–109 (1987)

Boyd, J.P.: Chebyshev and Fourier Spectral Methods. Dover, New York (2001)

Brun, R.: Introduction to Reactive Gas Dynamics. Oxford University Press, Oxford (2009)

Burden, R.L., Faires, J.D.: Numerical Analysis, 9th edn. Brooks/Cole, Boston (2011)

Burke, P.G.: R-Matrix Theory of Atomic Collisions: Application to Atomic, Molecular and Optical Processes. Springer, New York (2011)

Burke, K.: Perspective on density functional theory. J. Chem. Phys. **136**, 150901 (2012)

Burke, P.G., Joachain, C.J.: Theory of Electron Atom Collisions Part 1: Potential Scattering. Springer, New York (1995)

Canto, L.F., Hussein, M.S.: Scattering Theory of Molecules, Atoms and Nuclei. Springer, New York (2013)

Canuto, C., Hussaini, M.Y., Quarteroni, A., Zang, T.A.: Spectral Methods: Fundamentals in Single Domains. Springer, New York (2006)

Cassar, M.M., Drake, G.W.F.: High precision variational calculations for H_2^+. J. Phys. B: At. Mol. Opt. Phys. **37**, 2485–2492 (2004)

Chandrasekhar, S.: Radiative Transfer. Dover, New York (1960)

Chang, J.S., Cooper, G.: A practical difference scheme for Fokker-Planck equations. J. Comput. Phys. **6**, 1–16 (1970)

Chapman, S., Cowling, T.G.: The Mathematical Theory of Nonuniform Gases. Cambridge University Press, Cambridge (1970)

Chatfield, D.C., Truhlar, D.G., Schwenke, D.W.: Benchmark calculations for thermal reaction rates. I. Quantal scattering theory. J. Chem. Phys. **94**, 2040–2044 (1991)

Cheney, W., Kincaid, D.: Numerical Methods and Computing, 6th edn. Brooks/Cole Publishing Company, Calif (2008)

Child, M.S.: Molecular Collision Theory. Dover, New York (1996)

Clayton, D.D.: Principles of Stellar Evolution and Nucleosynthesis. McGraw-Hill, New York (1968)

Cohen, J.S.: Rapid accurate calculation of JWKB phase-shifts. J. Chem. Phys. **68**, 1841–1843 (1978)

Colbert, D.T., Miller, W.H.: A novel discrete variable representation for quantum-mechanical reactive scattering via the S-Matrix Kohn method. J. Chem. Phys. **96**, 1982–1991 (1992)

Cools, R.: An encyclopaedia of cubature formulas. J. Complexity **19**, 445–453 (2003)

Danailov, D.M., Viehland, L.A., Johnson, R., Wright, T.G., Dickinson, A.S.: Transport of O^+ through Argon gas. J. Chem. Phys. **128**, 134302 (2008)

Davis, P.J., Rabinowitz, P.: Methods of Numerical Integration. Academic Press, New York (1975)

Descouvemont, P., Adahchour, A., Angulo, C., Coc, A., Vangioni-Flam, E.: Compilation and R-matrix analysis of Big Bang nuclear reaction rates. At. Data Nucl. Data Tables **88**, 203–236 (2004)

Dickinson, A.S., Certain, P.R.: Calculation of matrix elements for one-dimensional quantum-mechanical problems. J. Chem. Phys. **49**, 4209–4211 (1968)

Dickinson, A.S., Shizgal, B.: Comparison of classical and quantum continuum expectation values. Mol. Phys. **30**, 1221–1228 (1975)

Drake, G.W.F.: High precision theory of atomic Helium. Phys. Scr. **T83**, 82–92 (1999)

Drake, G.W.F., Cassar, M.M., Nistor, R.A.: Ground-state energies for helium, H^- and Ps^-. Phys. Rev. A **65**, 054501 (2002)

Dulieu, O., Kosloff, R., Masnou-Seeuws, F., Pichler, G.: Quasibound states in long-range alkali dimers: grid method calculation. J. Chem. Phys. **107**, 10633–10642 (1997)

Durran, D.R.: Numerical Methods for Fluid Dynamics: With Applications to Geophysics. Springer, Berlin (2010)

El-Sherbiny, A., Poirier, R.A.: An evaluation of the radial part of the numerical integration commonly used in DFT. J. Comput. Chem. **25**, 1378–1384 (2004)

Ernst, M.H.: Nonlinear model Boltzmann equations and exact solutions. Phys. Rep. **78**, 1–171 (1981)

Fermi, E.: Un metodo statistico per la determinazione di alcune priopriet dell'atomo. Rend. Accad. Naz. Lincei **6**, 602607 (1927)

Ferziger, J.H., Kaper, H.G.: Mathematical Theory of Transport Processes in Gases. North-Holland, Amsterdam (1972)

Finlayson, B.A.: The Method of Weighted Residuals and Variational Principles. Academic Press, New York (1972)

Finlayson, B.A., Scriven, L.E.: The method of weighted residuals—a review. Appl. Mech. Rev. **19**, 735–748 (1966)

Fiolhais, C., Marques, M.A.L., Nogueira, F.: A Primer in Density Functional Theory. Springer, Berlin (2003)

Foch, J.D., Ford, G.W.: The linear Boltzmann equation. In: de Boer, J., Uhlenbeck, G.E. (eds.) Studies in Statistical Mechanics, pp. 127–154. Elsevier, Holland (1970)

Ford, G.W.: Matrix elements of the linearized collision operator. Phys. Fluids **11**, 515–521 (1968)

Fornberg, B.: A Practical Guide to Pseudospectral Methods. Cambridge University Press, Cambridge (1996)

Fornberg, B., Driscoll, T.A., Wright, G., Charles, R.: Observations on the behavior of radial basis function approximations near boundaries. Comput. Math. Appl. **43**, 473–490 (2002)

Frankowski, K., Pekeris, C.L.: Logarithmic terms in the wave functions of two-electron atoms. Phys. Rev. **146**, 46–49 (1966)

Funaro, D.: Polynomial Approximation of Differential Equations. Springer, Berlin (1992)

Gallas, J.A.C.: Some matrix elements for Morse oscillator. Phys. Rev. A **21**, 1829–1834 (1980)

Gautschi, W.: The numerical evaluation of a challenging integral. Numer. Algorithms **49**, 187–194 (2008)

Gibble, K.E., Gallagher, A.: Measurements of velocity-changing collision kernels. Phys. Rev. A **43**, 1366–1380 (1991)

Gibelli, L., Shizgal, B.D., Yau, A.W.: Ion energization by wave-particle interactions: comparison of spectral and particle simulation solutions of the Vlasov equation. J. Comput. Phys. **59**, 2566–2581 (2010)

Gill, P.M.W.: Molecular integrals over Gaussian basis functions. Adv. Quant. Chem. **25**, 141–205 (1994)

Gill, P.M.W., Chien, S.-H.: Radial quadrature for multiexponential integrands. J. Comput. Chem. **24**, 732–740 (2003)

Goldstein, H., Poole, C., Safko, J.: Classical Mechanics. Addison Wesley, San Francisco (2000)

Gombosi, T.I.: Gaskinetic Theory. Cambridge University Press, Cambridge (1994)

Gottlieb, D., Orszag, S.: Numerical Analysis of Spectral Methods: Theory and Applications. SIAM, Philadelphia (1977)

Grabowski, P.E., Chernoff, D.F.: Pseudospectral calculation of helium wave functions, expectation values, and oscillator strength. Phys. Rev. A **84**, 042505 (2011)

Hamilton, I.P., Light, J.C.: On distributed Gaussian bases for simple model multidimensional vibrational problems. J. Chem. Phys. **84**, 306–317 (1986)

Harris, D.O., Engerholm, G.G., Gwinn, W.D.: Calculation of matrix elements for one-dimensional quantum-mechanical problems and the application to anharmonic oscillators. J. Chem. Phys. **43**, 1515–1517 (1965)

Haubold, H.J., John, R.W.: Analytical representation of the thermonuclear reaction rate and fusion energy production in a spherical plasma shock wave. Plasma Phys. **23**, 399–411 (1981)

Haxton, D.J.: Lebedev discrete variable representation. J. Phys. B: At. Mol. Opt. Phys. **40**, 4443–4451 (2007)

Heidbrink, W.W., Sadler, G.J.: The behaviour of fast ions in Tokamak experiments. Nucl. Fusion **34**, 535–615 (1994)

Helgaker, T., Jorgensen, P., Olsen, J.: Molecular Electronic Structure Theory. Wiley, New York (2000)

Hesthaven, J.S., Gottlieb, S., Gottlieb, D.: Spectral Methods for Time Dependent Problems. Cambridge University Press, Cambridge (2007)

Hirschfelder, J.O., Curtiss, C.F., Bird, B.: The Molecular Theory of Gases and Liquids. Wiley, New York (1954)

Hoare, M.R.: The linear gas. Adv. Chem. Phys. **20**, 135–214 (1971)

Hoare, M.R., Kaplinsky, C.H.: Linear hard sphere gas: variational eigenvalue spectrum of the energy kernel. J. Chem. Phys. **52**, 3336–3353 (1970)

Hohenberg, P., Kohn, W.: Inhomogeneous electron gas. Phys. Rev. **136**, B864–B871 (1964)

Holloway, J.P.: Spectral discretizations of the Vlasov-Maxwell equations. Trans. Theory Stat. Phys. **25**, 1–32 (1996)

Holway, L.H.: Time varying weight functions and the convergence of polynomial expansions. Phys. Fluids **10**, 35–48 (1967)

Huang, K.: Statistical Mechanics. Wiley, New York (1967)

Hubert, D.: Auroral ion velocity distribution function: generalized polynomial solution of Boltzmann's equation. Planet. Space Sci. **31**, 119–127 (1983)

Hussein, M.S., Pato, M.P.: Uniform expansion of the thermonuclear reaction rate formula. Braz. J. Phys. **27**, 364–372 (1997)

Isaacson, S.A., Kirby, R.M.: Numerical solution of linear Volterra integral equations of the second kind with sharp gradients. J. Comput. Appl. Math. **235**, 4283–4301 (2011)

Iserles, A., Norsett, S.P.: Efficient quadrature of highly oscillatory integrals using derivatives. Proc. R. Soc. A **461**, 1383–1399 (2005)

Jamieson, M.J., Dalgarno, A., Wei, L.: Elastic scattering of hydrogen and deuterium atoms by oxygen atoms. J. Geophys. Res. **111**, A06308 (2006)

Jerri, A.J.: Introduction to Integral Equations with Applications, 2nd edn. Wiley, New York (1999)

Johnson, R.E., Liu, M., Tully, C.: Collisional dissociation cross sections for $O + O_2$, $CO + N_2$, $O_2 + O_2$, $N + N_2$ and $N_2 + N_2$. Planet. Space Sci. **50**, 123–128 (2002)

Jones, R.O., Gunnarsson, O.: The density functional formalism, its applications and prospects. Rev. Mod. Phys. **61**, 689–746 (1989)

Kabin, K., Shizgal, B.D.: Exact evaluation of collision integrals for the nonlinear Boltzmann equation. AIP Conf. Proc. **663**, 35–42 (2003)

Kakhiani, K., Tsereteli, K., Tsereteli, P.: A program to generate a basis set adaptive radial quadrature grid for density functional theory. Comput. Phys. Commun. **180**, 256–268 (2009)

Kallush, S., Kosloff, R.: Improved methods for mapped grids: applied to highly excited vibrational states of diatomic molecules. Chem. Phys. Lett. **433**, 221–227 (2006)

Kapral, R., Ross, J.: Relaxation in a dilute binary gas mixture. J. Chem. Phys. **52**, 1238–1243 (1970)

Karplus, M., Porter, R.N.: Atoms and Molecules: An Introduction for Students of Physical Chemistry. Benjamin, Menlo Park (1970)

Kennedy, M., Smith, F.J.: The efficient computation of JWKB phase shifts. Mol. Phys. **13**, 443–448 (1967)

Kern, C.W., Karplus, M.: Gaussian-transform method for molecular integrals. II. Evaluation of molecular properties. J. Chem. Phys. **43**, 415–429 (1965)

Kharchenko, V., Dalgarno, A.: Thermalization of fast $O(^1D)$ atoms in the stratosphere and mesosphere. J. Geophys. Res. **109**, D18311 (2004)

Kharchenko, V., Tharamel, J., Dalgarno, A.: Kinetics of thermalization of fast nitrogen atoms beyond the hard sphere approximation. J. Atmos. Sol. Terr. Phys. **59**, 107–115 (1997)

Kharchenko, V., Balakrishnan, N., Dalgarno, A.: Thermalization of fast nitrogen atoms in elastic and inelastic collisions with molecules of atmospheric gases. J. Atmos. Terr. Phys. **60**, 95–106 (1998)

Kohn, W., Sham, L.J.: Self-consistent equations including exchange and correlation effects. Phys. Rev. **140**, A1133–A1138 (1965)

Kokoouline, V., Dulieu, O., Kosloff, R., Masnou-Seeuws, F.: Mapped Fourier methods for long-range molecules: application to perturbations in the $Rb_2(0_u^+)$ photoassociation spectrum. J. Chem. Phys. **110**, 9865–9876 (1999)

Kremer, G.M.: An Introduction to the Boltzmann Equation and Transport Processes in Gases. Springer, New York (2010)

Krook, M., Wu, T.T.: Formation of Maxwellian tails. Phys. Rev. Lett. **36**, 1107–1109 (1976)

Kumar, A.S.: An analytical solution to applied mathematics-related Loves equation using the Boubaker polynomials expansion scheme. J. Frankl. Inst. **347**, 1755–1761 (2010)

Kythe, P.K., Puri, P.: Computational Methods for Linear Integral Equations. Birkhauser, Berlin (2002)

Kythe, P.K., Schaferkotter, M.R.: Handbook of Computational Methods for Integration. Chapman and Hall/CRC, London (2004)

Langer, R.E.: On the connection formulas and the solutions of the wave equation. Phys. Rev. **51**, 669–676 (1937)

Lebedev, V.I.: Spherical quadrature formulas exact to orders 25–29. Sib. Mat. Zh. **18**, 132–142 (1977)

Lemmon, E.W., Jacobsen, R.T.: Viscosity and thermal conductivity equations for Nitrogen, Oxygen, Argon, and Air. Int. J. Thermophys. **25**, 21–69 (2004)

LeVeque, R.J.: Finite Difference Methods for Ordinary and Partial Differential Equations. SIAM, Philadelphia (2007)

Levine, I.N.: Quantum Chemistry, 6th edn. Prentice Hall, New Jersey (2009)

Liao, P.F., Bjorholm, J.E., Berman, P.R.: Effects of velocity-changing collisions on two-photon and stepwise-absorption spectroscopic line shapes. Phys. Rev. A **21**, 1927–1938 (1980)

Liboff, R.L.: Introductory Quantum Mechanics, 4th edn. Addison-Wesley, New York (2002)

Liboff, R.L.: Kinetic Theory: Classical, Quantum, and Relativistic Descriptions, 3rd edn. Springer, New York (2003)

Lieb, E.H.: Thomas-Fermi and related theories of atoms and molecules. Rev. Mod. Phys. **53**, 603–641 (1981)

Light, J.C., Carrington Jr, T.: Discrete variable representations and their utilization. Adv. Chem. Phys. **114**, 263–310 (2000)

Light, J.C., Hamilton, I.P., Lill, J.V.: Generalized discrete variable approximation in quantum mechanics. J. Chem. Phys. **82**, 1400–1409 (1985)

Lindenfeld, M.J., Shizgal, B.: Matrix elements of the Boltzmann collision operator for gas mixtures. Chem. Phys. **41**, 81–95 (1979)

Lindfield, G.R., Penny, J.E.T.: Numerical Methods Using MATLAB. Elsevier, Amsterdam (2012)

Lindh, R., Malmqvist, P.A., Gagliardi, L.: Molecular integrals by numerical quadrature I. Radial integration. Theor. Chem. Acta **106**, 178–187 (2001)

Liou, K.-N.: A numerical experiment on Chandrasekhar's discrete-ordinate method for radiative transfer: applications to cloudy and hazy atmospheres. J. Atmos. Sci. **30**, 1303–1326 (1973)

Liu, Q.-J., Zhao, W.-Q.: Iterative solution for groundstate of H_2^+ ion. Commun. Theor. Phys (Beijing, China). **53**, 57–62 (2010)

Lo, J.Q.-W., Shizgal, B.D.: Spectral convergence of the quadrature discretization method in the solution of the Schrödinger and Fokker-Planck equations: comparison with Sinc methods. J. Chem. Phys. **125**, 194108 (2006)

Lo, J.Q.-W., Shizgal, B.D.: An efficient mapped pseudospectral method for weakly bound states: vibrational states of He_2, Ne_2, Ar_2 and Cs_2. J. Phys. B: At. Mol. Opt. Phys. **41**, 185103 (2008)

Love, E.R.: The electrostatic field of two equal circular co-axial conducting disks. Q. J. Mech. Appl. Math. **2**, 428–451 (1949)

Loyalka, S.K., Tipton, E.L., Tompson, R.V.: Chapman-Enskog solutions to arbitrary order in Sonine polynomials I: simple, rigid-sphere gas. Physica A **379**, 417–435 (2007)

Lyness, J.N.: When not to use an automatic quadrature routine. SIAM Rev. **25**, 63–87 (1983)

Lyness, J.N.: Integrating some infinite oscillating tails. J. Comput. Appl. Math. **12**, 109–117 (1985)

Mason, E.A., McDaniel, E.W.: Transport Properties of Ions in Gases. Wiley, New York (1988)

Mathai, A.M., Haubold, H.J.: Review of mathematical techniques applicable in astrophysical reaction rate theory. Astrophys. Space Sci. **282**, 265–280 (2002)

McCourt, F.R.W., Beenakker, J.J.M., Köhler, W.E.E., Kuščer, I.: Nonequilibrium Phenomena in Polyatomic Gases Volume. 2: Cross Sections, Scattering, and Rarefied Gases. Oxford University Press, Oxford (1991)

McDaniel, E.W., Mason, E.A.: The Mobility and Diffusion of Ions in Gases. Wiley, New York (1973)

McGuyer, B.H., Marslann III, R., Olsen, B.A., Happer, W.: Cusp kernels for velocity-changing collisions. Phys. Rev. Lett. **108**, 183202 (2012)

McQuarrie, D.A., Simon, J.D.: Physical Chemistry: A Molecular Approach. University Science Books, California (1997)

Meijering, E.H.W., Niessen, W.J., Viergever, M.A.: The Sinc-approximating kernels of classical polynomial interpolation. IEEE Int. Conf. Image Proc. **3**, 652–656 (1999)

Mitani, M.: An application of double exponential formula to radial quadrature grid in density functional calculation. Theor. Chem. Acc. **130**, 645–669 (2011)

Morgan, J.D.: Thomas-Fermi and other density—functional theories. In: Drake, G.W.F. (ed.) Atomic, Molecular and Optical Physics Handbook, pp. 233–242. AIP Press, New York (1996)

Mullen, W.J., Laloë, F., Richards, M.G.: Longitudinal relaxation times for dilute quantum gases. J. Low Temp. Phys. **80**, 1–13 (1990)

Munn, R.J., Mason, E.A., Smith, F.J.: Some aspects of the quantal and semiclassical calculation of phase shifts and cross sections for molecular scattering and transport. J. Chem. Phys. **41**, 3978–3988 (1964)

Mura, M.E., Knowles, P.J.: Improved radial grids for quadrature in molecular density-functional calculations. J. Chem. Phys. **104**, 9848–9858 (1996)

Murray, C.W., Handy, N.C., Lamming, G.L.: Quadrature schemes for integrals of density functional theory. Mol. Phys. **78**, 997–1014 (1993)

Nan, G., Houston, P.L.: Velocity relaxation of $S(^1D)$ by rare gases measured by Doppler spectroscopy. J. Chem. Phys. **97**, 7865–7872 (1992)

Napier, D.G., Shizgal, B.D.: Sound dispersion in single-component systems. Phys. A **387**, 4099–4118 (2008)

Newbury, N.R., Barton, A.S., Cates, G.D., Happer, W., Middleton, H.: Gaseous ^3He-^3He magnetic dipolar relaxation. Phys. Rev. A **48**, 4411–4420 (1993)

O'Hara, H., Smith, F.J.: Error estimation in the Clenshaw-Curtis quadrature formula. Comput. J. **11**, 213–219 (1968)

Oh, S.-K.: Modified Lennard-Jones potentials with a reduced temperature-correction parameter for calculating thermodynamic and transport properties: Noble gases and their mixtures (He, Ne, Ar, Kr, and Xe). J. Thermodyn. **2013**, 828620 (2013)

Olmos, D., Shizgal, B.D.: A pseudospectral method of solution of Fisher's equation. J. Comput. Appl. Math. **193**, 219–242 (2006)

O'Neal, D., Neff, J.E.: OH 1.563μ absorption from starspots on active stars. Astron. J. **113**, 1129–1137 (1997)

Ordzywolek, A.: Gaussian integration with rescaling abscissas and weights. Comput. Phys. Commun. **182**, 2533–2539 (2011)

Pack, R.T.: Space-fixed vs body-fixed axes in atom-diatomic molecule scattering. Sudden approximation. J. Chem. Phys. **60**, 633–639 (1974)

Parr, R.G.: Density functional theory. Annu. Rev. Phys. Chem. **34**, 631–656 (1983)

Parr, R.G., Gosh, S.W.: Thomas-Fermi theory for atomic systems. Proc. Natl. Acad. Sci. **83**, 3577–3579 (1986)

Pask, J.E., Sukumar, N., Monsavi, S.E.: Linear scaling solution of the all-electron Coulomb problem in solids. Int. J. Multiscale Comput. Eng. **10**, 83–99 (2012)

Pastore, P.: The numerical treatment of Love's integral equation having a small parameter. J. Comput. Appl. Math. **236**, 1267–1281 (2011)

Peyret, R.: Spectral Methods for Incompressible Viscous Flow. Springer, New York (2002)

Rasch, J., Whelan, C.T.: On the numerical evaluation of a class of integrals occurring in scattering problems. Comput. Phys. Commun. **101**, 31–46 (1997)

Reine, S., Helgaker, T., Lindh, R.: Multi-electron integrals. WIREs Comput. Mol. Sci. **2**, 290–303 (2012)

Robson, R.E., Prytz, A.: A discrete ordinate pseudo-spectral method: review and application from a physicist's perspective. Aust. J. Phys. **46**, 465–495 (1993)

Robson, R.E., Ness, K.F., Sneddon, G.E., Viehland, L.A.: Comment on the discrete ordinate method in the kinetic theory of gases. J. Comput. Phys. **92**, 213–229 (1991)

Rogers, G.L., Berman, P.R.: Exchange collision kernel. Phys. Rev. A **44**, 417–432 (1991)

Ross, J., Mazur, P.: Some deductions from a formal statistical mechanical theory of chemical kinetics. J. Chem. Phys. **35**, 19–28 (1961)

Rys, J., Dupuis, M., King, H.F.: Computation of electron repulsion integrals using Rys quadrature method. J. Comput. Chem. **4**, 154–157 (1983)

Sabbane, M., Tij, M., Santos, A.: Maxwellian gas undergoing a stationary Poiseuille flow in a pipe. Phys. A **327**, 264–290 (2003)

Safouhi, H.: The properties of sine, spherical Bessel and reduced Bessel functions for improving convergence of semi-infinite very oscillatory integrals: the evaluation of three-centre nuclear attraction integrals over B-functions. J. Phys. A: Math. Gen. **34**, 2801–2818 (2001)

Sandberg, J.A.R., Rinkevicius, Z.: An algorithm for the efficient evaluation of two-electron repulsion integrals over contracted Gaussian-type basis functions. J. Chem. Phys. **137**, 234105 (2012)

Santos, A.: Solutions of the moment hierarchy in the kinetic theory of Maxwell models. Contin. Mech. Thermodyn. **21**, 361–387 (2009)

Schumer, J.W., Holloway, J.P.: Vlasov simulations using velocity-scaled Hermite representations. J. Comput. Phys. **144**, 626–661 (1998)

Schwartz, C.: High-accuracy approximation techniques for analytic functions. J. Math. Phys. **26**, 411–415 (1985)

Secrest, D., Johnson, B.R.: Exact quantum-mechanical calculation of a collinear collision of a particle with a harmonic oscillator. J. Chem. Phys. **45**, 4556–4570 (1966)

Seinfeld, J.H., Pandis, S.N.: Atmospheric Chemistry and Physics: From Air Pollution to Climate Change, 2nd edn. Wiley, New York (2006)

Shapiro, D.A.: Spectral line narrowing in the Keilson-Storer model. J. Phys. B: At. Mol. Opt. Phys. **33**, L43–L49 (2000)

Sharipov, F., Bertoldo, G.: Numerical solution of the linearized Boltzmann equation for an arbitrary intermolecular potential. J. Comput. Phys. **228**, 3345–3357 (2009)

Shavitt, I., Karplus, M.: Gaussian-transform method for molecular integrals. I. Formulation of energy integrals. J. Chem. Phys. **43**, 398–414 (1965)

Shen, J., Tang, T., Wang, L.-L.: Spectral Methods: Algorithms Analysis and Applications. Springer, Berlin (2011)

Shizgal, B.: Kinetic theory calculation of NMR relaxation time for dilute ^{3}He gas. J. Chem. Phys. **58**, 3424–3431 (1973)

Shizgal, B.: Calculation of the NMR relaxation time for dilute ^{129}Xe gas. Chem. Phys. **5**, 464–470 (1974a)

Shizgal, B.: A method for the rapid calculation of matrix elements with highly oscillatory JWKB radial wavefunctions. Chem. Phys. Lett. **24**, 369–372 (1974b)

Shizgal, B.: A Gaussian quadrature procedure for the use in the solution of the Boltzmann equation and related problems. J. Comput. Phys. **41**, 309–328 (1981)

Shizgal, B.D.: An analysis of O-H interaction potentials, O-H and O-D cross sections and vibrational states. Planet. Space. Sci. **47**, 163–147 (1999)

Shizgal, B., Fitzpatrick, J.M.: Matrix elements of the linear Boltzmann collision operator for systems of two components at different temperatures. Chem. Phys. **6**, 54–65 (1974)

Shizgal, B., Lindenfeld, M.J.: Energy distribution function of translationally hot O(^3P) atoms in the atmosphere of earth. Planet. Space Sci. **27**, 1321–1332 (1979)

Shizgal, B., Blackmore, R.: A discrete ordinate method of solution of linear boundary value and eigenvalue problems. J. Comput. Phys. **55**, 313–327 (1984)

Shizgal, B., Hubert, D.: Nonequilibrium nature of ion distribution functions in the high latitude auroral ionosphere. In: Muntz, E.P., Weaver, D.P., Campbell, D.H. (eds.) Proceedings of the 16th International Symposium on Rarefied Gas Dynamics, pp. 3–22. AIAA, Washington (1989)

Shizgal, B.D., Chen, H.: The quadrature discretization method (QDM) in the solution of the Schrödinger equation with nonclassical basis functions. J. Chem. Phys. **104**, 4137–4150 (1996)

Shizgal, B.D., Chen, H.: The quadrature discretization method in the solution of the Fokker-Planck equation with nonclassical basis functions. J. Chem. Phys. **107**, 8051–8063 (1997)

Shu, C.: Differential Quadrature and Its Application in Engineering. Springer, Berlin (2000)

Siewert, C.E.: On computing the Chapman-Enskog functions for viscosity and heat transfer and the Burnett functions. JQRST **74**, 789–796 (2002)

Slevinsky, M., Safouhi, H.: Numerical treatment of a twisted tail using extrapolation methods. Numer. Algorithm **48**, 301–316 (2008)

Sospedra-Alfonso, R., Shizgal, B.D.: Henyey-Greenstein model in the shape relaxation of dilute gas mixtures. Trans. Theory Stat. Phys. **41**, 368–388 (2012)

Sospedra-Alfonso, R., Shizgal, B.D.: Energy and shape relaxation in binary atomic systems with realistic quantum cross sections. J. Chem. Phys. **139**, 044113 (2013)

St.-Maurice, J.-P., Schunk, R.W.: Use of generalized orthogonal polynomial solutions of Boltzmanns equation in certain aeronomy problems, Auroral ion velocity distributions. J. Geophys. Res. **81**, 2145–2154 (1976)

St.-Maurice, J.-P., Schunk, R.W.: Ion velocity distributions in the high-latitude ionosphere. Rev. Geophys. **17**, 99–134 (1979)

Stenger, F.: Numerical methods based on Sinc and analytic functions. Springer Series in Comp. Math. **20**, 91–96 (1993)

Stroud, A.H., Secrest, D.: Gaussian Quadrature Formulas. Prentice-Hall, New Jersey (1966)

Szabo, A., Ostlund, N.S.: Modern Quantum Chemistry, Introduction to Advanced Electronic Structure Theory. Dover, New York (1996)

Szalay, V.: Discrete variable representations of differential operators. J. Chem. Phys. **99**, 1978–1984 (1993)

Szalay, V., Szidarovsky, T., Czakó, G., Császár, A.G.: A paradox of grid-based representation techniques: accurate eigenvalues from inaccurate matrix elements. J. Math. Chem. **50**, 636–651 (2012)

Szalay, V., Czakó, G., Nagy, A., Furtenbacher, T., Császár, A.G.: On one-dimensional discrete variable representations with general basis functions. J. Chem. Phys. **119**, 10512–10518 (2003)

Tang, T.: The Hermite spectral method for Gaussian-type functions. SIAM J. Sci. Comput. **14**, 594–606 (1993)

Taylor, J.R.: Scattering Theory: The Quantum Theory on Nonrelativistic Collisions. Dover, New York (2012)

Thomas, L.H.: The calculation of atomic fields. Proc. Camb. Philos. Soc. **23**, 542–548 (1927)

Tomaschitz, R.: Multipole fine structure of the cosmic microwave background: reconstruction of the temperature power spectrum. Mon. Not. R. Astron. Soc. **427**, 1363–1383 (2012)

Tomaschitz, R.: Bessel integrals in epsilon expansion: squared spherical Bessel functions averaged with Gaussian power-law distributions. Appl. Math. Comput. **225**, 228–241 (2013)

Trefethen, L.N.: Is Gauss quadrature better than Clenshaw-Curtis? SIAM Rev. **50**, 67–87 (2008)

Treutler, O., Ahlrichs, R.: Efficient molecular numerical integration schemes. J. Chem. Phys. **102**, 346–354 (1995)

Truhlar, D.G., Wyatt, R.E.: History of H$_3$ kinetics. Annu. Rev. Phys. Chem. **27**, 1–43 (1976)

Tsuneda, T.: Density Functional Theory in Quantum Chemistry. Springer, New York (2014)

Ueda, M., Sargeant, A.J., Pato, M.P., Hussein, M.S.: Effective astrophysical S factor for nonresonant reactions. Phys. Rev. C **61**, 045801 (2000)

Viehland, L.A.: Velocity distribution functions and transport coefficients of atomic ions in atomic gases by a Gram-Charlier approach. Chem. Phys. **179**, 71–92 (1994)

Viehland, L.A., Chang, Y.: Transport cross sections for collisions between particles. Comput. Phys. Commun. **181**, 1687–1696 (2010)

Wei, H.: Ghost levels and near-variational forms of the discrete variable representation: application to H$_2$O. J. Chem. Phys. **106**, 6885–6900 (1997)

Wei, G.W.: Solving quantum eigenvalue problems by discrete singular convolution. J. Phys. B: At. Mol. Opt. Phys. **33**, 343–352 (2000a)

Wei, G.W.: Wavelets generated by using discrete singular convolution kernels. J. Phys. A: Math. Gen. **33**, 8577–8596 (2000b)

Weniger, E.J.: The strange history of B functions or how theoretical chemists and mathematicians do (not) interact. Int. J. Quant. Chem. **109**, 1706–1716 (2009)

Whittaker, J.M.: The Fourier theory of the Cardinal function. Proc. Roy. Soc. Edinb. **1**, 169–176 (1929a)

Whittaker, J.M.: On the Cardinal function of interpolation theory. Proc. Roy. Soc. Edinb. **1**, 41–46 (1929b)

Wick, G.C.: Über ebene diffusionsprobleme. Z. Phys. **121**, 702–718 (1943)

Wigner, E.P., Wilkins Jr, J.E.: Effect of temperature of the moderator on the velocity distribution of neutrons with numerical calculations for H as moderator. Technical Report AECD-2275, US Atomic Energy Commission (1944)

Willner, K., Dulieu, O., Masnou-Seeuws, F.: Mapped grid methods for long-range molecules and cold collisions. J. Chem. Phys. **120**, 548–561 (2004)

Wind, H.: Electron energy for H_2^+ in the ground state. J. Chem. Phys. **42**, 2371–2373 (1965)

Wright, J.S., Donaldson, D.J.: Potential energy and vibrational levels for local modes in water and acetylene. Chem. Phys. **94**, 15–23 (1985)

Zhang, P., Kharchenko, V., Dalgarno, A.: Thermalization of suprathermal $N(^4S)$ atoms in He and Ar gases. Mol. Phys. **105**, 1487–1496 (2007)